Exploring chemistry and magnetism in adlayers at surfaces

Inauguraldissertation

zur

Erlangung der Würde eines Doktors der Philosophie

vorgelegt der

Philosophisch-Naturwissenschaftlichen Fakultät

der Universität Basel

von

Jan Nowakowski

aus Bydgoszcz (Polen)

Villigen, 2016

Genehmigt von der Philosophisch-Naturwissenschaftlichen Fakultät

auf Antrag von:

Prof. Dr. Thomas Jung

Prof. Dr. Ernst Meyer

Basel, 21.06.2016

Prof. Dr. Jörg Schibler

Dekan

I'm not absolutely sure of anything.

I don't feel frightened by not knowing things.

Richard Feynman

Abstract

The goal of my thesis was to understand, design and modify the properties of surfaces as a whole, as well as of surface-supported atoms and molecules. This way I discovered exciting differences and similarities between two- and three-dimensional systems, *i.e.* between the surface and the bulk, which came as a natural consequence in the pursuit of this aim. I have observed physicochemical phenomena that strictly require the specific characteristics of surfaces and also a number of effects that proceed in a very similar fashion when compared to the gas or the liquid phase. One thesis is, however, not enough to study all of the interesting phenomena in surface science, *i.e.* the field concerned with effects occurring when the dimensionality of the arrangement of atoms is decreased below three. Therefore I focused on exploring on-surface chemistry and magnetism – phenomena that are closely related, as they both depend on the interaction of atoms' valence electrons with the surroundings.

The first example of how one can tune the properties of a surface is provided by adding a one-atom-thick layer of adsorbates – specifically O, N and Cl on Cu(001). During my work I discovered that this simple modification can drastically alter the reactivity of a surface, as studied using the self-metalation reaction of porphyrins, in which a metal atom is taken from the substrate and embedded in the molecule. Interestingly, this approach also allowed studying the interactions between the molecules, visualised in the formation of molecular self-assembled islands and clusters.

In the second studied system I investigated a surface covered by only single ad-atoms, not by a full layer of adsorbates. In this project I was interested in the influence of a substrate on the magnetic properties of single transition metal atoms. Isolated single atoms, due to their spherical symmetry, cannot possess any magnetic anisotropy – *i.e.* directional dependence of magnetic properties. The interaction with a surface can, however, induce such directional dependence, which in the case of Cr atoms deposited on a Bi substrate is found to reach the

theoretically possible limit. It is, to the best of my knowledge, the first observation of such a giant magnetic anisotropy on a non-insulating substrate.

Due to the very limited nature of the periodic table of elements, it is desirable to change the properties of paramagnetic atoms even before depositing them on a surface. Due to the vast possibilities given by organic chemistry, inserting an atom in easily modifiable molecule is a simple way to achieve that. In this thesis I show that such an organic 'cage' around an atom can additionally modify the magnetic interaction between the paramagnetic ion and the underlying substrate. I was able to tune the molecule-substrate magnetic exchange coupling energy by using molecules with different functional groups.

Interestingly, molecule-surface magnetic interactions can also be used to study molecular motion. I also discuss the use of X-ray Magnetic Circular Dichroism for detecting out-of-plane molecular rearrangement in a model case, in which two phthalocyanines, MnPc and FePc, showed different adsorption energies with the former being able to push the latter away from the substrate.

During this thesis I also developed a method for creating a supramolecular chessboard-like arrangement built from two different molecules, namely MnPc and FeFPc. This approach has been successfully used by me and my colleagues in many projects that strictly required a surface-supported, alternating arrangement of molecules. Fascinating properties of this low-dimensional magnetic layer were controlled by chemical ligation as well as by the choice of the underlying substrate – Au(111), Ag(111) or ferromagnetic O-covered Co(001). Those different supports enabled studying different magnetic coupling interactions that are strong on ferromagnetic supports, while weak on diamagnetic.

This thesis expands the range of tuneable surface properties. This was achieved by the use of on-surface supramolecular engineering, an approach combining the design and modifications of molecules and surfaces, as well as the interactions between them.

List of publications and manuscripts

First author:

- J. Nowakowski, C. Wäckerlin, J. Girovsky, D. Siewert, T.A. Jung, N. Ballav, *Porphyrin metalation providing an example of a redox reaction facilitated by a surface reconstruction*, Chemical Communications **49**, 2347 (2013).
- J. Nowakowski, S. Nowakowska, G. Srivastava, M. Baljozovic, J. Girovsky, N. Ballav, T.A. Jung, *Probing the reactivity of functionalized surfaces by porphyrin metalation*, ChemistrySelect **5**, 891 (2016)
- J. Nowakowski *et al.*, *Substrate-molecule distance dependence on the magnetic coupling energy*, in preparation
- J. Nowakowski *et al.*, *Detecting out-of-plane mobility in molecular bilayers*, in preparation
- J. Nowakowski and P. Kröger *et al.*, *Magnetic properties of single 3d transition metal atoms on Bi*, in preparation

Co-author:

- C. Wäckerlin, P. Maldonado, L. Arnold, A. Shchyrba, J. Girovsky, J. Nowakowski, E. Ali, T. Hählen, M. Baljozovic, D. Siewert, A. Kleibert, K. Müllen, P. M. Oppeneer, T. A. Jung, N. Ballav, *Magnetic exchange coupling of a synthetic Co (II)-complex to a ferromagnetic Ni substrate*, Chemical Communications **49**, 10736 (2013).

- C. Wäckerlin, K. Tarafder, J. Girovsky, J. Nowakowski, T. Hählen, A. Shchyrba, D. Siewert, A. Kleibert, F. Nolting, P. M. Oppeneer, T. A. Jung, N. Ballav, *Ammonia Coordination Introducing a Magnetic Moment in an On-Surface Low-Spin Porphyrin*, Angewandte Chemie International Edition **52**, 4568 (2013).

- C. Wäckerlin, J. Nowakowski, S.-X. Liu, M. Jaggi, D. Siewert, J. Girovsky, A. Shchyrba, T. Hählen, A. Kleibert, P. M. Oppeneer, F. Nolting, S. Decurtins, T. A. Jung, N. Ballav, *Two-Dimensional Supramolecular Electron Spin Arrays*, Advanced Materials **25**, 2404 (2013).

- J. Girovsky, M. Buzzi, C. Wäckerlin, D. Siewert, J. Nowakowski, P. M. Oppeneer, F. Nolting, T. A. Jung, A. Kleibert, N. Ballav, *Investigating magneto-chemical interactions at molecule–substrate interfaces by X-ray photo-emission electron microscopy*, Chemical Communications **50**, 5190 (2014).

- A. Shchyrba, C. Wäckerlin, J. Nowakowski, S. Nowakowska, J. Björk, S. Fatayer, J. Girovsky, T. Nijs, S. C. Martens, A. Kleibert, M. Stöhr, N. Ballav, T. A. Jung, L. H. Gade, *Controlling the Dimensionality of On-Surface Coordination Polymers via Endo-or Exoligation*, Journal of American Chemical Society **136**, 9355 (2014).

- M. N. Alberti, S. Nowakowska, M. D. Tzirakis, J. Nowakowski, P. Fesser, W. B. Schweizer, A. Shchyrba, C. Thilgen, T. A. Jung, F. Diederich, *Synthesis of trans-A2B2-and trans-A2BC-Porphyrins with Polar 4'-(Dimethylamino) tolan-4-yl Substituents, and a Screening Protocol for Vapor-Phase Deposition on Metal Surfaces*, European Journal of Organic Chemistry, 5705 (2014).

- J. Girovsky, K. Tarafder, C. Wäckerlin, J. Nowakowski, D. Siewert, T. Hählen, A. Wäckerlin, A. Kleibert, N. Ballav, T. A. Jung, P. M. Oppeneer, *Antiferromagnetic coupling of Cr-porphyrin to a bare Co substrate*, Physical Review B **90**, 220404(*R*) (2014).

- S. Nowakowska, A. Wäckerlin, S. Kawai, T. Ivas, J. Nowakowski, S. Fatayer, C. Wäckerlin, T. Nijs, E. Meyer, J. Björk, M. Stöhr, L. H. Gade, T. A. Jung, *Interplay of weak interactions in the atom-by-atom condensation of xenon within quantum boxes*, Nature Communications **6**, 6071 (2015).

- S. Nowakowska, A. Wäckerlin, I. Piquero-Zulaica, J. Nowakowski, S. Kawai, C. Wäckerlin, M. Matena, T. Nijs, S. Fatayer, O. Popova, A. Ahsan, S. F. Mousavi, T. Ivas, E. Meyer, M. Stöhr, J. Enrique Ortega, J. Björk, L. H. Gade, J. Lobo-Checa, T. A. Jung, *Configuring Electronic States in an Atomically Precise Array of Quantum Boxes*, accepted in SMALL.

- J. Girovsky, J. Nowakowski, Md. Ehesan Ali, M. Baljozovic, H. Rossmann, T. Nijs, E. Aeby, S. Nowakowska, D. Siewert, G. Srivastava, C. Wäckerlin, J. Dreiser, S. Decurtins, Shi-Xia Liu, P. M. Oppeneer, T. A. Jung, N. Ballav, *Long-range ferrimagnetic order in a two-dimensional supramolecular Kondo lattice*, submitted

- S. Nowakowska, F. Mazzola, M. Almperti, F. Song, T. Voigt, J. Nowakowski, A. Wäckerlin, C. Wäckerlin, J. Wiss, W. B. Schweizer, M. Broszio, C. Polley, M. Leandersson, S. Fatayer, T. Ivas, S. F. Mousavi, A. Ahsan, T. Nijs, O. Popova, J. Zhang, M Muntwiler, C. Thilgen, M. Stöhr, F. Diederich, J. Wells, T. A. Jung, *Adsorbate-induced modification of the confining barriers in a quantum box array*, submitted

- Ludovico G. Tulli, Mina Moradi, J. Nowakowski, Thomas A. Jung, and Patrick Shahgaldian, *Two-dimensional calix[4]arene-based metal-organic networks*, in preparation

Contents

List of abbreviations

General acronyms

2D	2-Dimensional
3D	3-Dimensional
BE	Binding Energy
B_J	Brillouin function
Cl/Cu	c(2x2)-Cl superstructure on Cu(001)
E_{ex}	Magnetic exchange energy
K	Magnetic anisotropy energy
k_B	Boltzmann constant
L	Langmuir, unit of exposure to a surface in UHV; 1L is equal to exposure of 10^{-6} torr for 1 second
M	Magnetisation
m	Magnetic moment
MAE	Magnetic anisotropy energy
μ_B	Bohr Magneton; the spin magnetic moment of an electron is approximately equal to 1 μ_B
MOF	Metal-Organic Framework
N/Cu	c(2x2)-N superstructure on Cu(001)

O/Co	c(2x2)-O superstructure on Co(001)
O/Cu	$(\sqrt{2}x2\sqrt{2})R45^{o}$-O reconstruction on Cu(001)
QCMB	Quartz Crystal Micro-Balance
T	Temperature or Tesla (unit of B)
TB	Terabit (10^{12} bits)
TEY	Total Electron Yield
UHV	Ultra-High Vacuum

Methods

DFT	Density Functional Theory
LEED	Low-Energy Electron Diffraction
STM	Scanning Tunnelling Microscopy
STS	Scanning Tunnelling Spectroscopy
UPS	Ultraviolet Photoelectron Spectroscopy
XAS	X-ray Absorption Spectroscopy
XMCD	X-ray Magnetic Circular Dichroism
XPS	X-ray Photoelectron Spectroscopy

Chemical compounds

2HTPP	5,10,15,20-tetraphenyl-porphyrin
M	Metal
MOEPCl	M 2,3,7,8,12,13,17,18-octaethyl-porphyrin chloride
MTPPCl	M 5,10,15,20-tetraphenyl-porphyrin chloride
MTTBPPCl	M tetrakis(3,5-di-tert-butylphenyl)-porphyrin chloride
MPc	M-phthalocyanine
MFPc	M 1,2,3,4,8,9,10,11,15,16,17,18,22,23,24,25-hexadecafluoro-Pc
NH_3	Ammonia
TM	Transition Metal

1 Introduction

1.1 Motivation and outline

Even though, or perhaps *because*, we live in a three-dimensional world, our physical interaction with the surroundings is mostly two-dimensional, i.e. occurs via surfaces. We walk on the surface of the earth, touch the surface of a warm coffee cup and use the surface of a desk as a working space. It was therefore natural that mankind started to exploit surfaces very early. They were, for example, used to store information, also in the form of art – e.g. as cave paintings or on papyrus.[1,2] In the 21st century we still save data on surfaces, even though the way we do it became much more sophisticated. Apart from writing on paper we use magnetic, electronic or optical properties of interfaces to store information – in magnetic hard drives, solid-state drives and optical drives, respectively.[3–5] We also have greatly increased the amount of data that can be stored per unit area; as an example, modern magnetic hard drives can save above 1 Tbit per square inch,[6] roughly 10 orders of magnitude more than hand-written text. The design and the large available surface area in all these technologies allows information to be stored and retrieved in a 'random-access' manner.

Beyond data storage, mankind also learned to exploit surface-specific properties like the adsorption of contaminants in filters and the surface-specific reactivity as found in heterogeneous catalysis.[7] This field of science attracted four Nobel prizes (for F. Haber and C. Bosch, I. Langmuir as well as Gerhart Ertl). Three of these four awards were given for the discovery, development and elucidation of the so-called Haber-Bosch process of synthesizing ammonia, mainly used in the production of fertilizers. This process has been termed the "detonator of the population explosion" and the most important invention of the 20th century, as it allowed for the world's population to grow from 1.6 billion at the beginning of the 20th

century to more than 7 billion today due to its impact on agriculture.[8] It is estimated that ammonia production by the Haber-Bosch process consumes more than 1% of the world's total energy supply.[9]

These examples of surface science and their role for society pose two important questions: **(i)** how can we modify surfaces to allow for new reactions and make existing ones more efficient, as well as **(ii)** what can represent the smallest addressable, surface-supported bit of information and how can they be manipulated. This thesis tackles the task of answering these questions by studying on-surface chemistry and magnetism. Chemical reactions, which are dynamic in their nature, and magnetism, which is more commonly encountered in static applications, might seem like two completely independent phenomena, but in reality they are closely related, as they both result from the interactions between valence electrons of neighbouring atoms and molecules. In addition, as shown in this thesis, they can work in tandem to shape structures of extraordinary properties. There are many degrees of freedom in the design and tunability of these systems, as provided by the unique approach of on-surface supramolecular engineering, combining self-assembly, surface chemistry and magnetism.

Designing functional systems with interesting properties has been successfully employed in metal-organic interfaces, weaving together the advantages of both organic and inorganic worlds. Most notably, porphyrins and phthalocyanines on metallic surfaces have become a vivid area of interest with many different phenomena studied, and each being able to extend the already large amount of porphyrin-based applications.[10–12] These on-surface phenomena include, but are not limited to (i) site-selective orbital doping,[13] (ii) self-metalation,[14,15] (iii) single-molecule rotation,[16] (iv) conductance switching via tautomerization,[17] (v) creation of catalytic 2D MOFs,[18] (vi) conformational switching[19] as well as (vii) magnetic switching.[20] The list is extensive because an appropriate substrate can be chosen and the molecules can be functionalised in many different ways, e.g. by ligands or by exchanging the metal centre.

Choosing the appropriate substrate, however, does not always yield the expected results. Due to the very finite nature of the periodic table of elements it is desirable to customize the native metallic surfaces. This brings us back to the question **(i)**, *i.e.* how to modify a surface in order to

control its physicochemical properties. The first part of this thesis (**chapter 2.1**) aims at answering this question by showing that simple surface functionalization can tune the chemical activation energy and reaction pathways. On-surface metalation reactions of free-base tetraphenyl porphyrins (2HTPP) on differently functionalized Cu(001) surfaces have been investigated and compared to the corresponding reaction proceeding on the native, non-functionalized surface. The surface functionalization involves atomically thin layers of adsorbates, namely O, N and Cl, exhibiting distinct and contrasting influences on the self-metalation reaction. Oxygen adlayer facilitates the metalation reaction to occur at a temperature ~150 K lower than on native Cu(001); nitrogen adlayer partially facilitates the reaction (*i.e.* with ~50 % reaction yield) while the Cl adlayer inhibits metalation up to the temperature of molecular desorption. In order to metalate the 2HTPP molecules adsorbed on the Cl-covered surface, metal atoms were deposited from the top, which resulted in an interesting two-step reaction mechanism; at room temperature a transition compound was created and only at elevated temperatures the final reaction product, CuTPP, was obtained. Moreover, it is shown that the adsorbate-induced surface modifications have a clear impact on the assembly of molecules; strong adsorption on bare Cu(001) significantly hinders molecular diffusion, O and N adsorbates surfaces facilitate diffusion and self-assembly while Cl causes molecules to assemble in small clusters that do not follow classical Poisson distribution. This study aids to elucidate the mechanism of on-surface self-metalation and shows how differently reactions on a surface can proceed when compared to the case in solution or in a gas phase.

This approach additionally suggests a method of “building up” metal-organic interfaces where molecules of desired properties might be synthesized directly on the surface by enhancing not only the reactivity of the interfaces, but also by allowing reactants to encounter each other by facilitating molecular diffusion. Therefore, perhaps surprisingly, the results from chapter 2.1 help to answer the question **(ii)** that can be re-phrased to: What is the ultimate size-limit of an easily-controllable, surface-supported magnetic information bit and how can we engineer it. As a simple example, by this approach Mn(II)TPP molecules could be synthesised on a surface, while they are not available in bulk due to their low stability. Only Mn(III)TPPCl is stable and commercially available.

Molecules, however, are clearly not the smallest objects that can possess spin, as already single atoms do. In order to discuss the difference between the magnetic properties of ad-atoms and ad-molecules, **chapter 2.2** presents a study of single transition metal atoms adsorbed on a Bi(111) substrate. Interestingly on this substrate Cr and Fe atoms exhibit out-of-plane magnetic anisotropy, which in Cr reaches the theoretically possible physical limit.

While single atoms provide the ultimate limit of single-spin systems and single surface-supported Ho atoms have recently been shown to exhibit magnetic remanence,[21] there are still many difficulties with this approach. Apart from the fact that these atoms have to be separated from each other and there is no easy and scalable way to achieve that, an atom also cannot be functionalized. Therefore inserting a single paramagnetic metal atom into molecules like porphyrins and phthalocyanines largely extends the range of spin systems to be investigated at surfaces. A molecule can be viewed at a first sight as a *"cage"*, as it creates a natural spacer between the magnetic atoms and allows for the up-scaling of ordered 2D domains by on-surface self-assembly. Notably, molecules also change the physicochemical properties of the inserted atom and modify its interaction with the substrate, allowing for an impressive level of tunability.

A seemingly simple method of changing the properties of surface-supported magnetic entities would be to modify the strength of the interaction with the substrate, for example by varying the substrate-adsorbate separation. This is close to impossible for atoms as we can barely control their adsorption site, but becomes straightforward when considering a molecule. **Chapter 2.3** reveals a method of manipulating the magnetic properties of metal-organic interfaces consisting of paramagnetic molecules adsorbed on ferromagnetic substrates, by simply varying the substrate-molecule distance. By using molecular substituents of different sizes we in turn control the magnetic exchange coupling strength. Specifically, three different Mn-based porphyrins adsorbed on Co and O-covered Co were studied – ligated with eight ethyl groups (MnOEPCl), four phenyl groups (MnTPPCl) or four di-tert-butylphenyl groups (MnTTBPPCl). The substrate-molecule distance varied between ~0.2 nm and ~0.5 nm and this way the magnetic exchange coupling energy was tuned between 30 meV and 80 meV. On the

bare Co substrate, where molecules adsorb strongly, the coupling strength changed monotonously between the three molecules. Interestingly, the changes in coupling energy are not as straightforward in the case of O-covered Co where molecules self-assemble, which suggests that molecular flexure can compensate the effect induced by ligands.

Molecular diffusion is a prerequisite to self-assembly. On-surface studies focused mostly on the diffusion of adsorbers along step edges and across the surface plane. Not as much attention, however, has been brought to out-of-plane rearrangement in molecular multilayers, because its investigation is not nearly as straightforward. Notably, inter-layer rearrangement effects were studied before in the case of delta-doped interfaces, i.e. thin layers of dopant atoms buried between thicker layers of a semiconductor. Inter-layer mixing of atoms in such interfaces was shown to significantly influence the performance of semiconductor devices.[22,23] Similar rearrangement of layers on a molecular scale could show an impact on the performance of thin films in future applications. In **chapter 2.4** a spectroscopic method of studying vertical molecular rearrangement on ferromagnetic substrates is proposed. XMCD is used to study bilayers consisting of two molecules with different metal centres (FePc and MnPc) and determine which molecule is in contact with a ferromagnetic O/Co substrate. An interesting vertical rearrangement of the bilayers is observed, with MnPc driving FePc away from the substrate.

An aim of this thesis is to show how closely related chemistry and magnetism are, and how they can influence each other. In the last result chapter, an extraordinary approach is shown in which chemistry, magnetism and surface science can be used together in order to create layers with properties unattainable in any other way than this supramolecular engineering. In **Chapter 2.5** the creation of novel 2D magnetic structures by co-deposition of different molecular building blocks is shown. The molecules used were two different phthalocyanines – MnPc and perfluorinated FeFPc, in which peripheral hydrogen atoms were substituted by fluorine. This resulted in the creation of a chessboard-like supramolecular assembly with alternating Mn-Fe metal centres, directed by C-H ··· F hydrogen bonds. Such an on-surface assembly exhibits fascinating magnetic properties depending on the underlying substrate. On Ag(111) it behaves

as a bimetallic, paramagnetic layer; when adsorbed on Au(111), it creates a 2D lattice exhibiting long-range ferrimagnetic order caused by intermolecular coupling mediated via the Au(111) surface electrons. On O-functionalized ferromagnetic Co(001) substrate on the other hand it serves as a magnetic array that can be selectively and reversibly controlled by chemical ligation.

1.2 Methods

The following section provides an overview of the preparatory as well as analytical techniques used in this thesis. In the presented studies a spectro-microscopy correlation approach was employed, combining both spatially-averaging and local-probe techniques. Scanning Tunnelling Microscopy and Low Energy Electron Diffraction were used to obtain structural information about the studied interfaces. Chemical composition of samples as well as evolution of chemical reactions was investigated using X-ray Photoelectron Spectroscopy. Ultraviolet Photoelectron Spectroscopy provided information about the electronic properties of studied systems. Magnetic properties, on the other hand, were elucidated with X-ray Magnetic Circular Dichroism and Scanning Tunnelling Spectroscopy.

Sample preparation

Single crystals of Cu(001), Ag(111) and Au(111) were cleaned by cycles of Ar^+ sputtering at ion energy of 2 keV and subsequent annealing to 600^{o}C. The Cu substrate modifications were performed on a clean Cu single crystal kept at 150^{o}C: O/Cu was obtained by dosing 2000 L of O_2 over 1000 s; N/Cu by sputtering with N^+ ions (E=500 eV) while Cl/Cu was prepared by depositing $CuCl_2$. All of the used molecules were deposited from a home-built Kundsen cell; the rate of deposition was monitored with a Quartz Crystal Micro-Balance (QCMB).

Ferromagnetic Co(001) substrate was prepared by depositing a 20 ML thick film on top of a Cu(001) single crystal. The deposition was performed in two steps: first 10 ML were deposited onto a crystal held at room temperature, followed by annealing to 150^{o}C and deposition of another 10 ML on the surface kept at this temperature. For O/Co, 20 L of O_2 were dosed onto the sample before the second Co deposition step.

The Si(111) substrate was cleaned by direct-current heating; after cooling down the substrate to 150 K, 60 MLs of Bi were deposited. The Fe and Cr atoms were deposited on the substrate kept at ~15 K in order to prevent clustering.

X-ray Photoelectron Spectroscopy (XPS)

In XPS the sample is irradiated with monochromatic x-ray light and it results in the emission of core electrons due to the photoelectric effect. These electrons are captured by an electron energy analyser, and the number of counted electrons is plotted vs. the electron energy. Each element in the periodic table leaves its specific fingerprint in such measured spectrum, which allows for a quantitative determination of the sample composition. Moreover, the signatures of each element shift in energy based on its chemical state and environment, and therefore make it possible to study the evolution of chemical reactions. Since XPS does not inherently require a tuneable x-ray source, it can be measured not only using a synchrotron, but also with radiation emitted from an x-ray tube. Very good introduction to XPS is provided in Refs. [24,25].

Ultraviolet Photoelectron Spectroscopy (UPS)

The fundamental phenomenon behind UPS is the same as in the case of XPS – it investigates the electrons emitted from the sample due to the photoelectric effect. The difference lies in the energy of used electromagnetic radiation. While in XPS, x-rays cause emission of electrons from core electronic levels, UPS utilizes ultraviolet light, which results in emission from valence energy levels. It allows electronic structure of solids and small molecules to be studied. In this thesis it is used mainly to determine the interface charge reorganization induced by different surface modifications; it is achieved by measuring the changes in work function. More details about UPS on solids can be found in Ref. [26], while in-depth information on the use of this technique at metal-organic interfaces is available in Refs. [27,28].

X-ray Magnetic Circular Dichroism (XMCD)

XMCD is an extension of the synchrotron-based X-Ray Absorption Spectroscopy (XAS) technique. In this method the sample is irradiated with circularly polarized light of tuneable energy. It takes advantage of the fact that, due to the angular momentum conservation

principle, exposure to circularly polarized light results in preferential excitation of spin-up or spin-down electrons. Each set of data requires acquiring two spectra – one obtained with left- and one with right-handed circularly polarized light. Then the difference of the two is taken, and the result of subtraction provides a vast amount of information about the magnetic properties of the sample. Most importantly, due to the fact that the absorption edge is at a different energy for each element, it is an element-specific technique. Additionally, owing to XMCD sum rules, it allows to quantify both the spin and the orbital magnetic moment separately.

While XMCD is not intrinsically a surface-sensitive technique, it can be if the total electron yield (TEY) is measured. In the TEY mode current flowing due to electrons being emitted from the sample are measured; these electrons have the mean-free path in the order of 1 nm, and therefore only absorption close to the surface is detected. More information about the XMCD technique can be found in Ref. [29]

Scanning Tunnelling Microscopy (STM)

STM technique is based on the phenomenon of quantum tunnelling, where a particle can pass through a barrier higher than its energy. In this local imaging technique an atomically sharp, metallic tip is used to scan over the sample's surface at an extremely close distance. A bias voltage applied between the tip and the sample results in a small current flow though the vacuum with this current depending exponentially on the tip-sample distance. In the most commonly used STM measurement mode, the tunnelling current is kept constant by a feedback loop. The extremely precise movement of the piezoelectric scanner reflects the convoluted information about the topography and the local density of states of the sample. Additionally, STM allows for studying the occupied and the unoccupied electronic states of the sample, depending on the direction of the current flow. An introduction to the STM can be found in the Ref. [30].

Scanning Tunnelling Spectroscopy (STS)

In the STS technique an STM tip is placed over the studied object and a bias voltage is swept in the desired range; during this procedure the tunnelling current is recorded. In modern scanning tunnelling microscopes the dI/dV derivative is directly recorded using a lock-in amplifier and it provides information about the electronic density of states in the sample as a function of electron energy. In this thesis STS was mainly used to study the Kondo effect, *i.e.* the screening of spin impurities by conduction electrons. It evidences itself in STS as a feature near zero bias voltage. More details are provided in Refs. [30,31].

Low Energy Electron DIffration (LEED)

In LEED low energy electrons (typically in the range of 20-300 eV) are diffracted from the sample and observed on a fluorescent screen. The pattern created by the diffracted electrons corresponds to the reciprocal space of the sample. It allows gaining information not only about the geometry of the studied surface, but also about the interatomic distances. In this thesis LEED was mainly used to determine the structure and symmetry of surface reconstructions and superstructures. In-depth description of this technique can be found in Ref. [32].

2 Results

2.1 Studying the influence of surface modifications on substrate's reactivity by porphyrin metalation

2.1.1 Porphyrin metalation providing an example of a redox reaction facilitated by a surface reconstruction

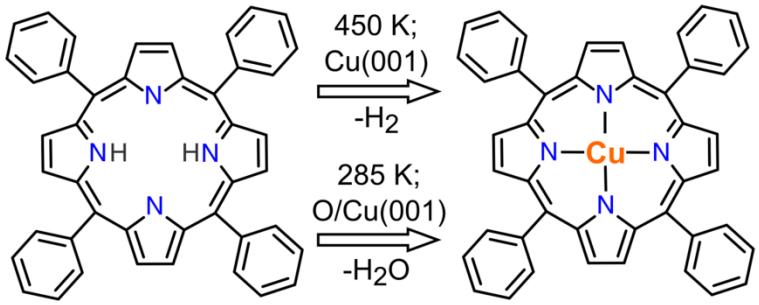

Summary: Here we demonstrate the decisive impact of an adsorbate-induced surface reconstruction on the self-metalation reaction of 2HTPP with the Cu atoms from the substrate. The reaction requires an elevated temperature of 450 K to proceed on bare Cu(001), while it occurs below room temperature on an O-reconstructed Cu(001). This lower activation energy of self-metalation on the O-reconstructed surface is attributed to the lower enthalpy of formation of H_2O, released during metalation on O/Cu(001), compared to H_2, which is formed during metalation on bare Cu(001).

ChemComm

RSC Publishing

COMMUNICATION

View Article Online
View Journal | View Issue

Porphyrin metalation providing an example of a redox reaction facilitated by a surface reconstruction†

Cite this: *Chem. Commun.*, 2013, **49**, 2347

Received 21st December 2012,
Accepted 4th February 2013

DOI: 10.1039/c3cc39134e

www.rsc.org/chemcomm

Jan Nowakowski,[a] Christian Wäckerlin,[a] Jan Girovsky,[a] Dorota Siewert,[a] Thomas A. Jung*[a] and Nirmalya Ballav*[b]

The presence of an oxygen reconstruction on the Cu(001) surface results in the self-metalation of 5,10,15,20-tetraphenylporphyrin (2HTPP) below room temperature (at ~285 K), in contrast to 2HTPP on the bare Cu(001) substrate, where a temperature of ~450 K is required. This study demonstrates the decisive impact of a surface reconstruction on the redox reaction in the solvent-free ultra-high vacuum environment.

On-surface reactions in general,[1] as well as on-surface redox chemistry[2] have gained significant attention in recent years. An important example of the latter is provided by the on-surface metalation of organic macrocycles, *e.g.*, 2HTPP.[3] For a surface-supported molecule under ultra-high vacuum (UHV) the metalation is usually realized in one of three ways: (i) by coordination with free metal atoms after their deposition onto a layer of 2*H*-porphyrin,[3a,b,d,f,h] (ii) by coordination of previously deposited hetero-adatoms (*e.g.* Zn on Ag(111))[3b,d,f,h] and (iii) by self-metalation, *i.e.* by coordination with atoms of the substrate, *e.g.*, on Cu(111).[3c,g,i,j] Very recently room-temperature (RT) self-metalation of 2HTPP has been achieved for the highly reactive Fe(110) and Ni(111) surfaces.[4] On the Cu(111) substrate, however, a significantly higher temperature to induce 2HTPP metalation is required.[3c,g,i,j]

Surface reconstructions are formed by the reorganisation of interacting ad-surface species and the topmost surface layers and often have decisive impact on metal-epitaxy.[5] Here we investigate their influence on on-surface redox reactions, in particular on the self-metalation of 2HTPP in a solvent-free UHV environment. We employ X-ray photoelectron spectroscopy (XPS) and scanning tunneling microscopy (STM) to present coherent evidence that the presence of a $(\sqrt{2} \times 2\sqrt{2})R45^\circ$ oxygen reconstruction[5a,b] on Cu(001) significantly lowers the temperature required for the metalation of 2HTPP from ~450 K (for atomically clean Cu(001)) to ~285 K. XPS provides particularly strong evidence towards metalation, since the precursor (2HTPP) consists of two different nitrogen species, whereas the product (Cu(II)TPP) contains only one, as depicted in Fig. 1a. STM data of the native and oxygen-reconstructed substrates are shown in Fig. 1b and c.

The two peaks observed in the XP spectra of N1s core levels of both 2HTPP/Cu(001) and 2HTPP/O/Cu(001) (Fig. 2a and c, bottom spectra) are characteristic of metal-free porphyrins.[3a] For 2HTPP/O/Cu (Fig. 2c), binding energies of 399.9 eV for pyrrolic (–NH–) and 397.9 eV for iminic (=N–) N1s are observed at 100 K.[3a,b,d,6] The binding energy of the iminic nitrogens is similar to the value obtained on Au(111) and Ag(111) substrates.[3c] This indicates little interaction between the molecules

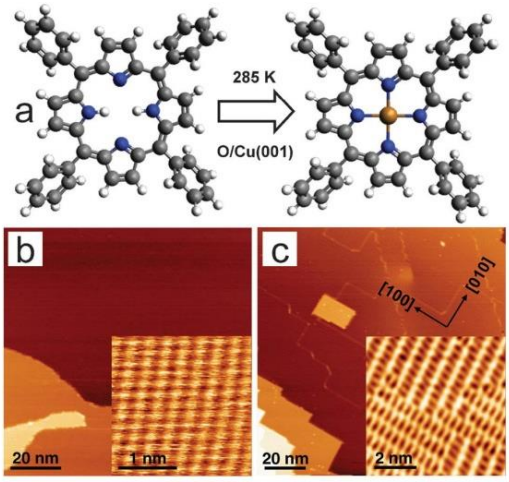

Fig. 1 (a) The chemical structure of 2HTPP (left) and CuTPP (right). The arrow between the models represents the observed reaction on the O/Cu(001) substrate at 285 K. (b, c) Constant-current STM images of the atomically clean Cu(001) and of the oxygen-$(\sqrt{2} \times 2\sqrt{2})R45^\circ$ reconstructed Cu(001) surfaces, respectively. The oxygen atoms are imaged as dark spots.

[a] *Laboratory for Micro- and Nanotechnology, Paul Scherrer Institute, 5232 Villigen, Switzerland. E-mail: thomas.jung@psi.ch; Fax: +41-56-310-2646; Tel: +41-56-310-4518*

[b] *Department of Chemistry, Indian Institute of Science Education and Research, Pune 411008, India. E-mail: nballav@iiserpune.ac.in; Fax: +91-20-2588-9790; Tel: +91-20-2590-8215*

† Electronic supplementary information (ESI) available: Sample preparation, STM/XPS data and general experimental conditions including STM tunneling parameters. See DOI: 10.1039/c3cc39134e

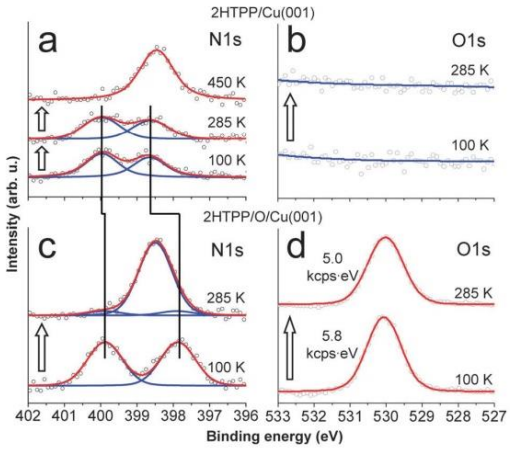

Fig. 2 XPS data of 2HTPP deposited on (a, b) Cu(001) and (c, d) oxygen-reconstructed Cu(001) substrates. (a) N1s spectra of 2HTPP on the native Cu(001) substrate demonstrating no chemical change in the molecules after heating up from 100 K to 285 K. Molecules metalate significantly above room temperature (~450 K). (b) O1s spectra of molecules on native Cu(001) showing the absence of oxygen on the surface. (c) N1s spectra of molecules on O/Cu(001). Two peaks at 100 K indicate nonmetalated molecules, while the single peak at 285 K implies transformation to CuTPP. (d) O1s spectra of the same sample showing a loss of oxygen at 285 K.

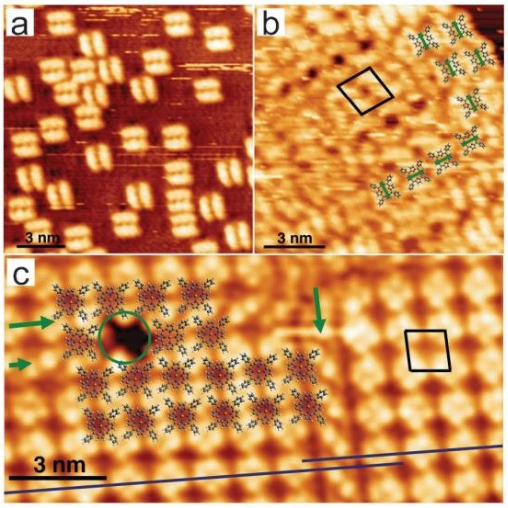

Fig. 3 Constant current STM images of (a) ~0.4 ML of 2HTPP on Cu(001) at RT. Bias voltage used to obtain the image was equal to V_b = 0.83 V; (b) ~1 ML of 2HTPP on O/Cu(001) at ~160 K, V_b = 2.22 V. Green lines connect the iminic nitrogens in the molecular models superimposed on the image. (c) The STM data for 2HTPP on O/Cu(001) after warming up to RT, V_b = 2.15 V. A vacancy defect (green circle) allows for the unambiguous determination of the adsorption geometry. In the image phase-shift boundaries can be identified (green arrows). They are most probably caused by the two domains of O-reconstruction rotated to each other by 90° (*cf.* the inset in Fig. 1c). Displacement of the molecules in the neighboring phases is marked by dark-blue lines. The unit cells of molecules before (b) and after (c) metalation (black squares) have the same, within the measurement error, lattice constant of ~1.3 nm. They are rotated by 30° with respect to each other because two different mirror domains are shown. For evidence that differences in scanning parameters (bias voltage, temperature) do not influence the conclusions *cf.* Fig. S2 and S3 (ESI†).

and the O/Cu(001) surface. In the case of 2HTPP/Cu(001), however, the binding energy of iminic N1s is 0.7 eV higher than that on O/Cu(001), while that of the pyrrolic N1s is virtually the same. Similar results have been found for free-base porphyrins on Cu(111), where it has been assigned to the interaction between the iminic nitrogens of the molecule and the Cu atoms of the substrate.[3c,6b] This is possible through the considerable flexibility of the porphyrin macrocycle, allowing for deformation into a so-called saddle-shape conformation with the imine groups pointing towards the substrate.[3e,7]

Heating up 2HTPP/Cu(001), *i.e.* in the absence of the oxygen reconstruction (*cf.* Fig. 2b), to 285 K has no effect on the N1s spectrum, indicating no metalation. However, annealing to ~450 K resulted in a single N1s peak at 398.5 eV, as expected for MTPP, where all four nitrogens are equivalent.[3] Note that our metalation temperature is in line with results obtained for the Cu(111) substrate, and that the N1s binding energy agrees well with values reported earlier.[3c,g,i,j]

For 2HTPP/O/Cu(001), in contrast, the self-metalation occurs at ~285 K, as evidenced by the single N1s peak at 398.5 eV in the upper spectrum of Fig. 2c. The metalation process is accompanied by a decrease in the oxygen amount in the sample by ~12.4% (*cf.* Fig. 2d), while concentrations of other elements did not change significantly (*cf.* Table S2, ESI†). One full monolayer (ML) of 2HTPP on O/Cu(001) contains ~6 times less porphyrin molecules than oxygen atoms, thus one would expect a ~16.7% decrease in the oxygen amount after the release of one O atom per metalated porphyrin. Therefore, we tentatively assign this reduction to the formation and release of one H_2O molecule per metalated porphyrin (one oxygen atom from the oxygen reconstruction and two hydrogen atoms from 2HTPP). Our findings are supported by similar results obtained from solution chemistry, where the metalation of *meso*-tetra(*p*-sulphophenyl) porphine has been reported to be facilitated by the presence of O_2.[8] The most probable side product of this reaction was identified to be H_2O.

On the basis of our STM data, we can conclude that 2HTPP does not freely diffuse at RT on the Cu(001) surface – the molecules do not create extended self-assembled domains, but are randomly distributed over the whole sample area (*cf.* Fig. 3a). For a similar system, 2HTPP on Cu(111), a relatively high diffusion barrier has been found and attributed to strong coordinative bonds between the iminic N atoms of 2HTPP and Cu atoms of the substrate.[3c] Our XPS data (*cf.* Fig. 2a and c), for 2HTPP on Cu(001) (*cf.* Fig. 2a) also supports such a mechanism as a possible cause of the immobilisation observed in STM. STM data for 2HTPP/O/Cu(001) (Fig. 3b and c), in contrast, show self-assembly evidencing diffusion after deposition of the molecules. Due to the change in binding energy of iminic N of 2HTPP on O/Cu(001) compared to bare Cu(001) (*cf.* Fig. 2a and c) we assign this lowered diffusion barrier to the O layer reducing the chemisorptive interaction between the Cu substrate and the iminic N atoms of 2HTPP.

The 2HTPP molecules on Cu(001) at RT are imaged in the saddle-shape conformation, *i.e.* exhibit two-fold symmetry

(*cf.* Fig. 3a), which is in line with the results obtained on Cu(111).[3g] 2HTPP molecules on O/Cu(001) at ~160 K are also observed in a saddle-shape conformation (Fig. 3b), even though their interaction with this substrate is evidenced to be lower here (XPS: Fig. 2a *vs.* c and STM Fig. 3) than on Cu(001). A significant transformation in the appearance of 2HTPP on O/Cu(001) is observed after warming up to RT (Fig. 3c). The molecules are now in a flat conformation and appear as four-leaf clovers, *i.e.* four-fold symmetric. This change is a sign of the metal-incorporation reducing the conformational flexibility of the porphyrin.[3g]

There is an important difference in the energetics of the self-metalation on metal and on oxygen-reconstructed metal. The first reaction is reported to release H_2 (*cf.* the mass spectrometry data for the metalation of 2DTPP)[3d] while our XPS data evidence loss of oxygen, which suggests H_2O liberation. Comparison of the formation enthalpies of the self-metalation on a Cu substrate (Cu + 2HTPP → CuTPP + H_2) with our proposed mechanism (Cu_2O + 2HTPP → Cu + CuTPP + H_2O) demonstrates that the latter involving the consumption of Cu_2O and the formation of H_2O is energetically favourable by ~73 kJ mol^{-1}. Note that this estimate is based on the formation energy of Cu_2O in order to mimic the unknown formation energy of the oxygen reconstruction.

One may argue that for a mechanistic understanding of the lowered temperature of metalation the structure of the oxygen-reconstructed Cu(001) should be considered. Several arguments, however, suggest that structural details are not decisive for this reaction: (i) on bare copper the temperature required for self-metallation does not significantly depend on the index of the surface (Cu(001) *vs.* Cu(111), *cf.* Fig. 2a and ref. 3*c*, *g*, *i* and *j*); (ii) co-deposition of 2HTPP and Cu atoms onto Au(111) also does not result in metalation at RT;[3g] (iii) we find that the metalation of 2HTPP does not proceed on Ni/Cu(001) at RT, while 2HTPP on O-c(2 × 2)-reconstructed Ni on Cu(001) is found to be fully metalated at RT (*cf.* Fig. S1, ESI†). These considerations suggest that the lowered temperature for metalation is determined by the chemical reactivity of the oxygen reconstruction, not by the structural changes it evokes.

The inclusion of the metal atom into the porphyrin involves its dehydrogenation. Shubina *et al.*[3d] identified the transfer of the hydrogen from a pyrrolic nitrogen to the metal as the rate-limiting step in the metalation. They determined, using *in vacuo* calculations, that the intermediate state before the dehydrogenation, where the iminic nitrogens exhibit a significant interaction with metal from the substrate (Fig. 2a), is accessible without barrier. A possible mechanism of self-metalation on the oxygen-reconstructed surface could involve an intermediate state containing an O–Cu dimer in the porphyrin, from where the reaction proceeds by the transfer of hydrogen to the oxygen atom. The bending of the porphyrin plane and the specific dynamics of the oxygen reconstruction, as studied in the context of surfactant mediated growth,[5b,c] may contribute to facilitate the reaction.

In summary, we have shown that the presence of a surface reconstruction significantly facilitates the on-surface self-metalation of 2HTPP. This observation is not limited to O/Cu(001): our experiments on O-c(2 × 2)-Ni/Cu(001) demonstrate that a surface reconstruction can critically affect the required reaction conditions. Our approach opens up a new field of research concerned with the exploration of surface reconstructions in the context of on-surface chemistry.

This work was financially supported by the Swiss National Science Foundation (SNSF), the National Center of Competence in Research (NCCR-Nano) and the Holcim Foundation for the Advancement of Scientific Research Switzerland. The authors thank R. Schelldorfer for technical support. J. N. thanks R. Czajka (Poznan University of Technology) for support during this work and S. Nowakowska (University of Basel) for valuable comments. N. B. thanks K. N. Ganesh (IISER Pune) for support during this work.

Notes and references

1 (*a*) G. A. Somorjai and Y. Li, *Proc. Natl. Acad. Sci. U. S. A.*, 2010, **108**, 917; (*b*) C. Diaz, E. Pijper, R. A. Olsen, H. F. Busnengo, D. J. Auerbach and G. J. Kroes, *Science*, 2009, **326**, 832; (*c*) K. R. Harikumar, J. C. Polanyi, A. Zabet-Khosousi, P. Czekala, H. Lin and W. A. Hofer, *Nat. Chem.*, 2011, **3**, 400.

2 (*a*) D.-T. Pham, K. Gentz, C. Zörlein, N. T. M. Hai, S.-L. Tsay, B. Kirchner, S. Kossmann, K. Wandelt and P. Broekmann, *New J. Chem.*, 2006, **30**, 1439; (*b*) C. Wäckerlin, C. Iacovita, D. Chylarecka, P. Fesser, T. A. Jung and N. Ballav, *Chem. Commun.*, 2011, **47**, 9146; (*c*) K. B. Holt, *Phys. Chem. Chem. Phys.*, 2010, **12**, 2048; (*d*) D. Skomski, S. Abb and S. L. Tait, *J. Am. Chem. Soc.*, 2012, **134**, 14165; (*e*) T21. B. Liu, A. Blaszczyk, M. Mayor and T. Wandlowski, *ACS Nano*, 2011, **5**, 5662.

3 (*a*) J. M. Gottfried, K. Flechtner, A. Kretschmann, T. Lukasczyk and H.-P. Steinrück, *J. Am. Chem. Soc.*, 2006, **128**, 5644; (*b*) A. Kretschmann, M. M. Walz, K. Flechtner, H.-P. Steinrück and J. M. Gottfried, *Chem. Commun.*, 2007, 568; (*c*) F. Buchner, J. Xiao, E. Zillner, M. Chen, M. Röckert, S. Ditze, M. Stark, H.-P. Steinrück, J. M. Gottfried and H. Marbach, *J. Phys. Chem. C*, 2011, **115**, 24172; (*d*) T. E. Shubina, H. Marbach, K. Flechtner, A. Kretschmann, N. Jux, F. Buchner, H.-P. Steinrück, T. Clark and J. M. Gottfried, *J. Am. Chem. Soc.*, 2007, **129**, 9476; (*e*) W. Auwärter, A. Weber-Bargioni, S. Brink, A. Riemann, A. Schiffrin, M. Ruben and J. V. Barth, *ChemPhysChem*, 2007, **8**, 250; (*f*) M. Chen, X. Feng, L. Zhang, H. Ju, Q. Xu, J. Zhu, J. M. Gottfried, K. Ibrahim, H. Qian and J. Wang, *J. Phys. Chem. C*, 2010, **114**, 9908; (*g*) J. Xiao, S. Ditze, M. Chen, F. Buchner, M. Stark, M. Drost, H.-P. Steinrück, J. M. Gottfried and H. Marbach, *J. Phys. Chem. C*, 2012, **116**, 12275; (*h*) F. Buchner, K. Flechtner, Y. Bai, E. Zillner, I. Kellner, H.-P. Steinrück, H. Marbach and J. M. Gottfried, *J. Phys. Chem. C*, 2008, **112**, 15458; (*i*) S. Ditze, M. Stark, M. Drost, F. Buchner, H.-P. Steinrück and H. Marbach, *Angew. Chem., Int. Ed.*, 2012, **51**, 10898; (*j*) K. Diller, F. Klappenberger, M. Marschall, K. Hermann, A. Nefedov, C. Wöll and J. V. Barth, *J. Chem. Phys.*, 2012, **136**, 014705.

4 A. Goldoni, C. A. Pignedoli, G. Di Santo, C. Castellarin-Cudia, E. Magnano, F. Bondino, A. Verdini and D. Passerone, *ACS Nano*, 2012, **6**, 10800.

5 (*a*) F. Jensen, F. Besenbacher, E. Laegsgaard and I. Stensgaard, *Phys. Rev. B*, 1990, **42**, 9206; (*b*) X. Liu, T. Iimori, K. Nakatsuji and F. Komori, *Appl. Phys. Lett.*, 2006, **88**, 133102; (*c*) R. Nünthel, T. Gleitsmann, P. Poulopoulos, A. Scherz, J. Lindner, E. Kosubek, C. Litwinski, Z. Li, H. Wende, K. Baberschke, S. Stolbov and T. Rahman, *Surf. Sci.*, 2003, **531**, 53; (*d*) K. Morgenstern, M. Voetz and H. Niehus, *Phys. Rev. B*, 1996, **54**, 17870.

6 (*a*) S. A. Krasnikov, N. N. Sergeeva, M. M. Brzhezinskaya, A. B. Preobrajenski, Y. N. Sergeeva, N. A. Vinogradov, A. A. Cafolla, M. O. Senge and A. S. Vinogradov, *J. Phys.: Condens. Matter*, 2008, **20**, 235207; (*b*) C. M. Doyle, S. A. Krasnikov, N. N. Sergeeva, A. B. Preobrajenski, N. A. Vinogradov, Y. N. Sergeeva, M. O. Senge and A. A. Cafolla, *Chem. Commun.*, 2011, **47**, 12134.

7 W. Auwärter, K. Seufert, F. Klappenberger, J. Reichert, A. Weber-Bargioni, A. Verdini, D. Cvetko, M. Dell'Angela, L. Floreano, A. Cossaro, G. Bavdek, A. Morgante, A. P. Seitsonen and J. V. Barth, *Phys. Rev. B*, 2010, **81**, 245403.

8 O. Herrmann, S. H. Mehdi and A. Corsini, *Can. J. Chem.*, 1978, **56**, 1084.

Supplementary Information

Porphyrin metalation providing an example of a redox reaction facilitated by a surface reconstruction†

Jan Nowakowski,[a] Christian Wäckerlin,[a] Jan Girovsky,[a] Dorota Siewert,[a] Thomas A. Jung*[,a] and Nirmalya Ballav*[,b]

[a] *Laboratory for Micro- and Nanotechnology, Paul Scherrer Institute, 5232 Villigen, Switzerland. Fax: +41-56-310-2646; Tel: +41-56-310-4518; E-mail: thomas.jung@psi.ch*
[b] *Department of Chemistry, Indian Institute of Science Education and Research, Pune 411008, India. Fax: +91-20-2588-9790; Tel: +91-20-2590-8215; E-mail: nballav@iiserpune.ac.in*

Experimental conditions

All experiments have been performed in an ultra-high vacuum (UHV) system with base pressure in the order of 10^{-10} mbar. Cu(001) single crystals were cleaned by Ar^+ sputtering and annealing cycles and their cleanness was confirmed by XPS. The $(\sqrt{2}x2\sqrt{2})R45^o$ O-reconstruction was prepared by dosing 3000 L of O_2 over 1000 s into the vacuum chamber with Cu(001) crystal annealed to ~500 K. 2HTPP molecules (Sigma-Aldrich, ≥ 99% purity) were sublimed onto atomically clean or O-reconstructed Cu(001) substrate kept at ~100 K. Samples were warmed up to RT by switching off the cooling. Rate of evaporation was controlled with a quartz-crystal microbalance. Monochromatised Al Kα line was used for XPS measurements. STM measurements were performed at ~160 K (Fig. 3b) and at RT (Fig. 1c, 1d, 3a and 3c) in constant current mode using electrochemically etched and in situ sputtered tungsten tips. Tunneling parameters used for each figure are given in Tab. S1; positive bias voltage corresponds to tunneling into unoccupied electronic states of the sample. The STM images were processed using WSxM software.[1]

Table S1 Bias voltage and tunneling current used to obtain presented STM images.

Figure	Sample	Bias voltage (V)	Tunneling current (pA)
1c	Cu(001)	-1.31	70
1b (inset)	Cu(001)	-0.034	930
1d	O/Cu(001)	1.03	20
1c (inset)	O/Cu(001)	1.03	10
3a	2HTPP/Cu(001)	0.83	10
3b	2HTPP/O/Cu(001)	2.22	30
3c	2HTPP/O/Cu(001)	2.15	10
S2a	2HTPP/Cu(001)	2.3	10
S2b	2HTPP/Cu(001)	2.1	10
S3a	2HTPP/O/Cu(001)	2.2	20
S3b	2HTPP/O/Cu(001)	2.2	10

Concentration of elements in XP spectra before and after the metalation

Table S2 Concentration of Cu, O, C and N elements before and after metalation showing decrease in the amount of oxygen, while concentrations of other elements did not significantly change.

Element	Cu	O	C	N
Concentration before metalation	87.16	3.06	8.78	1.00
Concentration after metalation	87.49	2.68	8.79	1.03
Change	+0.4%	-12.4%	+0.1%	+3.0%

Metalation of 2HTPP on Ni/Cu(001) and on O/Ni/Cu(001) surfaces

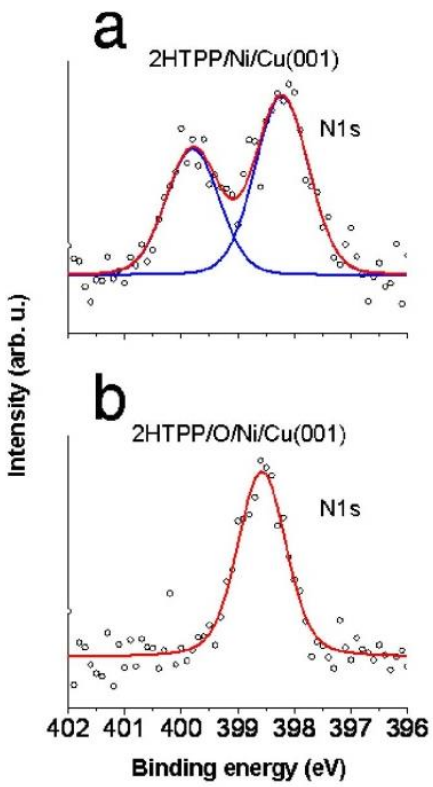

Figure S1 N1s XPS data of 2HTPP put on Ni/Cu(001) and oxygen-reconstructed Ni/Cu(001) substrates. (a) 2HTPP/Ni/Cu(001) at RT; two peaks indicate that molecules did not metalate. (b) 2HTPP/O/Ni/Cu(001) at RT; metalation reaction has been facilitated by the oxygen reconstruction.

Influence of bias voltage and temperature on the appearance of 2HTPP molecules in STM images

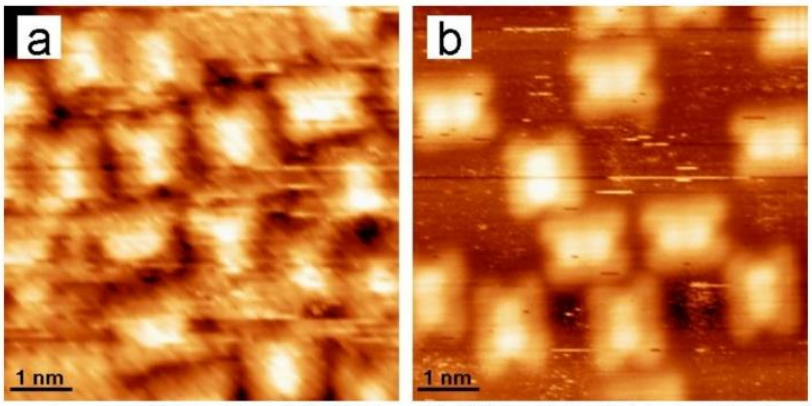

Figure S2 Constant current STM data of 2HTPP on Cu(001) obtained (a) at ~160 K with bias voltage V_b=2.3 V and (b) at RT with V_b=2.1 V. In both cases, not depending on the temperature of the sample or the bias voltage (cf. Fig. 3a), molecules are in saddle shape conformation.

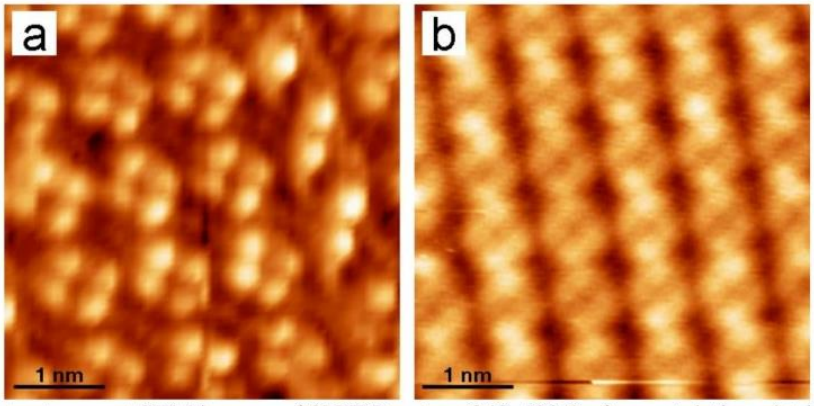

Figure S3 Constant current STM images of 2HTPP put on O/Cu(001) after metalation obtained (a) at ~160 K with V_b=2.2 V and (b) at RT with V_b=2.2 V. The temperature of the sample does not change the conformation of the molecules – in both images molecules appear four-fold symmetric, i.e. are in flat conformation. Please note, that images (a) and (b) were obtained using different scanning directions. They were, however, rotated for the crystallographic directions to match.

Notes and references

[1] I. Horcas, R. Fernández, J. M. Gómez-Rodríguez, J. Colchero, J. Gómez-Herrero, and A. M. Baro, *Rev. of Sci. Instrum.*, 2007, **78**, 013705.

2.1.2 Probing the Reactivity of Functionalized Surfaces by Porphyrin Metalation

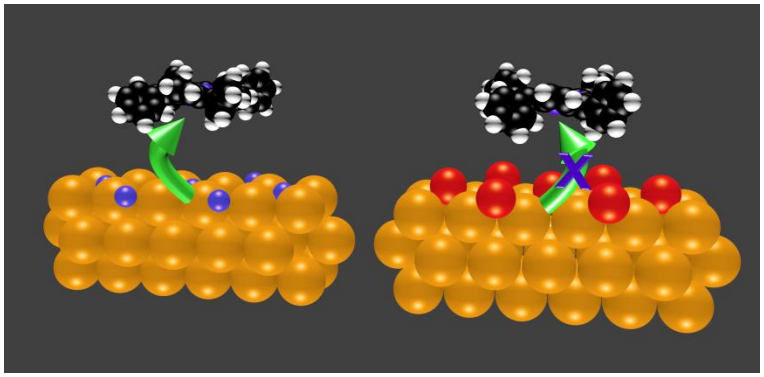

Summary: In this work the change in reactivity of the substrate depending on the adsorbate-induced superstructure is studied by investigating the self-metalation reaction of 2HTPP. The c(2x2) superstructures of N and Cl on Cu(001) are investigated and the results are compared to both bare Cu(001) as well as O-reconstructed Cu(001). The two adsorbates are shown to have drastically different influence on not only the on-surface reaction but also on the molecular assembly. N-induced superstructure is found to facilitate both the molecular diffusion the self-metalation. In contrast, Cl-induced superstructure inhibits the self-metalation reaction completely, requiring metal atoms to be deposited from above in order to overcome the steric hindrance imposed by the system. It also has a very interesting impact on the molecular assembly, namely causes the molecules to create small clusters that do not follow a classical Poisson distribution.

ChemPubSoc Europe

DOI: 10.1002/slct.201600215

Chemistry SELECT Communications

Materials Science inc. Nanomaterials & Polymers

Probing the Reactivity of Functionalized Surfaces by Porphyrin Metalation

Jan Nowakowski,*[a] Sylwia Nowakowska,[b] Gitika Srivastava,[a] Milos Baljozovic,[a] Jan Girovsky,[a] Nirmalya Ballav,*[c] and Thomas A. Jung*[a]

The presence of N- and Cl-induced superstructures is shown to drastically alter the physicochemical properties of the Cu(001) substrate. We present coherent evidence that N- and Cl-c(2x2) superstructures on Cu(001) decisively impact the metalation reaction of 5,10,15,20-tetraphenylporphyrin (2HTPP) as well as the on-surface diffusion and assembly of this molecule. The N superstructure facilitates the metalation reaction and self-assembled molecular domains of CuTPP are formed at room temperature (RT). In contrast, the Cl superstructure completely inhibits the self-metalation reaction requiring metal atoms to be deposited from the top and causes 2HTPP to assemble into small clusters. A spectro-microscopy correlation approach combining X-ray Photoelectron Spectroscopy (XPS), Ultraviolet Photoelectron Spectroscopy (UPS), Low Energy Electron Diffraction (LEED) and Scanning Tunneling Microscopy (STM) has been utilized in this study.

Key to the application-specific design of heterogeneous catalysis and surface reactions, for example in the field of photocatalytic water splitting, is the understanding of site-specific interactions.[1–3] Mechanistic understanding is particularly important for the realization of functional catalytic systems, which can be tuned e.g. by modifying reactants[4] and/or surfaces in order to maximize the energy efficiency. Reactions *at* surfaces, as demonstrated in catalysis,[5,6] or *on* surfaces, e.g. in coordination network formation,[7–10] are often influenced by the availability, the mobility and/or the site-specific reactivity of atoms. All these parameters strongly depend on the physicochemistry of the surface as well as on temperature. Recent studies focused also on single-atom catalysis,[11,12] and the modification of spin-states in surface-supported paramagnetic molecules.[13] Limited research, however, has been performed on the role of adsorbate-induced surface superstructures as they influence on-surface chemical reactions.

In our current work we establish the use of the metalation reaction of porphyrins (Figure 1a) as a probe of the reactivity of functionalized substrates and compare the results with the non-functionalized surface. The functionalization involves atomically thin c(2x2) superstructures of N and Cl, which are formed on Cu(001) (termed as N/Cu and Cl/Cu respectively, Figure 1b,c). The metalation reaction proved to be well suited for this purpose as it has been investigated on a wide range of surfaces[14–25] and it involves the movement of metal atoms in out-of-plane direction from the substrate to the initially metal free porphyrin. The evolution of the metalation can be conveniently assessed by XPS which is sensitive to the chemical environment

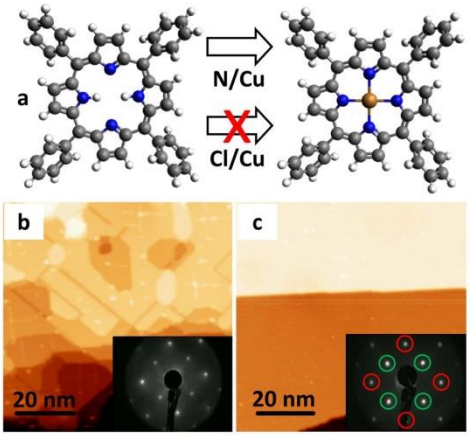

Figure 1. (a) Molecular schemes of 2HTPP (left) and CuTPP (right). The arrows are indicating the metalation reaction, which is facilitated on N/Cu and completely inhibited on Cl/Cu. (b) STM micrograph (I_t = 35 pA, V_s = -1 V) and LEED image (inset) of the N/Cu substrate (c) STM micrograph (I_t = 20 pA, V_s = -1 V) and the corresponding LEED image (inset) of the Cl/Cu substrate. Both presented LEED images were obtained with an electron energy of E = 130 eV. The Cu(001) substrate spots have been marked by red circles, whereas the spots originating from the c(2x2) surface superstructure have been marked with green circles.

[a] *J. Nowakowski, G. Srivastava, M. Baljozovic, J. Girovsky, Prof. Dr. T. A. Jung*
Laboratory for Micro- and Nanotechnology, Paul Scherrer Institute
5232 Villigen PSI (Switzerland)
E-mail: jan.nowakowski@psi.ch
thomas.jung@psi.ch

[b] *S. Nowakowska*
Department of Physics, University of Basel
Klingelbergstrasse 82, 4056 Basel (Switzerland)

[c] *Dr. N. Ballav*
Department of Chemistry, Indian Institute of Science Education and Research (IISER), Pashan, Pune – 411 008 (India)
E-mail: nballav@iiserpune.ac.in

Supporting information for this article is available on the WWW under http://dx.doi.org/10.1002/slct.201600215

of the porphyrin-nitrogen atoms within the precursor, 2HTPP, as well as in the reaction product, i.e. CuTPP.

In Figure 2 N1s and C1s XPS spectra of 2HTPP deposited on N/Cu and Cl/Cu substrates are shown. In both cases, after deposition of the molecules at 100 K two N1s peaks originating from the pyrrolic (–NH–) and the iminic (=N–) nitrogen are observed (both plotted in red), indicating that metalation has not occurred (note that the N1s peak at binding energy (BE) of 396.7 eV plotted in green in Figure 2a arises from the N-superstructure; see Figure S1 for comparison with the clean N/Cu substrate). After warming up the 2HTPP/N/Cu sample to 300 K, the signatures of pyrrolic (399.5 eV) and iminic (397.5 eV) nitrogen atoms (red) decrease in intensity, and a new peak appears at ~398.1 eV (blue). We attribute this transition to the formation of CuTPP. Thus, the N-superstructure on Cu(001) facilitates the metalation reaction, since it only occurs at ~400-450 K on atomically clean Cu(001) and Cu(111) substrates.[20,24,26] In analogy to the reaction of 2HTPP on O-reconstructed Cu(100) and the consequent release of H_2O,[26] one could expect the metalation on N/Cu to result in NH_2 creation (2 H atoms from 2HTPP and one N from the N/Cu substrate) and subsequently in the N/Cu N1s peak intensity loss of ~4% (after taking the 50% reaction yield into account). This loss of N is in quantitative agreement with the predicted amount, as shown in Figure S2. We did not observe, however, a loss of the total N1s peak intensity, which suggests that the reaction product is still adsorbed on the surface. It is most probably caused by the fact that NH_2 in its less stable monomeric (amidogen) and more stable dimeric (hydrazine) forms are known to adsorb strongly to the Cu surfaces.[27,28]

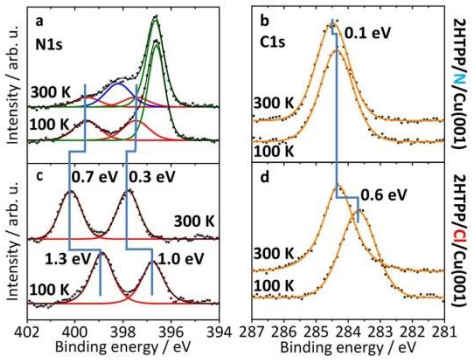

Figure 2. Temperature-dependent N1s and C1s XPS spectra of 1ML 2HTPP molecules deposited (a, b) on N/Cu and (c, d) on Cl/Cu. The N1s spectra are color-coded: Red lines indicate the signal component originating from non-metalated molecules, the blue line shows the spectral response of reacted CuTPP and green lines mark the signal originating from the N/Cu superstructure. (a) On N/Cu, molecules are not metalated after deposition at 100 K, but only after warming up the substrate to 300 K. About 50% of the 2HTPP molecules undergo a reaction to CuTPP as evidenced by the new N1s peak drawn with a blue line, whereas (b) the C1s signature remains virtually unchanged after the reaction. After warming up the substrate to 300 K N1s and C1s peaks of 2HTPP on Cl/Cu shift towards higher BE (c, d). All of the presented XPS spectra have been measured in normal emission.

The presence of the Cl-superstructure has a remarkably different influence on the chemical properties of Cu(001). The BEs of both N1s peaks and the C1s peak originating from 2HTPP after its cold-deposition (T = 100 K) on Cl/Cu (Figure 2c,d) are significantly lower than the respective BEs on N/Cu (Figure 2a,b) or on other substrates including Au(111), Ag(111), Cu(001) and O/Cu(001)[23,26,29] and amount to 398.9 eV, 396.8 eV and 283.7 eV for pyrrolic N1s, iminic N1s and C1s, respectively. We assign these uncommon binding energies to the presence of a much stronger Cl/Cu negative surface dipole as compared to N/Cu (cf. Figure S3); more detailed experimental and theoretical studies of these surface modifications can be found in the literature.[30–35] After warming up the sample to 300 K, a large shift of all three signatures towards higher BE is observed, specifically: the pyrrolic N1s is shifted by +1.3 eV to 400.2 eV, the iminic N1s peak is shifted by +1.0 eV to 397.8 eV and the C1s peak is shifted by +0.6 eV to 284.3 eV. Note that the Cl2p XPS is broadening with increasing temperature (see Figure S6). Interestingly, the Cl-superstructure blocks the metalation reaction (Figure 2c), as revealed by the absence of the N1s peak characteristic for metalated molecules (cf. Figure 2a, blue spectrum). Annealing of the sample to 550 K (i.e. a temperature higher than metalation temperature on bare Cu)[20,24,26] does not lead to metalation and at this temperature the molecules begin to desorb from the substrate, with the remaining molecules residing in an unreacted state (cf. Figure S4, top spectra).

To provide further evidence towards the detailed mechanism of the inhibited metalation on Cl/Cu, we measured XPS after depositing Ni atoms onto H2TPP/Cl/Cu at RT (Figure 3). The N1s spectra (Figure 3a) show that before Ni deposition there are two N1s signatures, about equal in intensity as typical for non-metalated porphyrins (plotted in blue). After depositing Ni and after subsequent annealing two main N1s features remain, but the ratios between their intensities changes significantly, to ~1:3 at 540 K. Such an inequivalency in the N1s intensities has been observed earlier for *metalated* porphyrins in which one of the pyrrole rings has been reduced by Cl.[36] Therefore, we assign this peculiar evolution of the N1s spectra to the changing ratio of two different adsorbed species: (A) An intermediate compound H-bonded to Cl/Cu in which the Ni atom is coordinated by the porphyrin, but without breaking the pyrrolic N–H bonds[23] and (B) the final product of the on-surface reaction with Ni, a NiTPP–Cl complex bound to ad-surface Cl via one of the pyrrole rings.[36] The precursor A is recognized by a characteristic N1s XPS signal at 399 eV and 400.5 eV (plotted in green) while the metalated form B is identified by signals at 398 eV and 400.2 eV (plotted in red). An estimate of the N1s peak intensities indicates a 45:55 ratio of the two compounds after deposition of Ni at RT. The precursor (A) is subsequently converted to the final compound (B) by progressive annealing; at 500 K ~19% of (A) remains and at 540 K no signature of the product (A) is observed. At 570 K ~69% of compound (B) desorbed. This assignment and the multiple stages of the process are further confirmed by identification of the

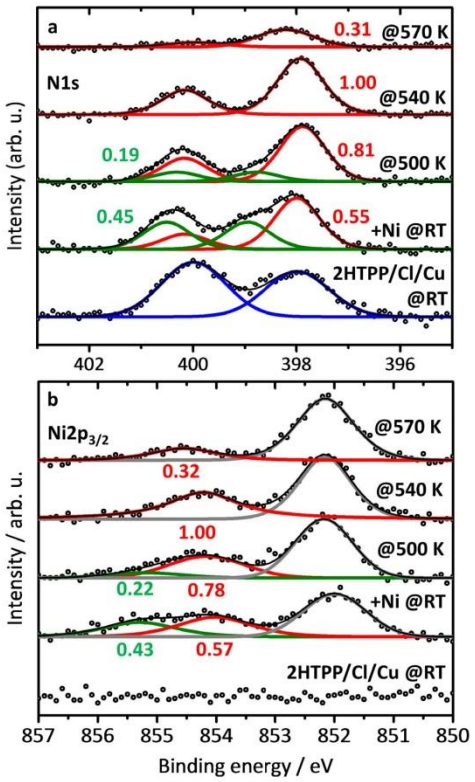

Figure 3. Temperature dependent metalation experiment with Ni atoms sublimed on top of 2HTPP/Cl/Cu - (a) N1s spectra and (b) $Ni2p_{3/2}$ spectra. After Ni deposition at RT two species could be identified both in N1s as well as Ni2p spectra, which we attribute to the intermediate and the final product of the on-surface metalation reaction (green and red lines, respectively). Note that the Ni2p signal at 852 eV (grey) originates from unreacted, excess Ni. Annealing results in full transformation to the final product at 540 K and to desorption of ~70% of the molecules at 570 K. All of the presented XPS spectra have been measured in normal emission.

two different Ni^{II} signatures originating from species A and B (Figure 2b). At room temperature, three Ni species are observed; from compound A (855 eV, green line); from compound B (854 eV, red line) and unreacted Ni^{0} (852 eV, grey line). In nearly perfect agreement with the evolution of the N1s signatures, the Ni2p signatures indicate a ratio of 43:57 between compounds (A) and (B) after deposition of Ni at RT. By annealing to 500 K ~22% of the area of the Ni^{II} signature at 855 eV, attributed to compound (A) remains; after warming up to 540 K the peak attributed to compound (A) disappears completely. Simultaneously the (B) peak at 854 eV nearly doubles in intensity in comparison to the data taken at RT. After warming up to 570 K, when molecular desorption starts, the Ni2p peak at 854 eV reduces to ~31%, again in very good agreement with the N1s spectra. The conforming evolution of $Ni2p_{3/2}$ and N1s peaks upon Ni exposure, metalation and annealing provides strong evidence for the assignment of the precursor and final state of the on-surface reaction in this two-step reaction mechanism.

Therefore, the reason for Cl/Cu blocking in the self-metalation reaction is two-fold: (a) the pyrrolic N atoms of 2HTPP molecules interact strongly with the Cl/Cu via H-bonding and (b) it forces molecules to change the conformation such, that iminic nitrogen atoms point away from the substrate, in contrast to 2HTPP on bare Cu substrates.[14,26] This causes steric hindrance which is overcome when metal atoms are deposited from the top.

We also performed an STM study of the molecular organization on both systems i.e. on ~0.3 ML of 2HTPP deposited on N/Cu (Figure 4a,b) and on Cl/Cu (Figure 4c,d). For better data

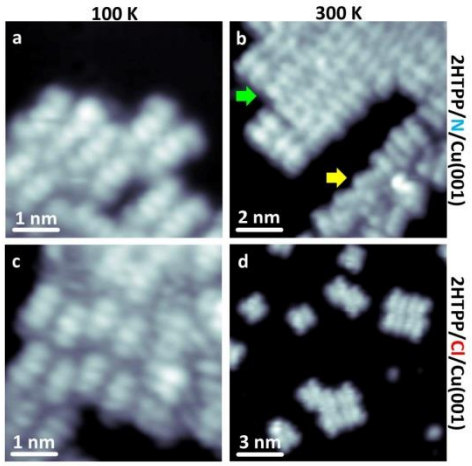

Figure 4. STM data after deposition of 0.3 ML of 2HTPP molecules on (a, b) a N/Cu substrate and on (c, d) a Cl/Cu substrate. The data on both systems have been measured (a, c) after cold deposition of the molecules and (b, d) after warming up of the same sample to 300 K. After cold deposition, molecules on both substrates self-assemble into disordered islands. (b) After warming up, two different appearances of molecules can be distinguished on N/Cu. The first type of molecule is adsorbed on a defect of the reconstruction and resembles two separated rods (yellow arrow). We attribute these molecules to the non-metalated 2HTPP. The second type of molecules, which we assign to metalated CuTPP (green arrow), is adsorbed in ordered self-assembled islands and appears as a letter **H**; we attribute the signature in the center of the molecule as a Cu atom inserted into the porphyrin backbone. (d) After warming up the 2HTPP/Cl/Cu sample to 300 K molecules are not self-assembled in large islands, but create clusters of up to 8 molecules (see Figure S3). Molecular schemes of 2HTPP or CuTPP were imposed on the image to guide the eye. All of the presented micrographs have been measured at 4.2 K in constant current mode with a set point of $I_t = 5$ pA and a sample bias of $V_s = -2.4$ V.

quality, STM measurements were performed at lower molecular coverage than the presented XPS and UPS data. After deposi-

tion of 2HTPP on samples held at 100 K (Figure 4a,c) disordered self-assembled islands were observed on both substrates. It can be seen that 2HTPP adsorbs in a typical saddle-shape conformation[29] on both superstructures. Significant differences between the two superstructures become apparent only after warming up the substrate to 300 K. In the case of N/Cu (Figure 4b), the self-assembled islands became ordered and moreover, molecules adsorb preferentially on the defects of the superstructure, which are also visible in Figure 1b, and are caused by the incommensurability of the N/Cu lattice.[37] Furthermore, there is a difference in the appearance of molecules adsorbed on the defects (yellow arrow) and in ordered self-assembled islands (green arrow). In the former case, molecules resemble two disjoined rods, whereas in the latter they appear like a letter H. We ascribe this new feature in the center of the latter molecules as the inserted Cu atom, and therefore assign the molecules in large islands to CuTPP. In majority of cases molecules change their initial saddle-shape conformation after on-surface metalation,[14,20,26] but a similar H-shape of metalated porphyrins has been observed before.[38] The molecules adsorbed on the defects, on the other hand, we attribute to unreacted 2HTPP. The Cl/Cu superstructure on the other hand has a very contrasting influence on the assembly of molecules in comparison to N/Cu. Remarkably, molecules on this substrate diffuse and self-assemble when cold-deposited (Figure 4c), but adsorb in small clusters after reaching 300 K (Figure 4d). Notably, the size of these clusters does not follow the classical Poisson binomial distribution (c.f. Fig. S7).[39]

The adsorption of the 2HTPP molecules on surfaces like Cu (111) or Cu(001) usually does not allow for their self-assembly.[24,26,29] This adsorption mode is of considerable strength and accompanied by a shift of the iminic N1s peak towards higher BE, thus decreasing the separation between the two N signatures, and has been explained by the interaction of the iminic N atoms with the substrate (cf. 2HTPP on Ag(111)[23] vs Cu (111)[29]). On the other hand, the peak separation on Cl/Cu becomes larger (from 2.1 eV at 100 K to 2.4 eV at 300 K, Figure 2c), suggesting that the interaction of 2HTPP with the substrate in this case is mediated through the pyrrolic (–NH–) groups. Furthermore, in UPS we observed that increasing the sample temperature results in a decrease of the work function (0.4 eV, Figure S3b, blue vs. red spectra), implying that molecules donate electrons to the Cl/Cu substrate. We assign this irreversible charge redistribution evidenced in XPS and UPS to H-bond formation between the two –NH– groups belonging to the porphyrin core and a Cl atom of the Cl/Cu surface. The STM results show that molecules adsorb weakly and self-assemble after being deposited on a cold substrate, but irreversibly adsorb in the form of small clusters after warming up the sample to 300 K. This observation also supports the assignment of a temperature-activated stronger bond, i.e. the above proposed H-bond to 2HTPP/Cl/Cu. This bonding model also provides support for an earlier published XPS-based assignment of 2HTPP molecules interacting via H-bonds with surface O atoms on TiO_2.[21]

In conclusion, we have identified and analyzed the distinctive influence of atomically thin N and Cl ad-layers on the on-surface metalation reaction of 2HTPP on Cu(001). The N/Cu substrate facilitates molecular diffusion as well as the studied redox reaction to occur below 300 K; the metalation temperature on N/Cu is equal to ~260 K, which is ~25 K lower than in the case of O/Cu.[26] In contrast, the Cl/Cu substrate blocks the self-metalation reaction completely, i.e. up to the desorption temperature of the molecules (~550 K); in order to metalate 2HTPP on the Cl/Cu substrate, Ni atoms were deposited from the top and in this situation the steric hindrance imposed by the strong interaction of 2HTPP interacting with Cl/Cu is overcome. Moreover, the Cl/Cu surface superstructure imposes a registry onto the adsorbates: 2HTPP molecules self-assemble freely when cold-deposited, but create limited size clusters, which do not follow classical Poisson distribution, after warming up to 300 K. While the former result demonstrates the use of the metalation reaction to assess the functionalization-induced change of a substrate's reactivity important for e.g. catalytic systems and provides further insight into the mechanism of on-surface metalation, the latter result may shed light onto the delicate balance of weak intermolecular and molecule-substrate interactions. Furthermore, the remarkable influence of the discussed surface termination layers on the metalation of porphyrins motivates more in-depth studies on the decisive role of the reaction mechanism with respect to the adsorption state, also for other on-surface reactions. Notably, surfaces functionalized by a monolayer of an adsorbate extend the range of chemically tunable physical and chemical surface properties for a wide range of scientific studies and in particular for surface chemical applications.

Supporting Information

The experimental section and additional information (XPS, UPS and STM data) are given in the supporting information.

Acknowledgements

We would like to acknowledge the financial support from the Swiss Nanoscience Institute (SNI) (Project P1204) and the Swiss National Science Foundation (grants no. 20020–162512, 200020–153549, 20602–144991 and 206021–121461) and the Swiss Commission for Technology and Innovation (CTI), grant no KTI 16465.1NM-NM as well as Ferrovac AG for the interaction about in-vacuum transfers. N.B. thanks K.N. Ganesh (IISER Pune) for the support. The authors thank Shigeki Kawai and Remy Pawlak (University of Basel) who helped to perform the STM experiments, Marco Martina (University of Basel) and Rolf Schelldorfer (Paul Scherrer Institute) for technical support, Christian Wäckerlin and Dorota Siewert (PSI) for helpful discussions as well as Mariah O' Doherty (Trinity College, Dublin) for language editing.

Keywords: Photoelectron Spectroscopy · Scanning Tunneling Microscopy · On-surface Redox Reactions · Surface Chemistry · Molecular Assembly

[1] A. Fujishima, K. Honda, *Nature* **1972**, *238*, 37–38.

[2] S. C. Marinescu, J. R. Winkler, H. B. Gray, *Proc. Natl. Acad. Sci.* **2012**, *109*, 15127–15131.
[3] T. M. McCormick, B. D. Calitree, A. Orchard, N. D. Kraut, F. V. Bright, M. R. Detty, R. Eisenberg, *J. Am. Chem. Soc.* **2010**, *132*, 15480–15483.
[4] Y. Wang, M. Lingenfelder, S. Fabris, G. Fratesi, R. Ferrando, T. Classen, K. Kern, G. Costantini, *J. Phys. Chem. C* **2013**, *117*, 3440–3445.
[5] M. F. Camellone, S. Fabris, *J. Am. Chem. Soc.* **2009**, *131*, 10473–10483.
[6] N. Lin, D. Payer, A. Dmitriev, T. Strunskus, C. Wöll, J. V. Barth, K. Kern, *Angew. Chem. Int. Ed.* **2005**, *44*, 1488–1491.
[7] G. Pawin, K. L. Wong, D. Kim, D. Sun, L. Bartels, S. Hong, T. S. Rahman, R. Carp, M. Marsella, *Angew. Chem. Int. Ed.* **2008**, *47*, 8442–8445.
[8] J. Lobo-Checa, M. Matena, K. Muller, J. H. Dil, F. Meier, L. H. Gade, T. A. Jung, M. Stohr, *Science* **2009**, *325*, 300–303.
[9] A. Langner, S. L. Tait, N. Lin, R. Chandrasekar, V. Meded, K. Fink, M. Ruben, K. Kern, *Angew. Chem.* **2012**, *124*, 4403–4407.
[10] J. I. Urgel, D. Ecija, W. Auwärter, D. Stassen, D. Bonifazi, J. V. Barth, *Angew. Chem. Int. Ed.* **2015**, *54*, 6163–6167.
[11] W. L. Wang, E. J. G. Santos, B. Jiang, E. D. Cubuk, C. Ophus, A. Centeno, A. Pesquera, A. Zurutuza, J. Ciston, R. Westervelt, et al., *Nano Lett.* **2014**, *14*, 450–455.
[12] K. Mao, L. Li, W. Zhang, Y. Pei, X. C. Zeng, X. Wu, J. Yang, *Sci. Rep.* **2014**, *4*, 5441.
[13] S. Vijayaraghavan, W. Auwärter, D. Ecija, K. Seufert, S. Rusponi, T. Houwaart, P. Sautet, M.-L. Bocquet, P. Thakur, S. Stepanow, et al., *ACS Nano* **2015**, 9, 3609–3616.
[14] W. Auwärter, A. Weber-Bargioni, S. Brink, A. Riemann, A. Schiffrin, M. Ruben, J. V. Barth, *ChemPhysChem* **2007**, *8*, 250–254.
[15] W. Auwärter, D. Écija, F. Klappenberger, J. V. Barth, *Nat. Chem.* **2015**, *7*, 105–120.
[16] J. M. Gottfried, *Surf. Sci. Rep.* **2015**, *70*, 259–379.
[17] M. Panighel, G. D. Santo, M. Caputo, C. Lal, B. Taleatu, A. Goldoni, *J. Phys. Conf. Ser.* **2013**, *470*, 012012.
[18] J. I. Urgel, M. Schwarz, M. Garnica, D. Stassen, D. Bonifazi, D. Ecija, J. V. Barth, W. Auwärter, *J. Am. Chem. Soc.* **2015**, *137*, 2420–2423.
[19] L. Smykalla, P. Shukrynau, D. R. T. Zahn, M. Hietschold, *J. Phys. Chem. C* **2015**, 119, 17228–17234.
[20] K. Diller, F. Klappenberger, M. Marschall, K. Hermann, A. Nefedov, C. Wöll, J. V. Barth, *J. Chem. Phys.* **2012**, *136*, 014705.
[21] C. Wang, Q. Fan, S. Hu, H. Ju, X. Feng, Y. Han, H. Pan, J. Zhu, J. M. Gottfried, *Chem Commun* **2014**, *50*, 8291–8294.
[22] J. M. Gottfried, K. Flechtner, A. Kretschmann, T. Lukasczyk, H.-P. Steinrück, *J. Am. Chem. Soc.* **2006**, *128*, 5644–5645.
[23] T. E. Shubina, H. Marbach, K. Flechtner, A. Kretschmann, N. Jux, F. Buchner, H.-P. Steinrück, T. Clark, J. M. Gottfried, *J. Am. Chem. Soc.* **2007**, *129*, 9476–9483.
[24] S. Ditze, M. Stark, M. Drost, F. Buchner, H.-P. Steinrück, H. Marbach, *Angew. Chem. Int. Ed.* **2012**, *51*, 10898–10901.
[25] A. Goldoni, C. A. Pignedoli, G. Di Santo, C. Castellarin-Cudia, E. Magnano, F. Bondino, A. Verdini, D. Passerone, *ACS Nano* **2012**, 6, 10800–10807.
[26] J. Nowakowski, C. Wäckerlin, J. Girovsky, D. Siewert, T. A. Jung, N. Ballav, *Chem. Commun.* **2013**, *49*, 2347.
[27] S. S. Tafreshi, A. Roldan, N. H. de Leeuw, *J. Phys. Chem. C* **2014**, *118*, 26103–26114.
[28] S. S. Tafreshi, A. Roldan, N. H. de Leeuw, *Phys Chem Chem Phys* **2015**, *17*, 21533–21546.
[29] F. Buchner, J. Xiao, E. Zillner, M. Chen, M. Röckert, S. Ditze, M. Stark, H.-P. Steinrück, J. M. Gottfried, H. Marbach, *J. Phys. Chem. C* **2011**, *115*, 24172–24177.
[30] S. M. Driver, J.-T. Hoeft, M. Polcik, M. Kittel, R. Terborg, R. L. Toomes, J.-H. Kang, D. P. Woodruff, *J. Phys. Condens. Matter* **2001**, *13*, L601–L606.
[31] L.-Q. Wang, A. E. Schach von Wittenau, Z. G. Ji, L. S. Wang, Z. Q. Huang, D. A. Shirley, *Phys. Rev. B* **1991**, *44*, 1292–1305.
[32] R. Pushpa, I. Williamson, B. Jones, *J. Chem. Phys.* **2011**, *135*, 084705.
[33] L. G. M. Pettersson, P. S. Bagus, *Phys. Rev. Lett.* **1986**, *56*, 500–503.
[34] A. Ferrón, J. L. Lado, J. Fernández-Rossier, *Phys. Rev. B* **2015**, *92*, 174407.
[35] S. Huemann, N. T. Minh Hai, P. Broekmann, K. Wandelt, H. Zajonz, H. Dosch, F. Renner, *J. Phys. Chem. B* **2006**, *110*, 24955–24963.
[36] D. K. Lavallee, J. Brace, N. Winograd, *Inorg. Chem.* **1979**, *18*, 1776–1780.
[37] T. Choi, C. D. Ruggiero, J. A. Gupta, *Phys. Rev. B* **2008**, *78*, 035430.
[38] J. Xiao, S. Ditze, M. Chen, F. Buchner, M. Stark, M. Drost, H.-P. Steinrück, J. M. Gottfried, H. Marbach, *J. Phys. Chem. C* **2012**, *116*, 12275–12282.
[39] J. G. Amar, F. Family, *Phys. Rev. Lett.* **1995**, *74*, 2066–2069.

Submitted: March 17, 2016
Accepted: March 31, 2016

Chemistry SELECT

Supporting Information

Probing the Reactivity of Functionalized Surfaces by Porphyrin Metalation

Jan Nowakowski,* Sylwia Nowakowska, Gitika Srivastava, Milos Baljozovic, Jan Girovsky, Nirmalya Ballav,* and Thomas A. Jung*

Experimental Section

All the presented experiments have been performed in an ultra-high vacuum (UHV) system with base pressure of 1x10-10 mbar. Cu(001) single crystals were cleaned by cycles of Ar+ sputtering (ion energy E=2keV, sputtering current Is=7μA, angle R=45˚) and annealing to ~700 K; their cleanness was confirmed by XPS. The c(2x2)R45o N superstructure on Cu(001) was prepared by pre-annealing for 15 minutes to ~500 K, N+ ion sputtering (E=500eV, Is=2 μA, R=0o) for 10 minutes and simultaneous annealing, finalized by post-annealing for another 15 minutes. The c(2x2)R45o Cl superstructure on Cu(001) was prepared by depositing anhydrous $CuCl_2$ on a clean Cu(001) crystal annealed to ~500 K. 2HTPP molecules (Sigma-Aldrich, ≥ 99% purity) were sublimed onto N/Cu or Cl/Cu substrates kept at ~100 K. Prior to deposition, evaporation rate of 2HTPP molecules and $CuCl_2$ was controlled with a quartz-crystal microbalance. Samples were warmed up to RT without annealing. Monochromatized Al Kα line was used for XPS measurements. All of the shown STM measurements were performed at liquid helium temperature in constant current mode using Pt-Ir tips (90% Pt, 10% Ir) prepared by mechanical cutting and in-situ sputtering. The STM images were processed using the WSxM software. [1]

N1s XPS on N/Cu

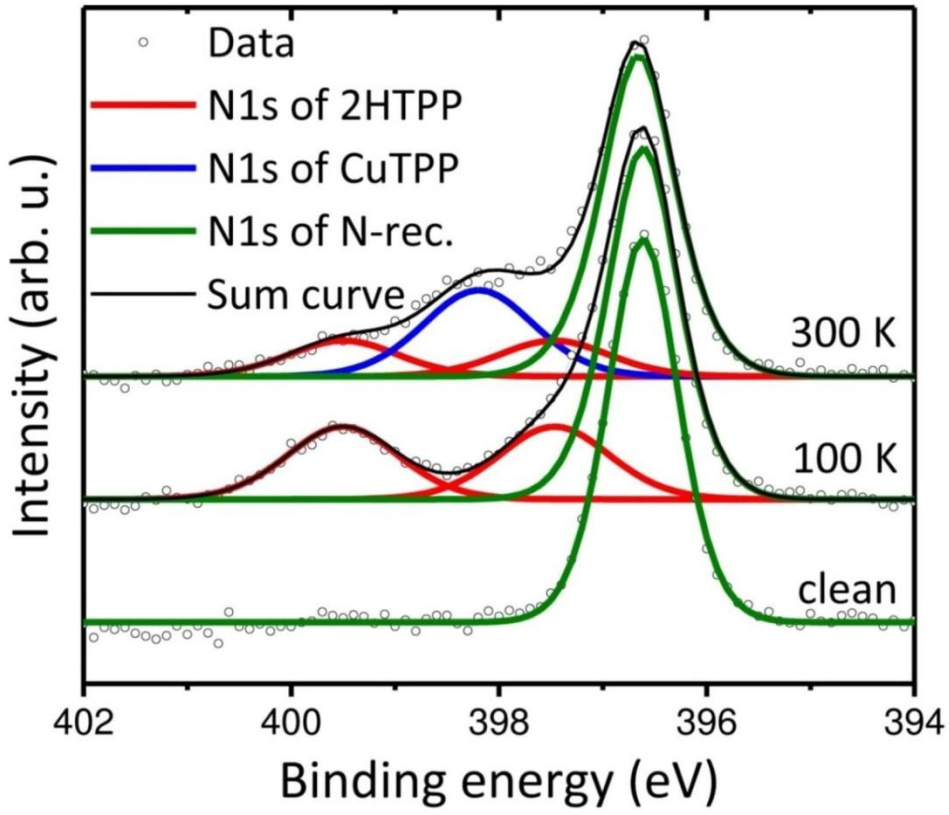

Figure 1: The N1s spectra measured on a clean N/Cu substrate (bottom), after cold-deposition of 2HTPP at 100 K (middle) and after warming up the sample to 300 K (top). The data are the same as presented in Fig. 2a in the main paper, but as a service to the interested reader here, also the substrate reference has been added.

N1s XPS before and after metalation of 2HTPP on N/Cu

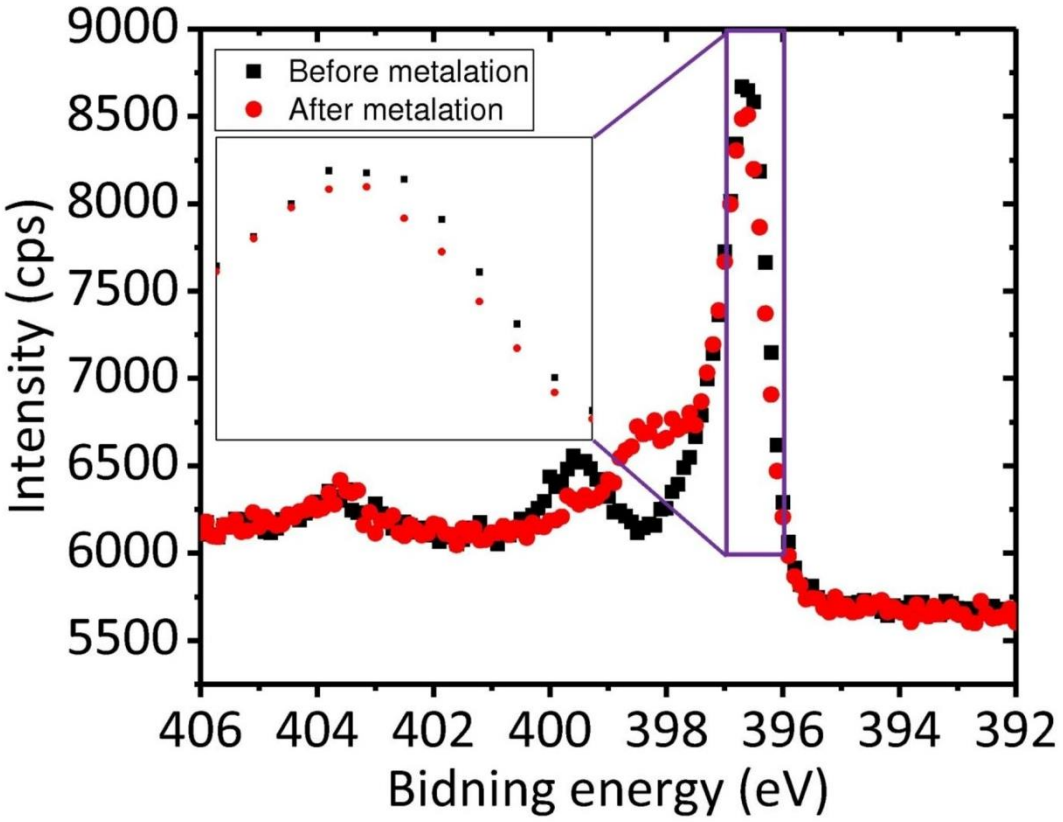

Figure 2: Comparison of raw data obtained in the N1s XPS region before and after metalation of 2HTPP on the N-superstructure of Cu. There is unambiguous evidence that metalation leads to a reduced intensity of the N1s peak from the N/Cu superstructure. Fitting is compromised by the four close lying peaks and by variable background from the Cu-LMM Auger signatures but depending on chosen parameters results in a decrease of 2-6% of the intensity of the N/Cu N1s peak at 397 eV by the metalation reaction, well within the 4% predicted in the main text of the publication.

Ultraviolet Photoelectron Spectroscopy data on Cl/Cu and N/Cu

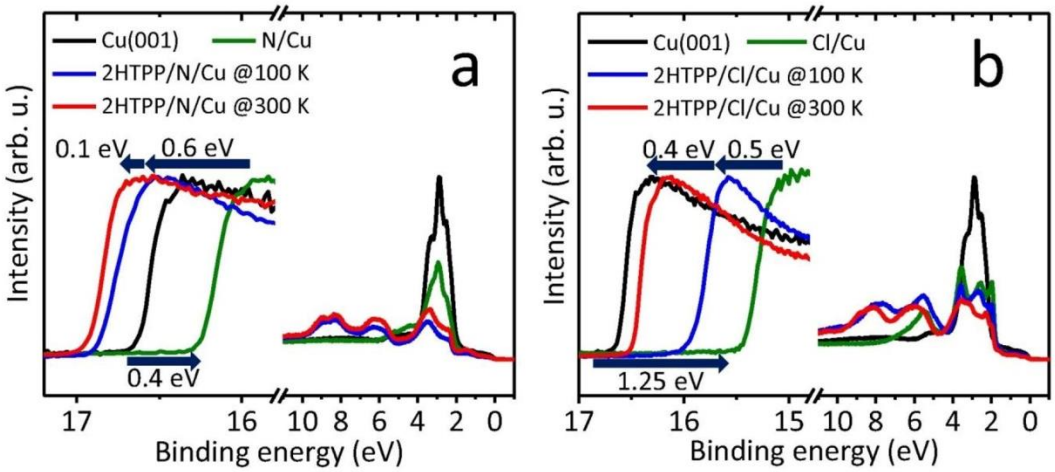

Figure 3: UP spectra taken after each step of sample preparation for (a) 1ML 2HTPP/N/Cu and (b) 1ML 2HTPP/Cl/Cu: of the clean Cu(001) (black); functionalized Cu(001) (green); after cold-deposition of 2HTPP (blue) and after warming up the sample to 300 K (red). The features present at BE between 0 eV and 4 eV arise from the electronic states of the substrate, whereas the ones visible between 4 eV and 10 eV originate mainly from the electronic states of the deposited molecules. The edge emerging between 15 eV and 17 eV is the secondary electron cut-off and relates to the workfunction ϕ of the sample, giving the values of ϕ=4.65 eV for clean Cu(001), ϕ=5.05 eV for N/Cu and ϕ=5.90 eV for Cl/Cu. Most importantly, it indicates that the surface dipole on Cl/Cu (b) (shift of 1.25 eV) is much stronger than on N/Cu (a) (shift of 0.4 eV). We attribute this to the significantly higher electron affinity of Cl atoms compared to N. The intensities of the edges at high BE have been normalized. All of the spectra have been measured 10° from normal emission.

2HTPP/Cl/Cu after annealing to 550 K

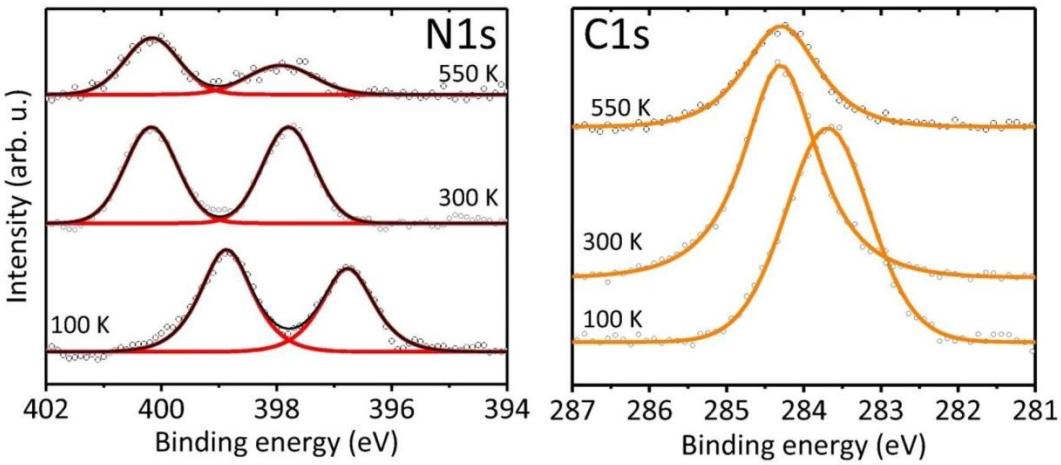

Figure 4: N1s and C1s XP spectra after cold deposition of 2HTPP at 100 K (bottom), after warming up to RT (middle) and after annealing to 550 K (top). After annealing to 550 K molecular desorption is observed. The remaining molecules are still not metalated; however, the N1s spectra show a significant discrepancy between the intensities of iminic and pyrrolic nitrogen atoms. Such disparity has been observed before and attributed to the X-ray Photoelectron Diffraction (XPD) effect [2], which is highly angle-dependent. It suggests that the remaining 2HTPP are in similar conformation after heating to 550 K (i.e. one specific conformation has a higher adsorption energy and that is the one that is still in contact with the substrate).

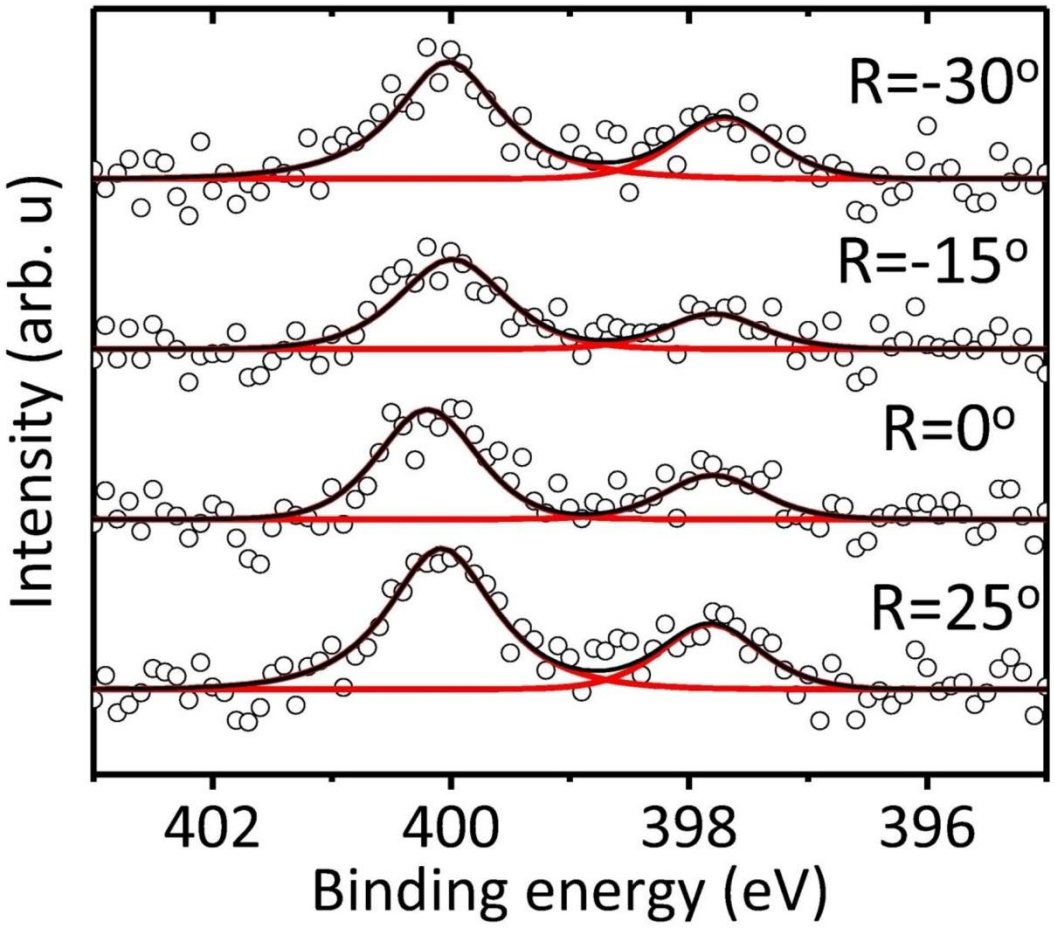

Figure 5: Angle-dependent N1s spectra of 2HTPP/Cl/Cu after annealing to 550 K providing evidence that the X-ray Photoelectron Diffraction (XPD) plays a role in the discrepancy between the N1s signatures. However, in our case, the ratio between –NH- and –N= nitrogen intensities changes only slightly with angle – between 2.8 for normal incidence to 2.2 for incidence of 30° which suggests that the XPD effect is not the sole reason for this difference. The increased N1s signal at 400 eV for all angles indicates a partial protonation of 2HTPP. This protonation might be facilitated by the H-free N atoms pointing away from the substrate as conformationally forced by NH forming H-bonds with the substrate.

Cl2p XPS on 2HTPP/Cl/Cu at different temperatures

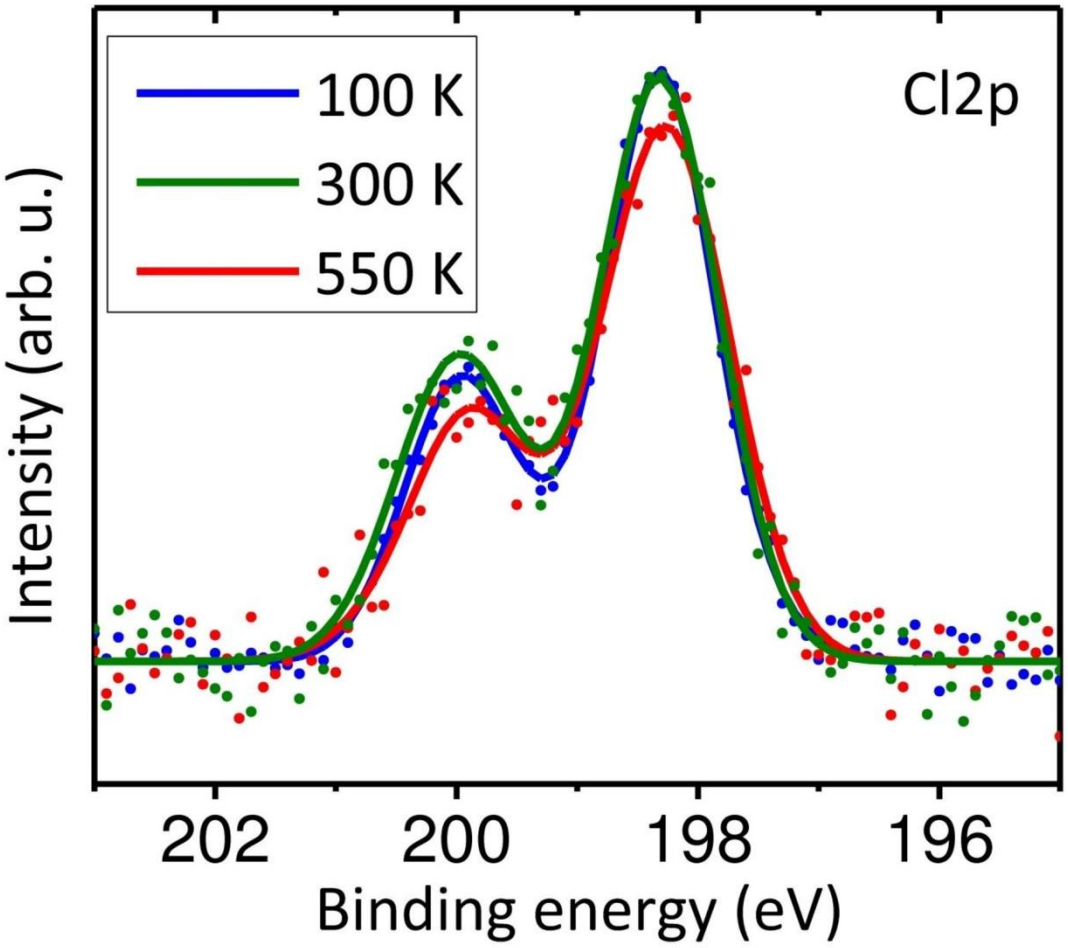

Figure 6: Cl2p XPS data measured on 2HTPP/Cl/Cu at (a) 100 K, (b) 300 K and (c) 550 K, i.e. the temperature of molecular desorption. There is virtually no chemical shift between the spectra and the biggest visible change is a slight broadening of the spectroscopic feature with temperature without significant changes in intensity.

Nucleation of 2HTPP clusters on Cl/Cu(001) at RT

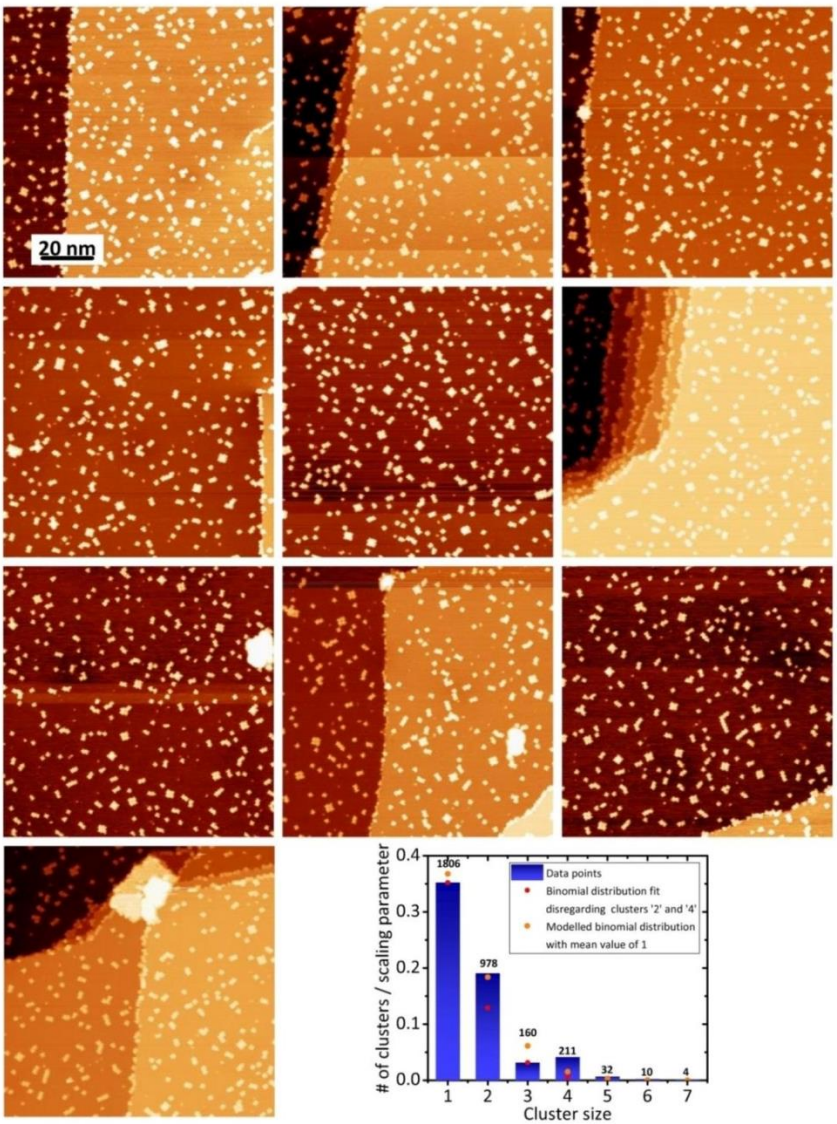

Figure 7: STM images used to calculate the cluster statistics and a cluster size distribution histogram together with a Poisson binomial distribution fit (red dots) and a modelled binomial distribution with a mean value of 1, both implying that clusters '2' and '4' appear more frequently than expected. The binomial distribution function was divided by a scaling parameter due to the undefined number of '0' clusters in this case. The scaling parameter is equal to the sum of number of clusters counted and the expected number of '0' clusters. The counted number of clusters of a certain size is indicated above each histogram bar.

[1] I. Horcas, R. Fernández, J. M. Gómez-Rodríguez, J. Colchero, J. Gómez-Herrero, A. M. Baro, *Rev. Sci. Instrum.* **2007**, *78*, 013705.

[2] Diller, K.; Klappenberger, F.; Marschall, M.; Hermann, K.; Nefedov, A.; Wöll, C.; Barth, J. V. *The Journal of Chemical Physics* **2012**, *136* (1), 014705.

2.2 Magnetic properties of single transition metal atoms on a Bi(111) substrate

Currently, there is an increasing interest in studying magnetic atoms at surfaces, also including the pursuit of single-atom magnets as the ultimate limit of magnetic data storage. This was accompanied by controversial discussion about the first STS-based report of stable magnetic moment in single Ho atoms on Pt(111)[33] which then could not be reproduced by other groups[34]. A few weeks before this thesis was written, magnetic remanence in single surface-supported rare-earth atoms has been reported in XMCD measurements; interestingly, the atoms in question were also Ho but deposited on a different substrate, namely MgO.[21]

We focused our investigation on magnetic properties of transition metal (TM) atoms on Bi/Si(111) surface. The choice of the substrate was motivated by the fact that it exhibits a large Rashba splitting, *i.e.* a momentum-dependent splitting of spin bands at the surface.[35] The electronic properties of TMs on Bi(111) were addressed by other groups using STM; interestingly, the transition metals were found to penetrate the first layer of Bi without any energy barrier and reside within the first bilayer.[36] This allows for a relatively high coverage of single paramagnetic atoms, *i.e.* without clustering. However, TMs on Bi(111) lacked the determination of their magnetic properties. Therefore, we decided to address these properties using the spatially-averaging XMCD technique aiming to achieve the fundamental understanding and control over single-atom spin systems at interfaces.

Isolated single atoms cannot exhibit a stable magnetic moment since they have spherical symmetry; hence, there is no preferential direction for the spin to align with, as long as there is no external magnetic field. Interaction with the substrate, however, can give the atoms a directional dependence of magnetic properties, called magnetic anisotropy (MA). MA is required to observe stable magnetic moments exhibiting a magnetic hysteresis and it can be studied by measuring the angle-dependent XMCD. [37] In order to decrease the size of surface-supported magnetic bits, each atom in the ferromagnetic domain should have as large

magnetic anisotropy energy as possible and it should be of easy-axis type, *i.e.* out-of-plane. Therefore it is interesting to see that both Fe and Cr single atoms show a significant out-of-plane magnetic anisotropy (Fig. 2.2.1), as in both cases the XMCD signal is stronger when measured in normal incidence as compared to grazing incidence. The difference is especially large for Cr.

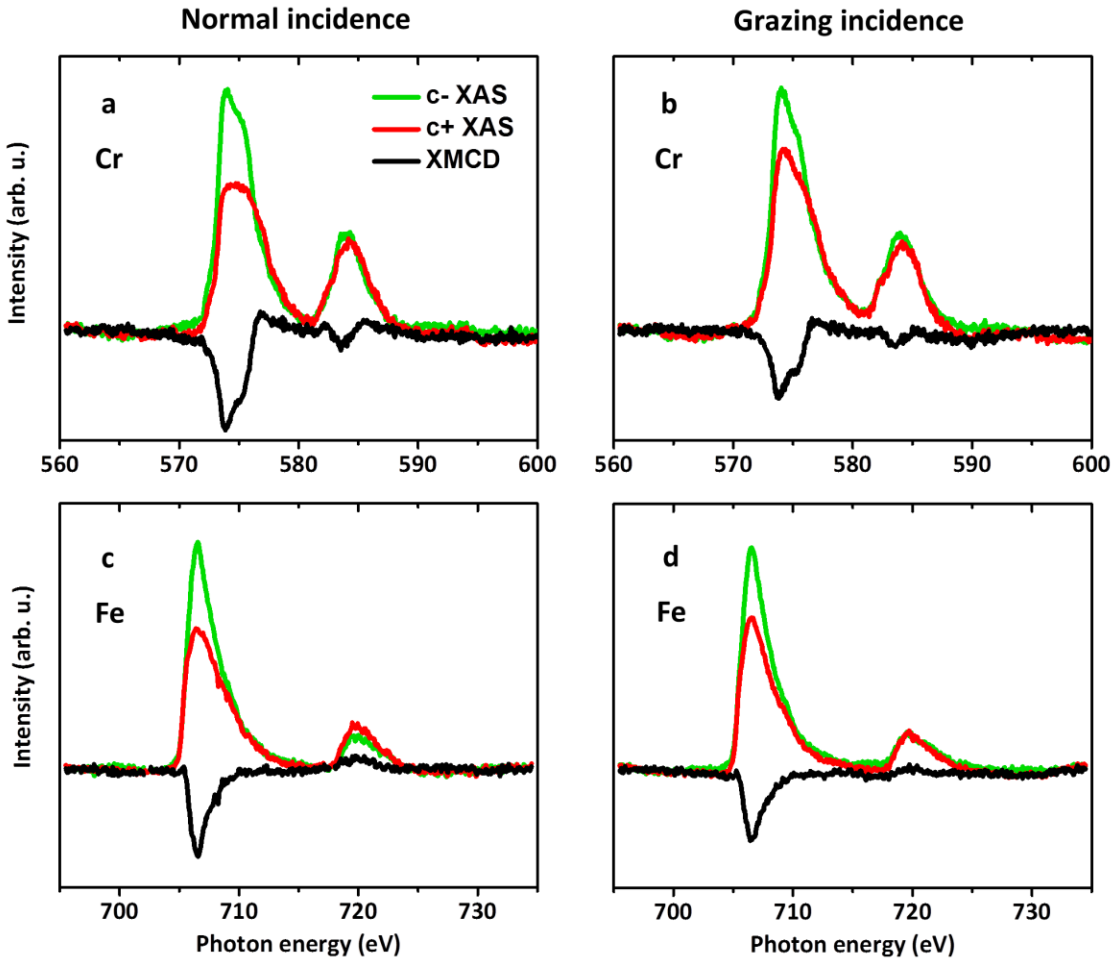

Figure 2.2.1 *The XMCD on Cr (a, b) and Fe (c, d) $L_{3,2}$ edges measured in normal incidence (a, c) and grazing incidence of 60^o (b, d) in the external magnetic field of 6.8 T. The intensity scale is the same for both angles for each element. It can be seen that both Cr and Fe show higher XMCD in normal incidence, indicating an out-of-plane magnetic anisotropy. The shape of XMCD signatures, especially for Cr, suggests a large orbital moment of the atoms (L_3 and L_2 edges pointing the same direction). The spectra were obtained at 7 K for Cr and at 13 K for Fe.*

To quantify this anisotropy, *i.e.* to determine the magnetic anisotropy energy (MAE), measuring

magnetisation curves at two angles is required. The obtained curves were fitted using a model described in Ref. [38], after slight modifications. It is a classical model that does not take magnetic moment quantisation into account, but was shown to give good results already for Co (S=3/2).[38] In the used procedure the magnetisation M was calculated as:

$$\boldsymbol{M} = \boldsymbol{m}\frac{\int_0^{2\pi} d\phi \int_0^{\pi} d\theta sin\theta cos\theta e^{-E(\theta_0,\theta,\phi)/k_B T}}{\int_0^{2\pi} d\phi \int_0^{\pi} d\theta sin\theta e^{-E(\theta_0,\theta,\phi)/k_B T}}$$

where ***m*** is the magnetic moment of a single atom, Θ_0 defines the easy axis of magnetisation, Θ is the polar and ϕ is the azimuthal coordinate of the measured magnetic moment while $E(\Theta_0, \Theta, \phi)$ is the magnetic energy function given by:

$$E = -\boldsymbol{mB}cos\theta - K(sin\theta_0 sin\theta cos\phi + cos\theta_0 cos\theta)^2$$

where *K* is the magnetic anisotropy energy of a single atom and ***B*** is the magnetic field. The magnetisation curves presented in Fig. 2.2.2 measured at two different angles were fitted *simultaneously* with a fitting procedure based on the above-described model with three free parameters: magnetic moment ***m***, magnetic anisotropy energy *K* and temperature *T*. The values of magnetic moment at B=6.8 T were calculated from the XMCD spectra (Fig. 2.2.1) using sum-rules,[39,40] after taking the correction factors[41] into account.

The magnetic anisotropy originates from the interaction between the spin and the orbital momentum of an atom and requires the ligand field breaking the spherical symmetry of the free ion.[42] In the vast majority of magnetic materials, however, the orbital magnetic moment is quenched due to ligand field effects and hybridization, thus leading to very low MAE in the order of K=0.01 – 1 meV.[43–45] Therefore, already the K=2.5 meV obtained for Fe is considered high. Interestingly, the Cr atoms exhibit more than an order of magnitude higher MAE than Fe, *i.e.* K=30.5 meV. The physical limit of magnetic anisotropy can be calculated as λL, where λ is the spin-orbit coupling constant and L is the atom's orbital angular momentum.[42,47] Assuming, in accordance with the XMCD results, that the occupancy of Cr and its spin state are $3d^5$ and S=3/2, respectively one can conclude that λ=10 meV[46] and L=3, resulting in λL =30 meV. It is nearly the same as the value of MAE of Cr, *i.e.* 30.5 meV, as obtained from the fits of

magnetisation curves. This is possible due to the fact that Cr atoms retain a large orbital magnetic moment (~ 1.2 μ_B, as estimated from the orbital XMCD sum rule). It can be seen in the XMCD spectra (Fig. 2.2.1a-b) as both L_3 and L_2 edges point in the same direction.[29] Before publishing, further analysis of the presented data will be supported by DFT+U calculations to gain a better understanding of the phenomena leading to such high MAE. The additional analysis will include the elucidation of the so-called T_Z term resulting in anisotropy of the spin magnetic moment itself, and might slightly change the obtained value of magnetic anisotropy. To the best of our knowledge the physical limit of MAE has been nearly reached for Co atoms on a thin layer of an insulator,[42] but so far never for other 3d transition metal atoms or on a semi-metal like Bi.

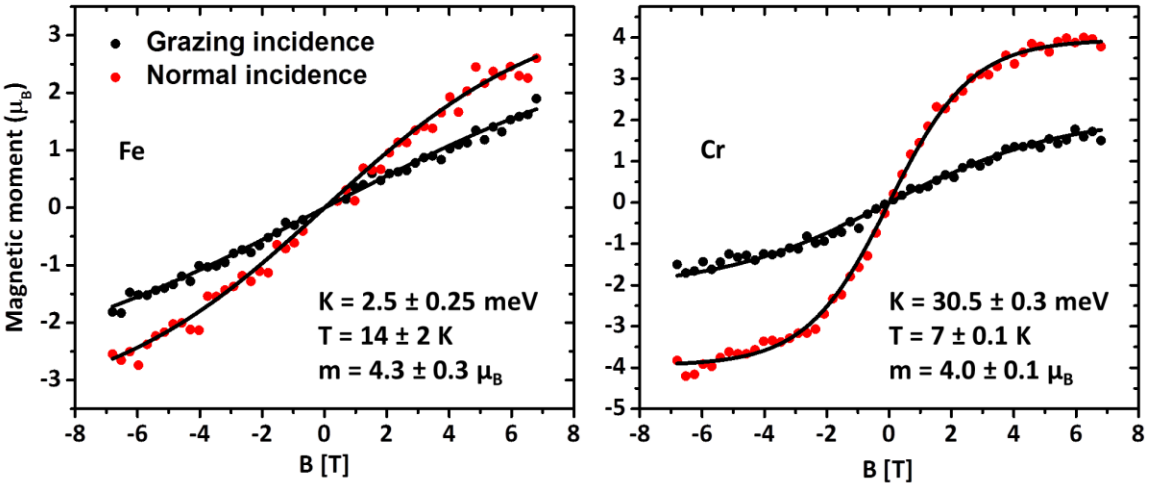

Figure 2.2.2 *Magnetisation curves obtained on ~3% of a ML of Fe (left) and Cr (right) deposited on Bi/Si(111). Red and black dots mark data points obtained in normal and grazing incidence, respectively. The black lines indicate the obtained fits, from which three given parameters were calculated – temperature **T**, magnetic moment **m** and magnetic anisotropy energy **K**. The higher uncertainty of calculated values in the case of Fe is due to the fact that even at the maximum field the magnetic moment of atoms is not saturated. The temperature difference is unintentional and caused by the different thermal conductivities of sample holders.*

2.3 Modifying the molecule-substrate coupling energy by molecular functionalization

For both application-targeted and fundamental investigations of magnetic interactions, paramagnetic organic molecules have many advantages when compared to single atoms. First of all, the molecular *"cage"* naturally separates the paramagnetic species and therefore prevents clustering while still allowing for similar coverage of transition metals like in the case of depositing single atoms, *i.e.* a few percent of a ML. Due to the bonding properties of the C atom and due to the diverse pre-established synthetic pathways, there are many ways of controlling the properties of paramagnetic species. Substitutions and ligations can change the oxidation state of the atom, its ligand field and symmetry as well as modify the interaction with the underlying substrate.[47,48] In the study presented here we deposited three different molecules – Mn(III) 2,3,7,8,12,13,17,18-octaethyl-porphyrin chloride (MnOEPCl), Mn(III) 5,10,15,20-tetraphenyl-porphyrin chloride (MnTPPCl) and Mn (III) tetrakis(3,5-di-tert-butylphenyl)-porphyrin chloride (MnTTBPPCl) on two different ferromagnetic substrates, *i.e.* Co and O/Co (*c.f.* Fig. 2.3.1). The adsorption results in a different distance between the macrocycle of each molecule and the substrate. Owing to that we were able to tune the substrate-molecule magnetic exchange coupling energy.

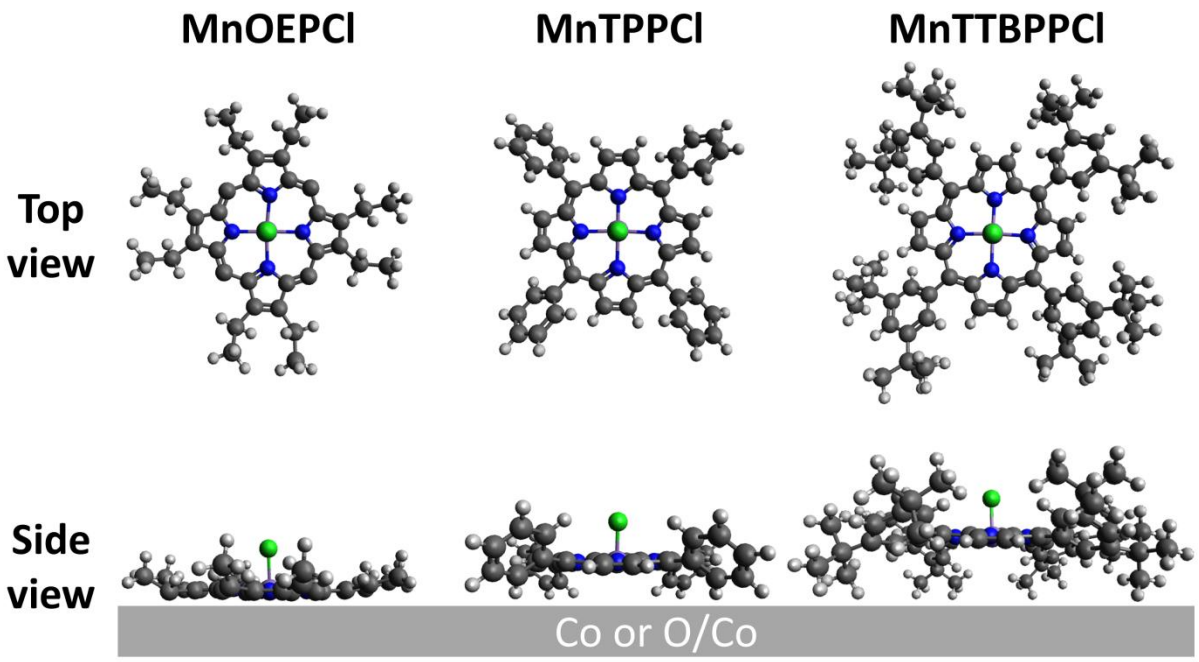

Figure 2.3.1 *The top- and side-view of the models of the studied molecules deposited on a Co or an O/Co support – MnOEPCl (left), MnTPPCl (centre) and MnTTBPPCl (right), illustrating the changing distance between the molecules' macrocycles and the substrate.*

In order to study the substrate-molecular exchange coupling we used the XMCD technique. In Fig. 2.3.2 example spectra measured at RT for each of the six studied systems are shown. The direction on the XMCD peaks indicates that all of the molecules couple ferromagnetically (FM) to a bare Co substrate and antiferromagnetically (AFM) to an O/Co substrate. Porphyrins on Co couple to the substrate by the 90^{o} indirect exchange mechanism via the four N atoms surrounding the metal centre.[49] On O/Co on the other hand the coupling mechanism has been identified as 180^{o} superexchange via the O atoms of the substrate.[50,51] This suggests that the N-Co distance is important for the molecules adsorbed on bare Co, whereas the Mn-O distance plays a more important role for the molecules on O/Co. Additionally, in agreement with the literature, the position of the Mn L_3 edge suggests that the oxidation state of the Mn ion is different on each substrate.[51] On O/Co the molecules' metal ion remains as Mn(III); on bare Co, however, Mn(II) is detected due to the loss of Cl ligand from most of the molecules.[51]

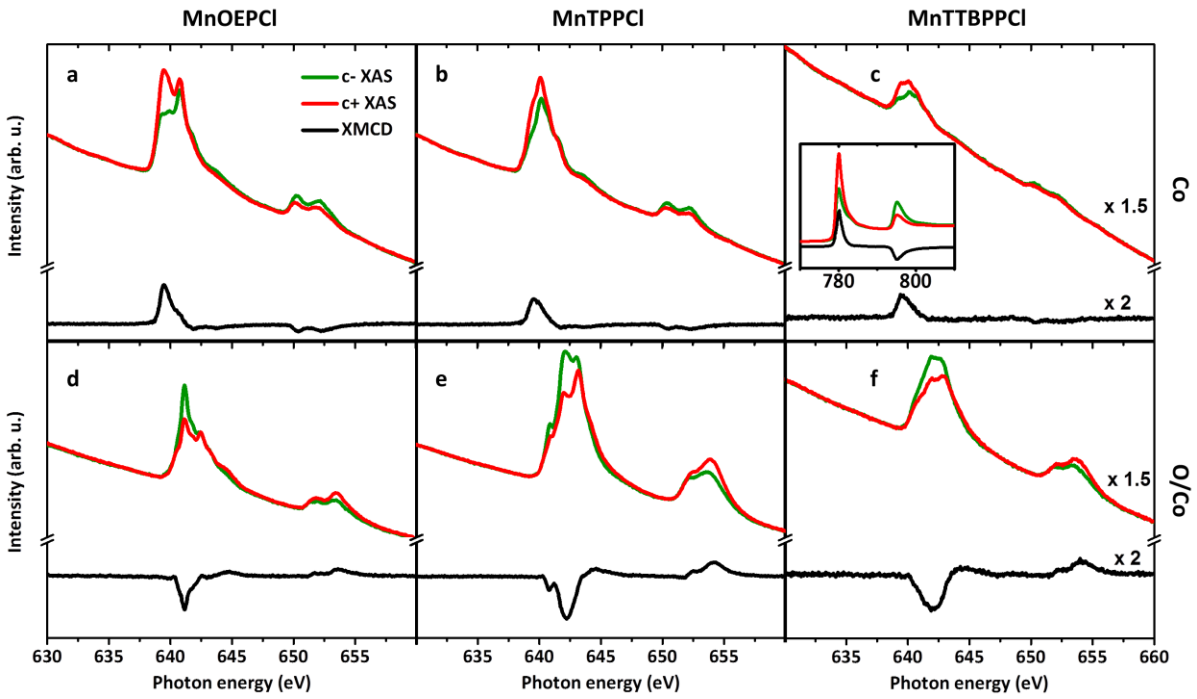

Figure 2.3.2 *The example XMCD spectra obtained at the Mn $L_{3,2}$ edges of MnOEPCl (a, d), MnTPPCl (b, e) and MnTTBPPCl (c, f) deposited on bare Co (a, b, c) and O/Co (d, e, f). In the inset of (c) XAS and XMCD of the underlying Co substrate are shown, which were virtually identical for all six systems. All molecules couple ferromagnetically to a bare Co substrate and antiferromagnetically to an O/Co substrate. The XAS and XMCD for MnTTBPPCl were multiplied by the indicated values due to a lower amount of Mn atoms. All of the spectra were measured at room temperature.*

In order to quantify the molecule-substrate magnetic coupling energy, temperature-dependent XMCD studies have been performed; the results are shown in Fig. 2.3.3. The six measurements plotted in the Fig. 2.3.2 provided six out of thirty data-points in Fig. 2.3.3. From each measured XMCD spectrum the ratio between the XMCD and XAS (*i.e.* (c+ + c-)/2) intensity was calculated. The rate at which this ratio changes with temperature is proportional to the coupling energy; a weak dependence of XMCD on temperature corresponds to large coupling energy and *vice versa*. The coupling energy can be quantified by modelling the temperature dependence using the so-called Brillouin function $B_J(x)$:[50]

$$B_J(x) = \frac{2 \cdot J + 1}{2 \cdot J} \coth\left(\frac{2 \cdot J + 1}{2 \cdot J} \cdot x\right) - \frac{1}{2 \cdot J} \coth\left(\frac{1}{2 \cdot J} \cdot x\right)$$

where *J* is usually a positive integer or half-integer (in this case the total magnetic moment of a molecule). In this model the molecule-substrate coupling is treated like an effective magnetic field and the coupling energy E_{ex} can be calculated from:

$$M_{mol}(T) = M_{sub}(T) \cdot B_J\left(\frac{E_{ex}}{k_B T}\right)$$

where M_{mol} and M_{sub} are the magnetisation of the molecule and the substrate, respectively, k_B is the Boltzmann constant and T is the temperature. Due to the very high Curie temperature of the used 20 ML Co films (~1000 K), however, M_{sub} is nearly independent on the temperature in the range of 50 – 300 K (change of less than 5%) and therefore was neglected.

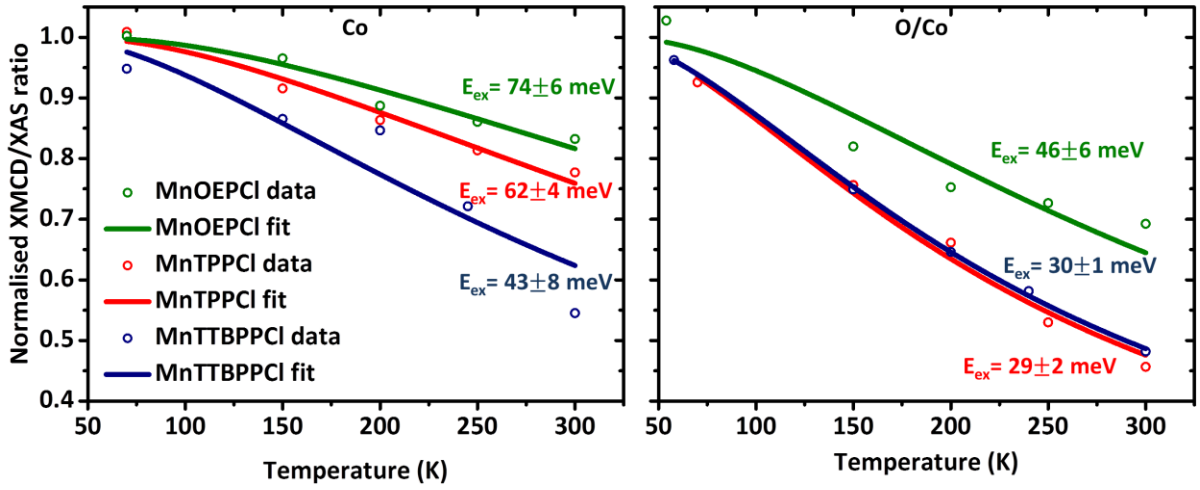

Figure 2.3.3 *The XMCD/XAS ratios obtained from temperature-dependent XMCD data of Mn L_3 edge of MnOEPCl (green), MnTPPCl (red) and MnTTBPPCl (blue) deposited on bare Co (left) and O/Co (right). The rate of change of the XMCD/XAS ratio with temperature is an indication of the magnetic coupling strength between the molecules and the substrate and is fitted with the Brillouin function. The magnetic exchange energy can thus be quantified and is given for each system next to the corresponding fits.*

The results obtained on the bare Co substrate follow the expected dependency: the further away the molecule's macrocycle is, the weaker the coupling – specifically 74 meV for MnOEPCl, 62 meV for MnTPPCl and 43 meV for MnTTBPPCl. Interestingly, on O/Co the exchange energy is the same, within the uncertainty margin, for both MnTPPCl and MnTTBPPCl molecules and equal to ~30 meV. The coupling energy of MnOEPCl on O/Co is only ~50% larger, while on bare

Co it is almost double that of MnTTBPPCl. This all suggests that molecular flexure of molecules deposited on the less-reactive O/Co can mitigate the effect induced by the size of the molecular substituents. It would be very interesting to deduce an empirical dependency of the coupling energy with distance, but in order to achieve this the knowledge about the exact distances between substrate and molecule atoms is required. Thus, X-ray Photoelectron Diffraction experiments as well as DFT+U calculations are currently ongoing.

To summarize, the presented data shows significant tunability of metal-organic interfaces by simple functionalization of the spin-bearing molecule. The range of attainable exchange energy values can be further extended by changing the ferromagnetic substrate[50] as well as by axial ligation that can pull the metal ion away from the plane of the molecule, introducing the so-called spin-trans effect.[52]

2.4 Detecting out-of-plane mobility in molecular bilayers

At an interface, there exist many dynamic phenomena occurring parallel to the surface plane, exemplified by the well-studied molecular diffusion.[51,53–55] The effect of out-of-plane motion is, however, frequently neglected, since it is not nearly as easy to study and not as common. The following results show a convenient XMCD-based method of investigating the phenomenon of molecular inter-layer rearrangement. This effect could significantly alter the properties of organic layered structures and therefore would need to be taken into account in the design and fabrication of metal-organic systems, similarly to the case of atomic inter-layer mixing in, by design ultra-thin, delta-doped layers in semiconductor devices[22] as well as layered oxide films.[56]

In the Fig. 2.4.1 Mn and Fe $L_{3,2}$ XAS and XMCD spectra of different molecular films on O/Co are shown: ~1.1 ML of FePc (a, b), the same sample after adding 1ML of MnPc (c, d) and after reversed order of molecular deposition. Before the deposition of MnPc, the single layer of FePc couples antiferromagnetically to the underlying substrate, as expected. After the deposition of the second molecular layer, however, the XMCD signal of Fe decreases significantly (*i.e.* ~5 times) and is accompanied by the appearance of XMCD in Mn, suggesting that the MnPc molecules drive FePc away from the substrate with a yield of ~80%. Interestingly, no such effect is observed after a reversed order of deposition, *i.e.* first MnPc then FePc (*c.f.* Fig. 2.4.1e, f). It suggests that this effect is not solely caused by the kinetic energy of the molecules deposited in the second step, but rather is an outcome of their different adsorption energies. The reason of this difference is most likely two-fold: firstly, MnPc molecules have a higher spin state than FePc and therefore interact stronger with the magnetic field generated by the O/Co film and secondly, MnPc molecules undergo a charge transfer to the substrate changing the oxidation state from Mn(II)Pc to Mn(III)Pc.[57] Therefore, the interaction of FePc is predominantly of physisorption type whereas for MnPc it is a mixture of physisorption and chemisorption,

according to the recently-proposed criteria on how to discriminate between these two phenomena for large π-conjugated organic molecules.[58]

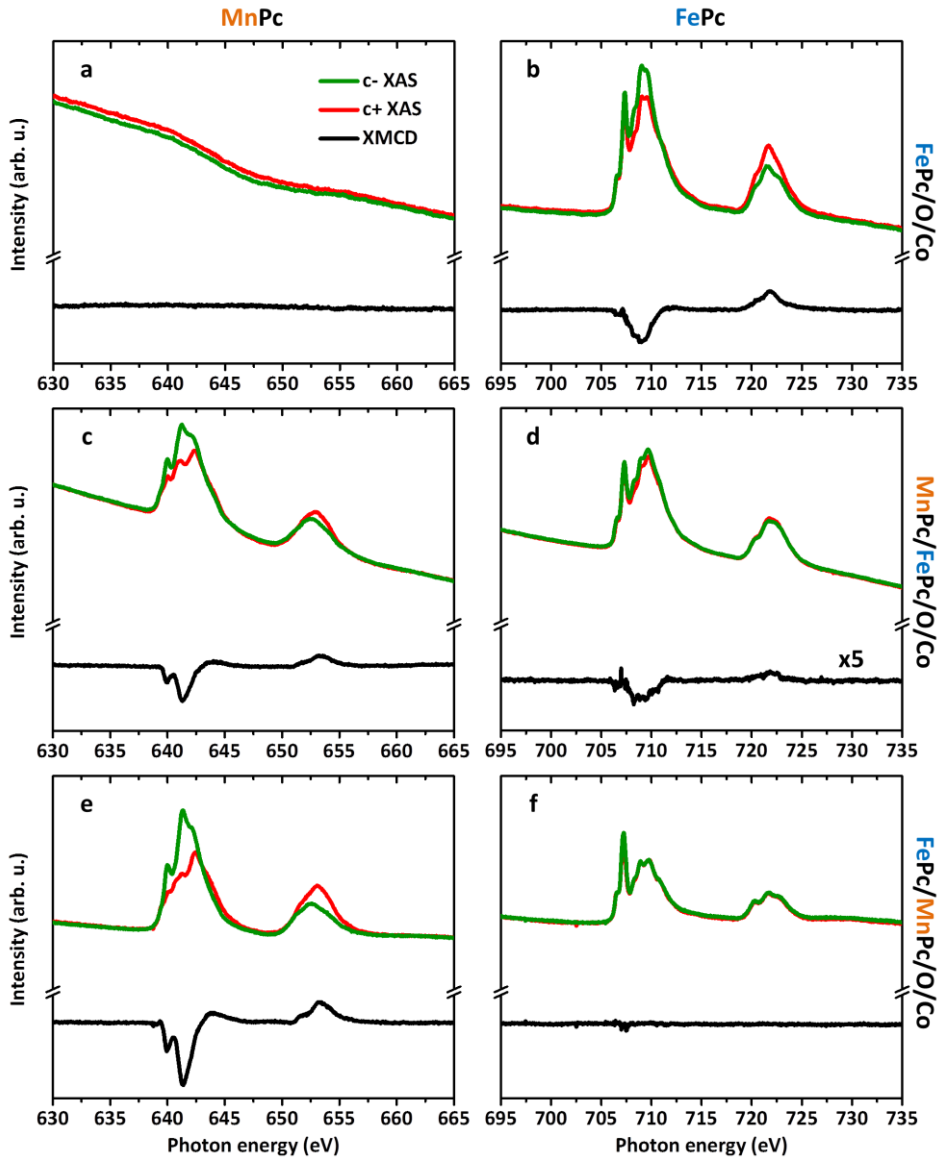

Figure 2.4.1 *The Mn and Fe $L_{3,2}$ XAS and XMCD spectra of different molecular films on O/Co: (a, b) 1 ML FePc, (c, d) after adding MnPc on top and (e, f) after reversed order of deposition, i.e. first MnPc and then FePc. After depositing MnPc on a full monolayer of FePc the XMCD/XAS ratio of Fe significantly decreases due to most of FePc being pushed away from the substrate (c.f. b vs d). No such phenomenon is observed after reversed order of deposition. The intensity of the XMCD spectrum in (d) has been multiplied by 5. The molecules in all cases were deposited on a substrate held at RT. All spectra were measured at 5 K.*

In principle the presence of XMCD, *i.e.* of a magnetic moment on the central metal ion, measured on the molecules deposited in the second step could also be caused by intermolecular coupling of the 2nd layer to the substrate through the 1st layer, not due to inter-layer mixing. In such a case of a different coupling mechanism, however, one would expect a different coupling energy of molecules adsorbed in the 1st and in the 2nd layer. In order to estimate the coupling energy and verify that the observed XMCD changes in Fig. 2.4.1 are due to layer rearrangement rather than intermolecular coupling, in the Fig. 2.4.2 T-dependent XMCD results are shown. The obtained fits indicate that the molecule-substrate magnetic coupling energy of MnPc in both single- and double-layer samples is the same within error margin; the same applies to FePc. It indicates that in both monolayer and bilayer cases the magnetic signal in molecules originates from the interaction with the substrate.

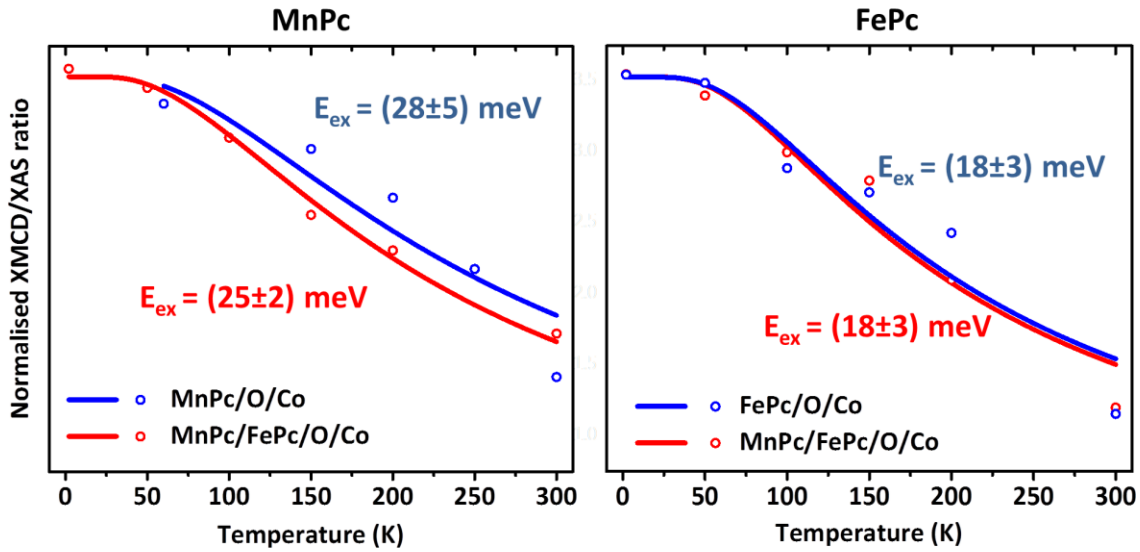

Figure 2.4.2 *Temperature-dependent XMCD/XAS ratio from Mn (left) and Fe (right) L_3 edges. The same, within uncertainty margin, values of exchange energy obtained on single- and bi-layer samples indicate that the observed XMCD in bilayers is due to molecule-substrate coupling rather than intermolecular interactions.*

It is important to note that in the presented experiments, the molecules were deposited on a substrate kept at room temperature. The molecular rearrangement was, therefore, occurring in a non-equilibrium state as the molecules deposited in the second step arrived with a high

kinetic energy (due to the sublimation temperature of ~300^{o}C). It would be also interesting to study how this effect would proceed under close to equilibrium conditions, *i.e.* by depositing the molecules at a very low substrate temperature and then slowly warming up the sample. It would allow for the deduction of the energy barrier involved in the inter-layer mixing, also as a function of thickness of the bottom molecular film. Notably, this use of XMCD technique to study mixing of phthalocyanine layers could be extended to other systems of molecular bi-/multilayers, *e.g.* mixtures of phthalocyanines and TCNQ.[59] It is also possible to use this method for non-magnetic substrates as the XAS line shape is affected by the adsorption site as can be seen in the Fig. 2.4.1: b *vs.* d.

2.5 Two-dimensional supramolecular spin arrays

2.5.1 Molecules assembled in a chessboard

Since the seminal work of Scheybal *et al.*[60] it is known that the magnetic moment of paramagnetic organic molecules, like porphyrins and phthalocyanines, can be exchange coupled to a ferromagnetic substrate.[60] Afterwards many similar systems were studied and it was also shown that the magnetic moment of molecules can be controlled by gas dosing.[20,61] This lead to the idea of creating a selectively-addressable spin array. One of the main goals of this thesis was to prepare and characterize 2D supramolecular layers built from two phthalocyanines with different metal centres self-assembled alternatively, *i.e.* in a chessboard-like structure, in order to use them in novel magnetic systems. A chessboard-like supramolecular array has already been obtained for mixed porphyrin-phthalocyanine systems on Au(111);[62,63] however, it was not certain that it would apply to a mixture of two fully planar phthalocyanines. It was debated that a non-planar interaction, like in the case of phenyl/pentafluorophenyl assembly,[64] might be necessary. Such a chessboard-like supramolecular structure has also never been achieved before on reactive, ferromagnetic substrates, which normally do not allow for molecular diffusion. Molecular self-assembly on a ferromagnetic substrate can, however, be achieved if the substrate is covered with an atomically thin layer of oxygen.[51]

The molecules chosen for this study were commercially available MnPc as well as FeFPc synthesized by our collaborators from University of Bern (from the group of Prof. S. Decurtins). These two molecular species were co-evaporated onto the substrate of choice, *i.e.* O/Co, Au(111) or Ag(111), held at RT. The evaporation rate of molecules was controlled independently using a QCMB; to investigate the deposition rate for one molecule, the crucible with the other species was kept under a shutter. Due to a significantly higher molecular weight of FeFPc than MnPc, a higher mass of the former had to be deposited in order to obtain the

desired 1:1 ratio, which was extremely important for the planned magnetic investigations. Once the desired and stable rate of both molecules was confirmed, ~1 ML in total of both species was deposited simultaneously.

Before using the sample for synchrotron-based measurements, its quality was investigated using lab-based techniques. Most importantly, XPS was measured on every prepared sample with special attention given to C1s, F1s and N1s signatures. In the Fig. 2.5.1 typical XPS spectra for the co-assembled MnPc and FeFPc are shown. A quantitative analysis of these spectra gives a lot of information about the prepared sample: (i) the intensity of the C1s peak confirms the ~1ML molecular coverage (ii) the ratio of C1s to N1s provides evidence that molecules are still intact and that there are no C-based impurities and (iii) a comparison of C1s to F1s intensities provides information about the ratio between the molecular species. Since a phthalocyanine consists of 32 C atoms and a perfluorinated phthalocyanine is additionally made up from 16 F atoms, an ideal C1s:F1s proportion is 4:1, indicating a perfect 1:1 ratio of MnPc and FeFPc. Samples consisting of up to 60% of one molecular species were used for synchrotron investigations.

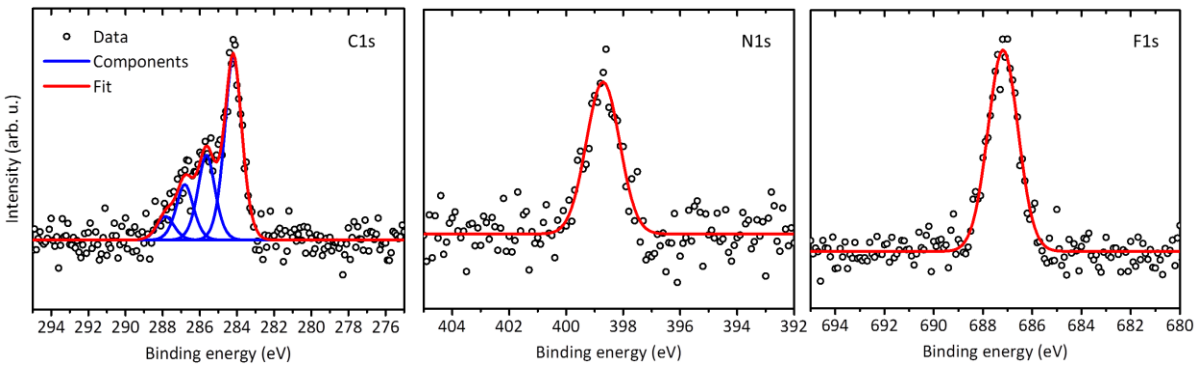

Figure 2.5.3: *Typical XP spectra of ~1ML of MnPc-FeFPc co-assembly deposited on Au(111). The quantified ratios between elements are: C/N = 3.8 (ideal = 4.0) and C/F = 3.6 (ideal 4.0), suggesting that the sample consists of 55% MnPc and 45% FeFPc.*

After obtaining satisfactory XPS results, STM measurements were performed to confirm the chessboard-like structure of the molecular layer. The MnPc-FeFPc co-assembly was extensively studied on three different substrates: O/Co, Au(111) and Ag(111). In the Fig. 2.5.2 STM micrographs of co-assemblies on these surfaces are shown. In all three cases the molecular species are easily distinguishable; the smaller and brighter species are MnPc, while FeFPc are imaged as larger and darker.

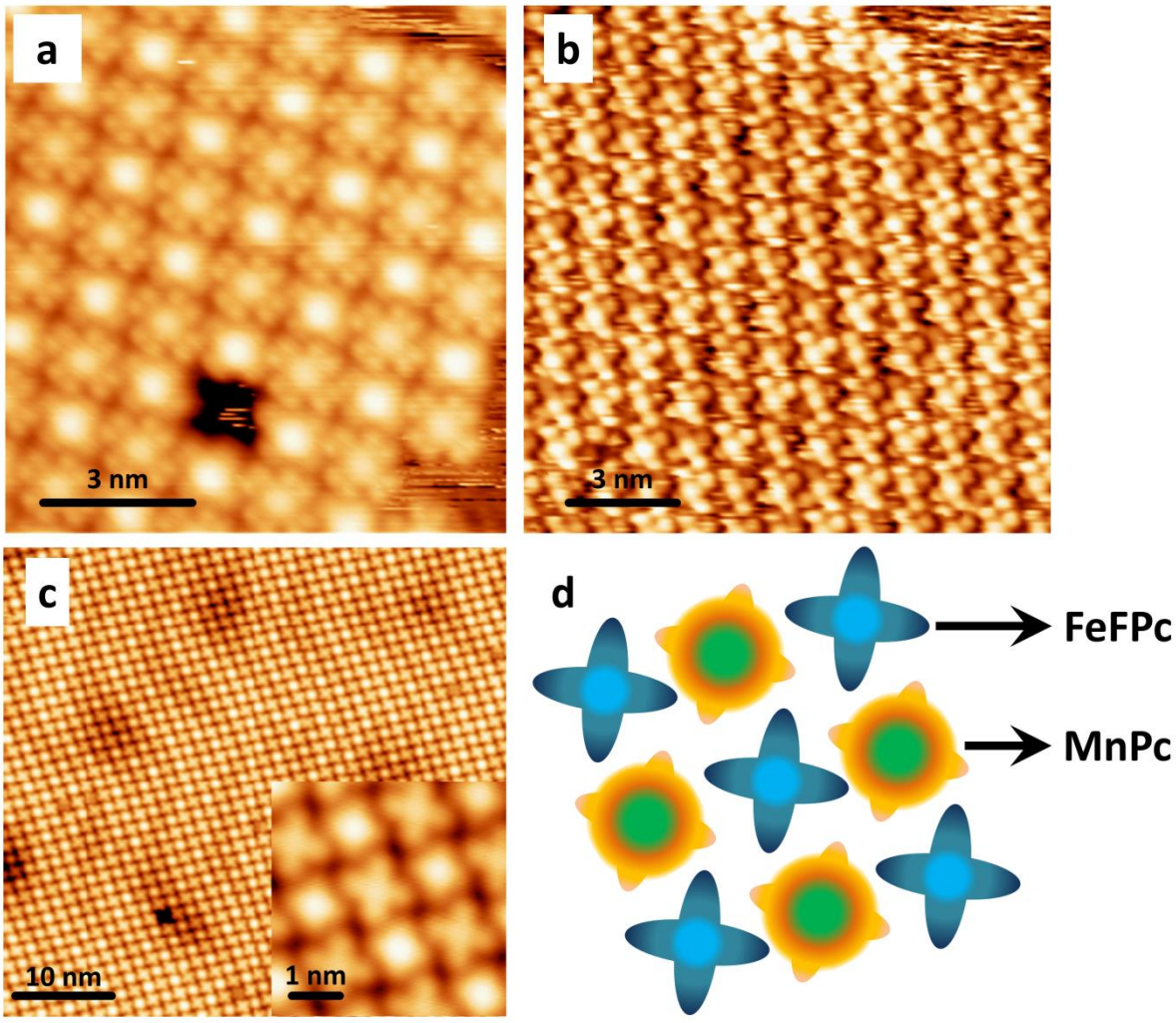

Figure 2.5.4: *STM micrographs of MnPc + FeFPc co-assembly deposited on a (a) O/Co, (b) Ag(111) and (c) Au(111) substrate. (d) Model of the chessboard shown in the inset of (c). The distance between nearest neighbours in the co-assembly does not vary significantly between the different substrates and is equal to ~1.4 nm. All of the presented micrographs were measured at V_s=2 V and I_t=10 pA; images (a) and (b) were measured at RT, while image (c) was measured at 4.2 K.*

Self-assembly occurs through a balance of repulsive and attractive interactions.[65] Since we observe the supramolecular chessboard, the interactions between MnPc and FeFPc are favourable compared to MnPc-MnPc or FeFPc-FeFPc interactions. To know why, it is required to discuss the involved forces between (a) C-H···H-C, (b) C-F···H-C and (c) C-F···F-C. In all three cases there will be an attractive dispersion force involved,[66] which is also the dominant one in (a) due to the weakly polar nature of a C-H bond.[47] As a result of a much higher electronegativity of F on comparison to C, (c) interactions will also involve a strong electrostatic repulsion of negatively-charged F atoms.[66] The situation is much more favourable in the case of C-F···H-C interactions, in which the weak C-H and stronger F-C dipole attract each other, creating H-bond type interaction. Two other forces that allow for the system to reach the balance of repulsive and attractive interactions are the Pauli repulsion that prevents the molecules and therefore the supramolecular assembly from collapsing, as well as the 2D analogue of pressure caused by mobile molecules. The molecules that are constantly diffusing can be seen as noise in the top-right corners of Fig. 2.5.2a,b.

In order to achieve a molecular chessboard, the surface has to be well prepared and exhibit wide (*i.e.* > 100 nm) terraces: they are necessary since any steps and defects will act as adsorption sites. Low adsorption energy of molecules is also required, as it allows for a high diffusion coefficient and therefore large diffusion length, which is necessary to create such an extended supramolecular structure. Notably, the smaller the diffusion length, the slower the layer should be deposited: it enables the molecules to create the most favourable structure before random assembly occurs.

2.5.2 Influence of the substrate on the magnetic properties of 2D supramolecular chessboard-like assemblies

As shown before, the supramolecular 2D arrangement of molecules had been prepared on all studied substrates. Therefore, we found it conceptually interesting to investigate how the underlying substrate influences the magnetic properties of the MnPc-FeFPc co-assembly. The first clear difference between different substrates is the relative strength as well as the nature of the interactions. While on ferromagnetic supports the magnetic exchange interaction is the dominant interaction with the substrate, choosing a diamagnetic surface allows for other phenomena to be observed. Specifically, the interactions *via* and *with* the conduction electrons of the substrate can be investigated. Interaction v*ia* conduction electrons implies the so-called Ruderman-Kittel-Kasuya-Yosida (RKKY) coupling, *i.e.* the interaction mediated by propagating spin density waves. The RKKY coupling is commonly known for its effect on magnetic layers separated by a diamagnetic conductor, where depending on the thickness of the spacer layer the coupling between the magnetic films can be either ferromagnetic or antiferromagnetic.[67,68] This effect, however, occurs also in the case of surface-supported molecular monolayers and it can result in intermolecular coupling.[69] The interaction *with* conduction electrons on the other hand is expected to result in the Kondo effect, *i.e.* in the screening of magnetic moment. It has been first observed as a resistance minimum in dilute magnetic alloys,[70] whereas at present it is extensively studied in surface-supported atoms, molecules and quantum dots by means of STS.[71–73]

Figure 2.5.3 shows XMCD results obtained for the MnPc-FeFPc co-assembly adsorbed on O/Co.[57] On this ferromagnetic substrate, the magnetic coupling of the molecules to the underlying substrate is dominating and any realistic intermolecular coupling mechanism is too weak to be investigated, since the large size of organic molecules do not allow for the hybridisation of neighbouring metal centres. However, this strong interaction can be modified by ligation, which causes a change in the spin state of the molecules. For example, the spin

state of surface-adsorbed CoTPP molecules could be reversibly changed from S=1/2 to S=0 by NO (S=1/2) ligation and subsequent annealing.[20] The inspiration of spin switching originates from the nature: when O_2 is transported by blood in the human body, it binds to Fe from the haem molecule and changes its spin state from S=2 to S=0.[74] In the here shown example of control over the supramolecular assembly, we were able to switch the initial ON/ON state (Fig. 2.5.3a,b) to the ON'/OFF state (Fig 2.5.3c,d) by simple ligation of both molecules with NH_3. The NH_3 changes the spin state of both building blocks; however, MnPc remains paramagnetic whereas FeFPc becomes diamagnetic, as evidenced by the lack of XMCD signal (Fig. 2.5.3c). Interestingly, NH_3 can change the spin state of metal-organic molecules even though it is a compound with S=0. This change is possible because NH_3 ligation causes a rearrangement of 3d orbital energy levels of the porphyrin metal centre; specifically, the interaction of NH_3 via its lone-pair increases the energy of the $3dz^2$ orbital, and in turn changes the electronic configuration and the spin state of the porphyrin molecules.

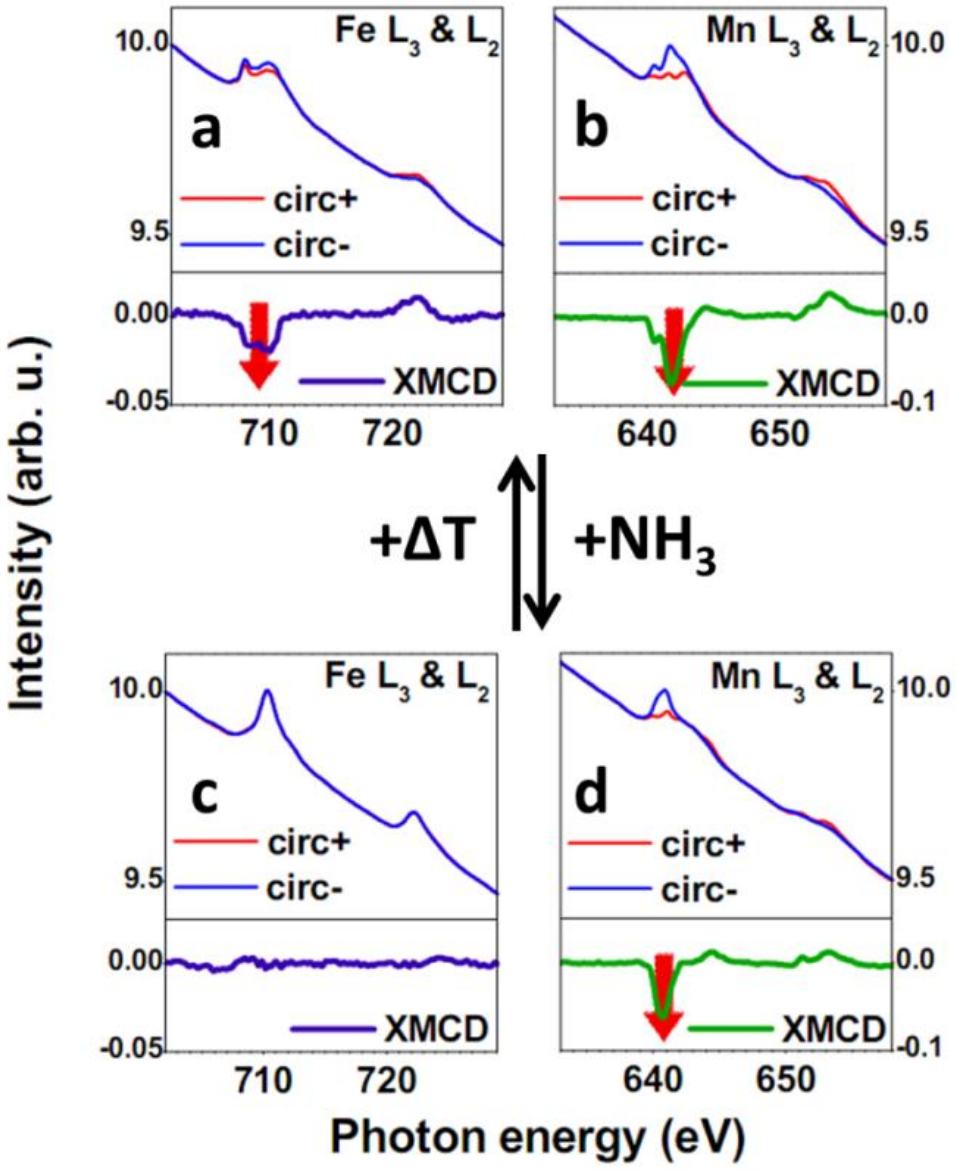

Figure 2.5.5 *Mn and Fe L-edge XAS and XMCD measured on the MnPc-FeFPc co-assembly adsorbed on the O/ Co substrate. Fe (a) and Mn (b) $L_{3,2}$ spectra showing that both molecules couple to the underlying substrate. Fe (c) and Mn (d) $L_{3,2}$ spectra after exposure to 100 L of NH_3 onto the sample held at 70 K. Ligation caused a change of the spin state of both molecules, resulting in a ON/ON to ON/OFF switch. This effect is fully reversible by thermal desorption of NH_3 after annealing of the sample to 300 K. Graphs adapted from Ref. [*57*].*

The interaction of paramagnetic molecules with an underlying ferromagnetic substrate conceals any weaker, intermolecular effects, which we were interested to study. Therefore, we decided to investigate the co-assembly prepared on (111)-cut noble, diamagnetic substrates. At the beginning we used a Ag(111) substrate, and the results are shown in Fig. 2.5.4. It can be seen that the molecular layer behaves like a paramagnet, with both molecules aligning their magnetic moment with the external magnetic field (green curves), but exhibiting no net magnetisation when the magnetic field is switched off (red curves).

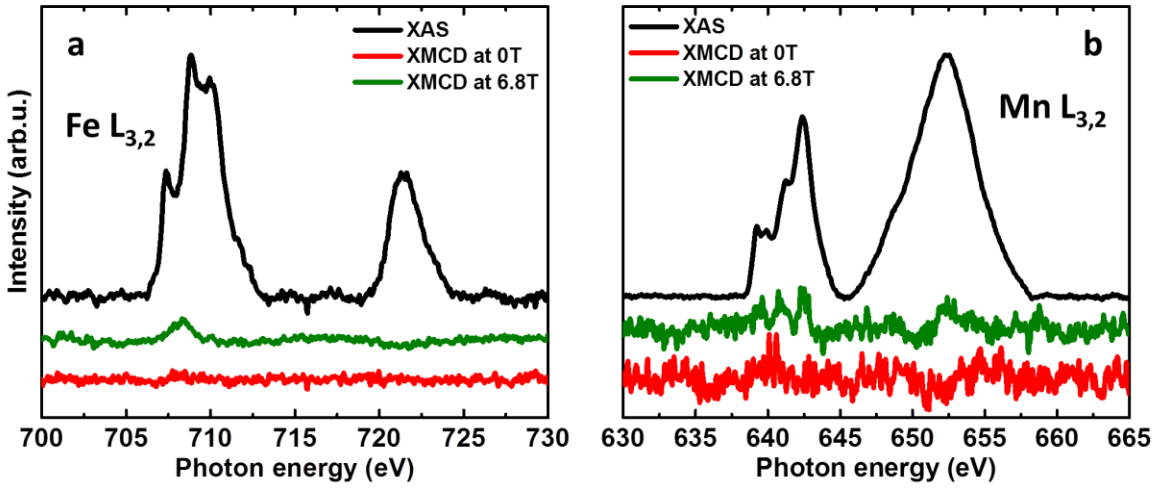

Figure 2.5.6 *The XAS and XMCD of Fe (a) and Mn (b) $L_{3,2}$ edges measured on MnPc-FeFPc co-assembly adsorbed on Ag(111). On this substrate the molecules exhibit paramagnetic properties, i.e. they align their spin in the magnetic field, but show no magnetic remanence. The apparently large Mn L_2 edge is due to an overlap with M absorption edges of Ag. The spectra were measured at 2.5 K in normal incidence.*

One could expect a similar paramagnetic behaviour of co-assembly fabricated on Au(111). However, as can be seen in the Figure 2.5.5, this is not the case. Surprisingly, the MnPc-FeFPc supramolecular arrangement on Au(111) shows XMCD even without the external magnetic field (red curves in Fig 2.5.5a,b). Moreover, the FeFPc molecules flip their magnetization direction when compared to the data measured in the magnetic field. This indicates that there is AFM coupling between the two molecular species. As the magnetic moment of the two metal centres is different, the molecular layer is a 2D *ferrimagnet*. To the best of our knowledge this

system provides the first example of such a structure. Moreover, this is the first example of an on-surface organometallic layer exhibiting properties of a permanent magnet, as the only similar 2D system with permanent magnetic moment was presented recently in a fully organic layer of TCNQ on graphene, where the coupling between molecules was found to be ferromagnetic.[75]

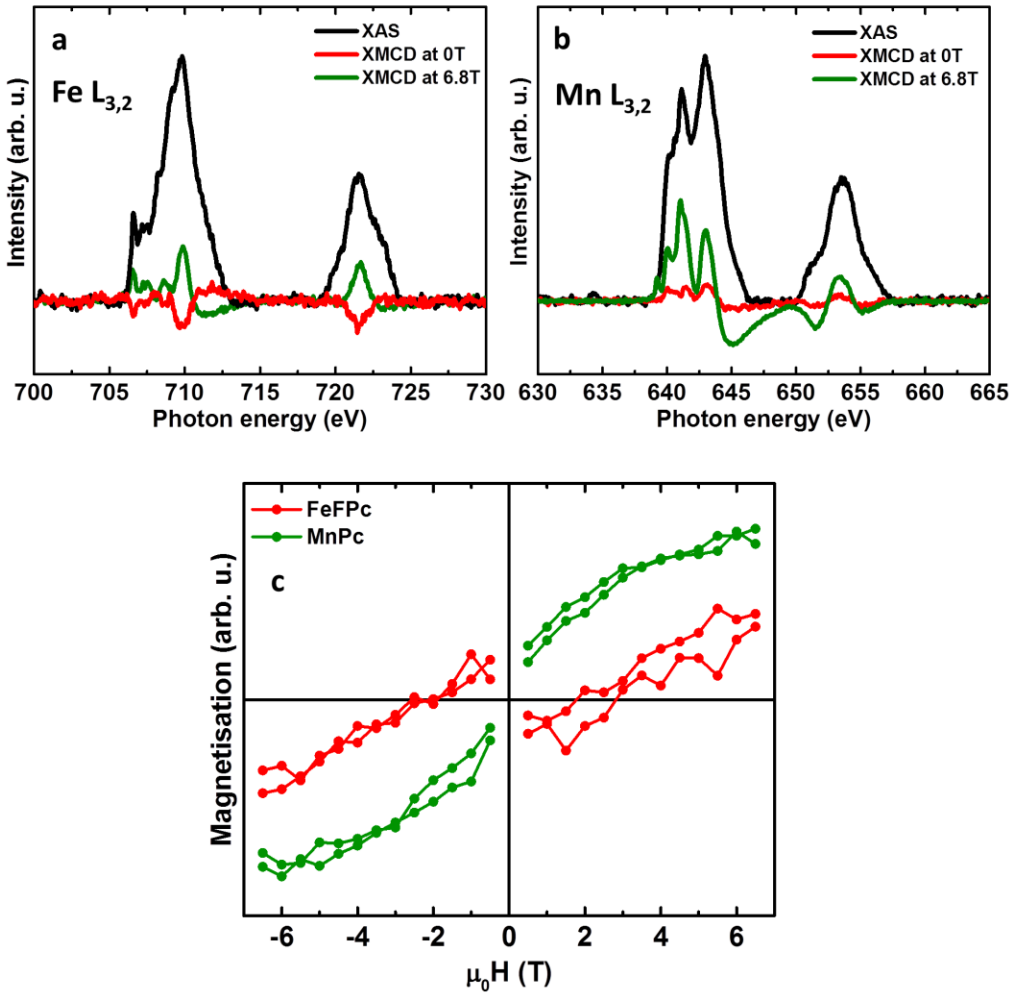

Figure 2.5.7 *The XAS and XMCD of Fe (a) and Mn (b) $L_{3,2}$ edges as well as the magnetisation curves (c) measured on MnPc-FeFPc co-assembly adsorbed on Au(111). Interestingly, molecules exhibit a magnetic moment not only in the external magnetic field, but also without it. In remanence the molecules couple antiferromagnetically to each other, as evidenced by the opposite signs of XMCD spectra (c.f. red curves of (a) and (b)). Both of the molecules exhibit a large orbital moment, as indicated by both XMCD edges pointing in the same direction. The magnetisation curve (c) shows that the intermolecular coupling is*

overcome by an external magnetic field higher than ~2.5 T (c.f. the red curve crossing zero magnetisation). In the Mn data a small opening of the hysteresis curve is observed between -2.5 T and +2.5 T (green curve). The data was measured at 2.5 K in normal incidence.

The magnetic curve of Fe crossing zero at B_0=2.5 T means that at this point the intermolecular coupling mediated by the substrate is equal in strength but reverse in sign to the interaction with the external magnetic field; this allows for the estimation of the intermolecular coupling energy. Assuming a magnetic moment of FeFPc equal to $m_{Fe}=2\ \mu_B$ and taking into account that the spin-orbit splitting energy is equal to E_{split}=58 μeV per T,[29] the intermolecular magnetic coupling strength can be estimated as $E=B_0 \cdot m_{Fe} \cdot E_{split} \approx 0.3$ meV. This result is more than two orders of magnitude smaller than that for the molecule-surface interaction strength on a ferromagnetic substrate, accentuating that any such interactions, even if present, would be virtually impossible to detect on ferromagnetic surfaces.

The fact that such a 2D ferrimagnetic structure exists becomes even more interesting, when considering the fact that the RKKY coupling is not the only physical effect induced by gold. The interaction with conduction electrons from gold causes also the so-called Kondo effect which results in screening of the magnetic moment. Figure 2.5.6 presents temperature-dependent STS data measured with the STM tip positioned above the centre of FeFPc (top) and MnPc (bottom) molecules. The zero bias feature is a dip in the case of FeFPc and a step for MnPc, in agreement with literature data for homo-molecular layers on Au(111) substrate.[69,76]

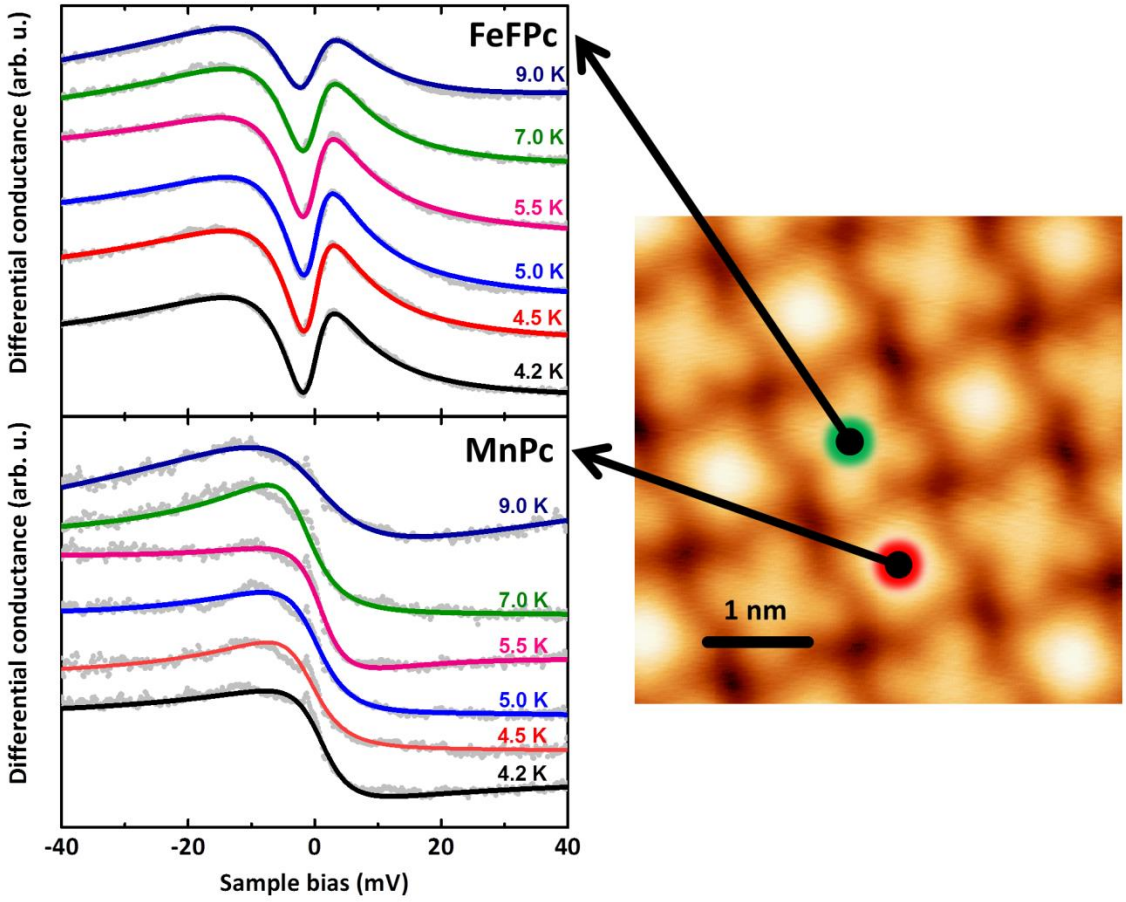

Figure 2.5.8 *Temperature-dependent STS spectra measured above the centre of FeFPc (top) and MnPc (bottom) co-assembled on Au(111). The data in both cases shows a zero-bias feature that is broadening with increasing temperature due to the Kondo effect. The data points for all temperatures are plotted in grey, while the coloured lines represent fits at the respective temperatures. The data for different temperatures have been vertically translated for clarity. The STM image on the right shows the molecules STS was measured above. All of the data had to be measured on the same molecules, as the intensity of the Kondo resonance was highly varying between molecules due to the inhomogeneous nature of the underlying herring-bone reconstruction of Au(111).*

In order to unambiguously prove that these features are due to the Kondo effect, the measured data has been fitted with a phenomenological Frota line shape in the following form:[77]

$$\frac{dI}{dV} \backsim a \cdot Im\left[-ie^{i\phi}\sqrt{\frac{i\Gamma}{eV - e_0 + i\Gamma}}\right] + b \cdot V + c$$

where ϕ is the phase factor that determines the shape of the Kondo resonance, Γ is the resonance width, e_0 defines the centre of the resonance while a, b and c are dimensionless factors. The change of Γ with temperature allows in turn for the determination of the Kondo temperature defining the energy scale that limits the validity of Kondo results. Thus, the Γ parameter depends on the interaction strength between the conduction electrons and the magnetic impurity.[78] Interestingly, the extracted Kondo temperature T_K of both molecules is very similar and equal to T_K=10.5 ± 1.2 K for FeFPc and T_K=12.8 ± 1.0 K for MnPc. These results fall in between the values obtained for single FePc (T_K=2.6 K)[69] and MnPc (T_K=36 K)[76], confirming the electronic coupling between the molecules and the creation of a 2D Kondo lattice.

To understand why the coupling between MnPc and FeFPc molecules is possible, even though the spin moments of molecules are partially screened by the Kondo effect, as well as why it occurs only on Au(111) and not on Ag(111), we have to consider the nature of the electronic states interacting with the molecular adlayer. The first factor to consider is the Fermi wave vector k_F of the surface-state electrons. On Au(111) due to Rashba splitting there are two different wave vectors for opposite spins: k_F=1.62 nm^{-1} and k_F=1.85 nm^{-1},[79] while on Ag(111) there is one wave vector of k_F=0.8 nm^{-1}.[79] It would be sensible to consider whether bulk electrons also contribute to this coupling; the spin density waves of bulk electrons in Au and Ag, however, have an order of magnitude shorter wavelength, therefore decay much faster and their contribution to the coupling is negligible.[69,80] Taking all this into account, the RKKY coupling mediated by the surface-state electrons can be calculated using the equation:[81]

$$J = J_0 \frac{\sin(2k_F r)}{(2k_F r)^2}$$

where J_0 is a constant and r is the distance between two magnetic atoms. The results obtained from this equation for both Ag(111) and Au(111) are shown in the Fig. 2.5.7. It explains why

Au(111) is the ideal substrate to mediate antiferromagnetic coupling within the studied supramolecular chessboard. The distance between the nearest neighbours, *i.e.* 1.4 nm between MnPc and FeFPc, lies almost at the maximum of AFM coupling while the distance between next-nearest neighbours (1.98 nm between two FeFPc or two MnPc molecules) lies in the FM coupling range.

Looking at only the Fig. 2.5.7 one might then expect a ferromagnetic coupling between the MnPc and FeFPc molecules in the supramolecular assembly on Ag(111), as the nearest neighbour distance lies in the strong FM coupling range. It is, however, also important to realise that the right wavelength is not the only prerequisite to intermolecular coupling. The spin density waves also have to interact strongly with the surface-supported spin impurity (*i.e.* the molecular metal centre). The interaction between the molecules and the surface electrons depends on many factors including the adsorption site of the metal centre, its chemical environment, distance between the metal centre and the surface, symmetry of the system and the available local density of states of the surface electrons; it has been shown for example, that the Kondo effect can be switched on and off by ligation, by introducing intermolecular interactions or by dehydrogenating and therefore bending the molecule.[82–84] Interestingly, the Kondo effect and the RKKY coupling are closely related as they both arise from the interaction of unpaired magnetic moments and conduction electrons of the underlying substrate. Therefore, counter-intuitively, the observation of Kondo resonance might be necessary for the long-range order. In the case of Ag(111), however, no Kondo resonance was observed for MnPc molecules,[85] suggesting weak interaction between the molecules and the conduction electrons of Ag(111) and hence explaining the lack of intermolecular coupling in the MnPc-FeFPc chessboard-like arrangement on this substrate.

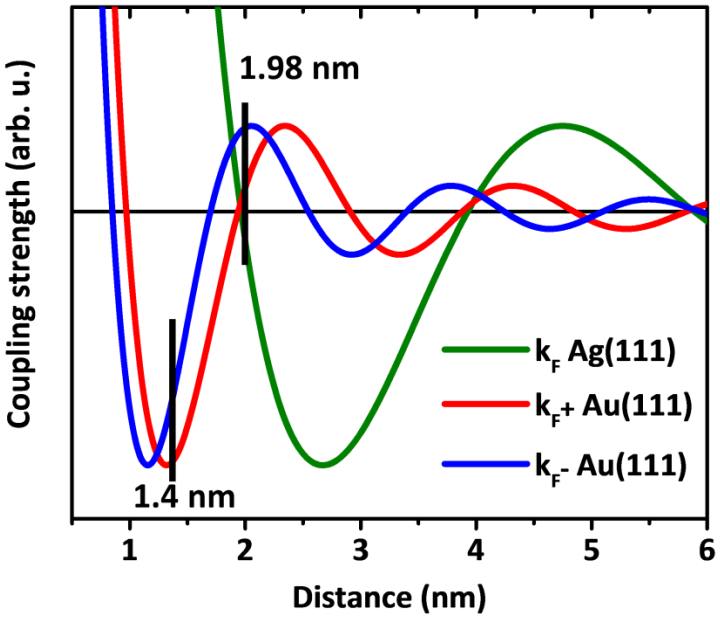

Figure 2.5.9 *Simulated RKKY coupling strength between two spins vs. distance on Ag(111) and Au(111) substrates. There are two curves for Au(111) because this substrate exhibits two Rashba-split surface states. The black vertical lines indicate that the spin density waves on Au(111) have a virtually ideal wavelength to mediate AFM coupling between nearest neighbours (1.4 nm apart) and FM coupling between next-nearest neighbours (1.98 nm apart).*

Importantly, such a 2D ferrimagnet is highly unexpected, because theory of magnetism predicts that stabilisation of magnetic moments is not possible in low dimensional systems (d≤2) even at T=0 K.[86] The only reason we can observe this effect is due to the influence of the substrate, not only in the form of the coupling mediated by the surface state, but also due to the magnetic anisotropy imposed on the molecules.

3 Summary and outlook

During my studies I explored fascinating systems exhibiting multidimensional tunability combining the advantages of two different, organic and inorganic, worlds. This tunability was provided by the extensive selection of possible molecular substituents (organic chemistry), the ability to create the intended organic species directly on the surface (metalation), together with the possibility to choose and design the properties of the metallic support (surface modification). The presented examples show the differences and similarities between the phenomena of magnetism and chemical reactions and how they can influence each other.

By studying porphyrin metalation I have observed that simple, atomically thin surface modifications can change the intermolecular interactions and the assembly of molecules, as well as the activation energy, the pathway and the products of a chemical reaction. Interestingly, metalation involves removing a metal atom from the surface and inserting it in an organic molecule, where its properties resemble more those of single atoms. This provides an example of how a chemical reaction can influence magnetic properties of a system and accentuates the difference between the properties of bulk, surface and single Cu atoms, since only the last exhibit paramagnetic properties.[87,88]

A reaction involving the insertion of a metal into an organic molecule is, however, not the only way to tune magnetic properties of atoms. Also by mere adsorption on a well-chosen surface, the magnetic properties of an atom may significantly change. The large out-of-plane magnetic anisotropy, as here observed in Fe and Cr single atoms adsorbed on a Bi(111) substrate, provides an interesting example of a tunable magnetic property that is important in order to decrease the size or magnetic information bits.

The surface-adsorbed metal atoms can be further modified by inserting them in an organic molecule – either directly on the surface as exemplified by the self-metalation reaction, or via

organic chemistry. The latter approach was chosen in the here presented study showing the influence of molecular substituents on the magnetic exchange coupling energy. I was able to tune it by a factor of three by modifying the substrate and using molecules with different substituents.

This interaction of metal-organic molecules and their ferromagnetic support lead to a phenomenon of inter-layer molecular rearrangement, caused by higher adsorption energy of MnPc when compared to FePc. I was able to study this effect using XMCD, as the magnetic response of paramagnetic molecules depends on whether or not it is in direct contact with the ferromagnetic substrate.

Interestingly, changing the substrate does not only modify the molecule-substrate interactions, but can additionally enable and tune the intermolecular coupling. I have shown that a MnPc-FeFPc chessboard-like supramolecular arrangement can be prepared on both diamagnetic (Ag(111) or Au(111)) and ferromagnetic (O/Co) substrates, exhibiting drastically different behaviour on different surfaces. On O/Co it behaved as a reversible switch, on Ag(111) it exhibited properties of a purely paramagnetic layer, while the intermolecular coupling through the Au(111) substrate enabled the molecular chessboard to become the first, to the best of my knowledge, observed 2D ferrimagnet.

These results may, in the future, help in modifying the properties of magnetic/spintronic devices or in surface catalytic applications, in both their design and realisation. A better, mechanistic understanding of the role of adatoms in chemical reactions, for example, could allow increasing their efficiency. Decreasing the energy required to obtain NH_3 would be of great interest from both the economic and ecological standpoints, as the currently-used Haber-Bosch process is inefficient and utilised in an almost-unchanged way since a hundred years. Modifying the magnetic properties of surface-supported atoms and molecules on the other hand could not only increase the storage density of magnetic hard drives, but also make new applications possible, like a 2D organic spin-valve controllable by *e.g.* ligation. The ability to selectively address only a part of the supramolecular layer or even just single molecules by STS/STM, as shown by my co-workers and me, extends the possibilities even further.[57]

Naturally, there are many technical difficulties to overcome before we will be able to build a device using, for example, a 2D ferrimagnet. First of all, it would need to be protected from the influence of ambient pressure and room temperature. These tasks might look extremely difficult, but I believe they are not impossible. Coating the molecular layer with a protective layer and using ligation or surface modifications in order to increase the magnetic ordering temperature could solve these issues. There is also a lot of work required before surface superstructures could be used in industrial-scale chemical reactors.

Possible applications, however, are not the only reason to do research and we would all like to know more about the laws of nature. At the time of submission of this thesis, I was not able to answer all of the fundamental questions I asked, and there are many more that I did not even think of asking. I would like to understand the delicate balance of intermolecular interactions that causes 2HTPP molecules to assemble in clusters that do not follow the Poisson distribution. I would be very interested to better understand why MnPc molecules push FePc away from the O/Co substrate – whether the nature of this effect is more chemical or magnetic, or maybe there are other effects that I did not take into account. What I also consider worth pursuing in the future is extending the limit of attainable magnetic coupling energies between surface-adsorbed molecules and ferromagnetic substrates – by *e.g.* utilising different substrate modifications, using even bigger molecular substituents or by ligation that can pull the metal atom away from the substrate. Moreover, a phenomenological dependency of the magnetic coupling energy on the molecule-substrate separation is still missing.

I am curious how the idea of the 2D supramolecular chessboard and the 2D ferrimagnet can be expanded further, as I can imagine many different ways of modifying its properties. Apart from investigating the effects of ligation in more detail, one could use, for example use different metal centres and study the relative importance of different molecular orbitals. By using larger or smaller organic molecules as well as different substrates, the intermolecular coupling energy and possibly also the direction of the magnetic anisotropy would be modified. This opens the door to create other magnetic 2D structures, not only a ferrimagnet. It is also interesting to think of changing the dimensionality of the chessboard arrangement – to 1D, where they could

serve as molecular, spintronic wires or even to 3D where the interaction between molecular layers could also be investigated.

I hope these questions will be answered in the future, some of them maybe by the next PhD student.

Bibliography

(1) Pike, A. W. G.; Hoffmann, D. L.; Garcia-Diez, M.; Pettitt, P. B.; Alcolea, J.; De Balbin, R.; Gonzalez-Sainz, C.; de las Heras, C.; Lasheras, J. A.; Montes, R.; Zilhao, J. *Science* **2012**, *336* (6087), 1409–1413.

(2) Lewis, N. *Papyrus in classical antiquity.*; Fondation égyptologique reine Élisabeth: Bruxelles, 1989.

(3) Terris, B. D.; Thomson, T. *J. Phys. Appl. Phys.* **2005**, *38* (12), R199–R222.

(4) *Inside solid state drives (SSDs)*; Micheloni, R., Marelli, A., Eshghi, K., Eds.; Springer series in advanced microelectronics; Springer: Dordrecht, 2013.

(5) Feringa, B. L.; Jager, W. F.; de Lange, B. *Tetrahedron* **1993**, *49* (37), 8267–8310.

(6) Mallary, M.; Torabi, A.; Benakli, M. *IEEE Trans. Magn.* **2002**, *38* (4), 1719–1724.

(7) Masel, R. I. *Principles of adsorption and reaction on solid surfaces*; Wiley series in chemical engineering; Wiley: New York, 1996.

(8) Vaclav Smil. *Nature* **1999**, *400* (6743), 415.

(9) Kitano, M.; Inoue, Y.; Yamazaki, Y.; Hayashi, F.; Kanbara, S.; Matsuishi, S.; Yokoyama, T.; Kim, S.-W.; Hara, M.; Hosono, H. *Nat. Chem.* **2012**, *4* (11), 934–940.

(10) *The porphyrin handbook*; Kadish, K. M., Smith, K. M., Guilard, R., Eds.; Academic Press: San Diego, Calif., 2000.

(11) Auwärter, W.; Écija, D.; Klappenberger, F.; Barth, J. V. *Nat. Chem.* **2015**, *7* (2), 105–120.

(12) Gottfried, J. M. *Surf. Sci. Rep.* **2015**, *70* (3), 259–379.

(13) Krull, C.; Robles, R.; Mugarza, A.; Gambardella, P. *Nat. Mater.* **2013**, *12* (4), 337–343.

(14) Auwärter, W.; Weber-Bargioni, A.; Brink, S.; Riemann, A.; Schiffrin, A.; Ruben, M.; Barth, J. V. *ChemPhysChem* **2007**, *8* (2), 250–254.

(15) Shubina, T. E.; Marbach, H.; Flechtner, K.; Kretschmann, A.; Jux, N.; Buchner, F.; Steinrück, H.-P.; Clark, T.; Gottfried, J. M. *J. Am. Chem. Soc.* **2007**, *129* (30), 9476–9483.

(16) Écija, D.; Auwärter, W.; Vijayaraghavan, S.; Seufert, K.; Bischoff, F.; Tashiro, K.; Barth, J. V. *Angew. Chem. Int. Ed.* **2011**, *50* (17), 3872–3877.

(17) Auwärter, W.; Seufert, K.; Bischoff, F.; Ecija, D.; Vijayaraghavan, S.; Joshi, S.; Klappenberger, F.; Samudrala, N.; Barth, J. V. *Nat. Nanotechnol.* **2011**, *7* (1), 41–46.

(18) Hod, I.; Sampson, M. D.; Deria, P.; Kubiak, C. P.; Farha, O. K.; Hupp, J. T. *ACS Catal.* **2015**, *5* (11), 6302–6309.

(19) Qiu, X. H.; Nazin, G. V.; Ho, W. *Phys. Rev. Lett.* **2004**, *93* (19).

(20) Wäckerlin, C.; Chylarecka, D.; Kleibert, A.; Müller, K.; Iacovita, C.; Nolting, F.; Jung, T. A.; Ballav, N. *Nat. Commun.* **2010**, *1* (5), 1–7.

(21) Donati, F.; Rusponi, S.; Stepanow, S.; Wackerlin, C.; Singha, A.; Persichetti, L.; Baltic, R.; Diller, K.; Patthey, F.; Fernandes, E.; Dreiser, J.; ljivan anin, .; Kummer, K.; Nistor, C.; Gambardella, P.; Brune, H. *Science* **2016**, *352* (6283), 318–321.

(22) Schubert, E. F. *Delta-doping of semiconductors*; Cambridge University Press: New York, 2005.

(23) Simbrunner, C.; Wegscheider, M.; Quast, M.; Li, T.; Navarro-Quezada, A.; Sitter, H.; Bonanni, A.; Jakiela, R. *Appl. Phys. Lett.* **2007**, *90* (14), 142108.

(24) *Surface analysis: the principal techniques*, 2. ed.; Vickerman, J. C., Gilmore, I. S., Eds.; Wiley: Chichester, 2009.

(25) *Handbook of X-ray photoelectron spectroscopy: a reference book of standard spectra for identification and interpretation of XPS data*; Moulder, J. F., Stickle, W. F., Sobol, P. E., Bomben, K. D., Chastain, J., King Jr., R. C., Physical Electronics, Incorporation, Eds.; Physical Electronics: Eden Prairie, Minn., 1995.

(26) Leckey, R. In *Surface Analysis Methods in Materials Science*; O'Connor, D. J., Sexton, B. A., Smart, R. S. C., Eds.; Ertl, G., Gomer, R., Mills, D. L., Lotsch, H. K. V., Series Eds.; Springer Berlin Heidelberg: Berlin, Heidelberg, 1992; Vol. 23, pp 291–300.

(27) Braun, S.; Salaneck, W. R.; Fahlman, M. *Adv. Mater.* **2009**, *21* (14-15), 1450–1472.

(28) Bussolotti, F.; Yang, J.; Hinderhofer, A.; Huang, Y.; Chen, W.; Kera, S.; Wee, A. T. S.; Ueno, N. *Phys. Rev. B* **2014**, *89* (11).

(29) Stöhr, J.; Siegmann, H. C. *Magnetism from fundamentals to nanoscale dynamics*; Springer: Berlin, 2006.

(30) Chen, C. J. *Introduction to scanning tunneling microscopy*; Oxford series in optical and imaging sciences; Oxford Univ. Press: New York, NY, 1993.

(31) Hipps, K. W. In *Handbook of Applied Solid State Spectroscopy*; Vij, D. R., Ed.; Springer US: Boston, MA, 2006; pp 305–350.

(32) Hove, M. A.; Weinberg, W. H.; Chan, C.-M. *Low-Energy Electron Diffraction Experiment, Theory and Surface Structure Determination*; Springer Berlin Heidelberg: Berlin, Heidelberg, 1986.

(33) Miyamachi, T.; Schuh, T.; Märkl, T.; Bresch, C.; Balashov, T.; Stöhr, A.; Karlewski, C.; André, S.; Marthaler, M.; Hoffmann, M.; Geilhufe, M.; Ostanin, S.; Hergert, W.; Mertig, I.; Schön, G.; Ernst, A.; Wulfhekel, W. *Nature* **2013**, *503* (7475), 242–246.

(34) Steinbrecher, M.; Sonntag, A.; Dias, M. dos S.; Bouhassoune, M.; Lounis, S.; Wiebe, J.; Wiesendanger, R.; Khajetoorians, A. A. *Nat. Commun.* **2016**, *7*, 10454.

(35) Bihlmayer, G.; Blügel, S.; Chulkov, E. V. *Phys. Rev. B* **2007**, *75* (19).

(36) Klein, C.; Vollmers, N. J.; Gerstmann, U.; Zahl, P.; Lükermann, D.; Jnawali, G.; Pfnür, H.; Tegenkamp, C.; Sutter, P.; Schmidt, W. G.; Horn-von Hoegen, M. *Phys. Rev. B* **2015**, *91* (19).

(37) Aharoni, A. *Introduction to the theory of ferromagnetism*, Reprinted.; International series of monographs on physics; Clarendon Press: Oxford, 1998.

(38) Gambardella, P. *Science* **2003**, *300* (5622), 1130–1133.

(39) Carra, P.; Thole, B. T.; Altarelli, M.; Wang, X. *Phys. Rev. Lett.* **1993**, *70* (5), 694–697.

(40) Thole, B. T.; Carra, P.; Sette, F.; van der Laan, G. *Phys. Rev. Lett.* **1992**, *68* (12), 1943–1946.

(41) Teramura, Y.; Tanaka, A.; Jo, T. *J. Phys. Soc. Jpn.* **1996**, *65* (4), 1053–1055.

(42) Rau, I. G.; Baumann, S.; Rusponi, S.; Donati, F.; Stepanow, S.; Gragnaniello, L.; Dreiser, J.; Piamonteze, C.; Nolting, F.; Gangopadhyay, S.; Albertini, O. R.; Macfarlane, R. M.; Lutz, C. P.; Jones, B. A.; Gambardella, P.; Heinrich, A. J.; Brune, H. *Science* **2014**, *344* (6187), 988–992.

(43) Eriksson, O.; Johansson, B.; Albers, R. C.; Boring, A. M.; Brooks, M. S. S. *Phys. Rev. B* **1990**, *42* (4), 2707–2710.

(44) Weller, D.; Stöhr, J.; Nakajima, R.; Carl, A.; Samant, M. G.; Chappert, C.; Mégy, R.; Beauvillain, P.; Veillet, P.; Held, G. A. *Phys. Rev. Lett.* **1995**, *75* (20), 3752–3755.

(45) Gambardella, P.; Dallmeyer, A.; Maiti, K.; Malagoli, M. C.; Eberhardt, W.; Kern, K.; Carbone, C. *Nature* **2002**, *416* (6878), 301–304.

(46) Francisco, E.; Pueyo, L. *Phys. Rev. A* **1987**, *36* (5), 1978–1982.

(47) Huheey, J. E.; Keiter, E. A.; Keiter, R. L. *Inorganic chemistry: principles of structure and reactivity*, 4. ed., [repr.].; Harper: Cambridge, 2009.

(48) Wäckerlin, C.; Tarafder, K.; Siewert, D.; Girovsky, J.; Hählen, T.; Iacovita, C.; Kleibert, A.; Nolting, F.; Jung, T. A.; Oppeneer, P. M.; Ballav, N. *Chem. Sci.* **2012**, *3* (11), 3154.

(49) Chylarecka, D.; Kim, T. K.; Tarafder, K.; Müller, K.; Gödel, K.; Czekaj, I.; Wäckerlin, C.; Cinchetti, M.; Ali, M. E.; Piamonteze, C.; Schmitt, F.; Wüstenberg, J.-P.; Ziegler, C.; Nolting, F.; Aeschlimann, M.; Oppeneer, P. M.; Ballav, N.; Jung, T. A. *J. Phys. Chem. C* **2011**, *115* (4), 1295–1301.

(50) Bernien, M.; Miguel, J.; Weis, C.; Ali, M. E.; Kurde, J.; Krumme, B.; Panchmatia, P. M.; Sanyal, B.; Piantek, M.; Srivastava, P.; Baberschke, K.; Oppeneer, P. M.; Eriksson, O.; Kuch, W.; Wende, H. *Phys. Rev. Lett.* **2009**, *102* (4).

(51) Chylarecka, D.; Wäckerlin, C.; Kim, T. K.; Müller, K.; Nolting, F.; Kleibert, A.; Ballav, N.; Jung, T. A. *J. Phys. Chem. Lett.* **2010**, *1* (9), 1408–1413.

(52) Wäckerlin, C.; Tarafder, K.; Siewert, D.; Girovsky, J.; Hählen, T.; Iacovita, C.; Kleibert, A.; Nolting, F.; Jung, T. A.; Oppeneer, P. M.; Ballav, N. *Chem. Sci.* **2012**, *3* (11), 3154.

(53) Dobbs, K. D.; Doren, D. J. *J. Chem. Phys.* **1993**, *99* (12), 10041.

(54) Buchner, F.; Xiao, J.; Zillner, E.; Chen, M.; Röckert, M.; Ditze, S.; Stark, M.; Steinrück, H.-P.; Gottfried, J. M.; Marbach, H. *J. Phys. Chem. C* **2011**, *115* (49), 24172–24177.

(55) Xiao, J.; Ditze, S.; Chen, M.; Buchner, F.; Stark, M.; Drost, M.; Steinrück, H.-P.; Gottfried, J. M.; Marbach, H. *J. Phys. Chem. C* **2012**, *116* (22), 12275–12282.

(56) Lee, J. H.; Luo, G.; Tung, I. C.; Chang, S. H.; Luo, Z.; Malshe, M.; Gadre, M.; Bhattacharya, A.; Nakhmanson, S. M.; Eastman, J. A.; Hong, H.; Jellinek, J.; Morgan, D.; Fong, D. D.; Freeland, J. W. *Nat. Mater.* **2014**, *13* (9), 879–883.

(57) Wäckerlin, C.; Nowakowski, J.; Liu, S.-X.; Jaggi, M.; Siewert, D.; Girovsky, J.; Shchyrba, A.; Hählen, T.; Kleibert, A.; Oppeneer, P. M.; Nolting, F.; Decurtins, S.; Jung, T. A.; Ballav, N. *Adv. Mater.* **2013**, *25* (17), 2404–2408.

(58) Müller, K.; Seitsonen, A. P.; Brugger, T.; Westover, J.; Greber, T.; Jung, T.; Kara, A. *J. Phys. Chem. C* **2012**, *116* (44), 23465–23471.

(59) Wakayama, Y.; de Oteyza, D. G.; Garcia-Lastra, J. M.; Mowbray, D. J. *ACS Nano* **2011**, *5* (1), 581–589.

(60) Scheybal, A.; Ramsvik, T.; Bertschinger, R.; Putero, M.; Nolting, F.; Jung, T. A. *Chem. Phys. Lett.* **2005**, *411* (1-3), 214–220.

(61) Wende, H.; Bernien, M.; Luo, J.; Sorg, C.; Ponpandian, N.; Kurde, J.; Miguel, J.; Piantek, M.; Xu, X.; Eckhold, P.; Kuch, W.; Baberschke, K.; Panchmatia, P. M.; Sanyal, B.; Oppeneer, P. M.; Eriksson, O. *Nat. Mater.* **2007**, *6* (7), 516–520.

(62) Hipps, K. W.; Scudiero, L.; Barlow, D. E.; Cooke, M. P. *J. Am. Chem. Soc.* **2002**, *124* (10), 2126–2127.

(63) Scudiero, L.; Hipps, K. W.; Barlow, D. E. *J. Phys. Chem. B* **2003**, *107* (13), 2903–2909.

(64) Ponzini, F.; Zagha, R.; Hardcastle, K.; Siegel, J. S. *Angew. Chem. Int. Ed.* **2000**, *39* (13), 2323–2325.

(65) Whitesides, G. M.; Boncheva, M. *Proc. Natl. Acad. Sci.* **2002**, *99* (8), 4769–4774.

(66) Kawai, S.; Sadeghi, A.; Xu, F.; Peng, L.; Orita, A.; Otera, J.; Goedecker, S.; Meyer, E. *ACS Nano* **2015**, *9* (3), 2574–2583.

(67) Bruno, P.; Chappert, C. *Phys. Rev. Lett.* **1991**, *67* (12), 1602–1605.

(68) Yafet, Y. *J. Appl. Phys.* **1987**, *61* (8), 4058.

(69) Tsukahara, N.; Shiraki, S.; Itou, S.; Ohta, N.; Takagi, N.; Kawai, M. *Phys. Rev. Lett.* **2011**, *106* (18).

(70) Kondo, J. *Prog. Theor. Phys.* **1964**, *32* (1), 37–49.

(71) Cronenwett, S. M. *Science* **1998**, *281* (5376), 540–544.

(72) Minamitani, E.; Tsukahara, N.; Matsunaka, D.; Kim, Y.; Takagi, N.; Kawai, M. *Phys. Rev. Lett.* **2012**, *109* (8).

(73) Park, J.; Pasupathy, A. N.; Goldsmith, J. I.; Chang, C.; Yaish, Y.; Petta, J. R.; Rinkoski, M.; Sethna, J. P.; Abruña, H. D.; McEuen, P. L.; Ralph, D. C. *Nature* **2002**, *417* (6890), 722–725.

(74) Friedman, J. M.; Scott, T. W.; Stepnoski, R. A.; Ikeda-Saito, M.; Yonetani, T. *J. Biol. Chem.* **1983**, *258*, 10564–10572.

(75) Garnica, M.; Stradi, D.; Barja, S.; Calleja, F.; Díaz, C.; Alcamí, M.; Martín, N.; Vázquez de Parga, A. L.; Martín, F.; Miranda, R. *Nat. Phys.* **2013**, *9* (6), 368–374.

(76) Liu, L.; Yang, K.; Jiang, Y.; Song, B.; Xiao, W.; Song, S.; Du, S.; Ouyang, M.; Hofer, W. A.; Castro Neto, A. H.; Gao, H.-J. *Phys. Rev. Lett.* **2015**, *114* (12).

(77) Prüser, H.; Dargel, P. E.; Bouhassoune, M.; Ulbrich, R. G.; Pruschke, T.; Lounis, S.; Wenderoth, M. *Nat. Commun.* **2014**, *5*, 5417.

(78) Nagaoka, K.; Jamneala, T.; Grobis, M.; Crommie, M. F. *Phys. Rev. Lett.* **2002**, *88* (7).

(79) Reinert, F. *J. Phys. Condens. Matter* **2003**, *15* (5), S693–S705.

(80) Ashcroft, N. W.; Mermin, N. D. *Solid state physics*, Repr.; Brooks/Cole Thomson Learning: South Melbourne, 2012.

(81) Fischer, B.; Klein, M. W. *Phys. Rev. B* **1975**, *11* (5), 2025–2029.

(82) Liu, L.; Yang, K.; Jiang, Y.; Song, B.; Xiao, W.; Li, L.; Zhou, H.; Wang, Y.; Du, S.; Ouyang, M.; Hofer, W. A.; Castro Neto, A. H.; Gao, H.-J. *Sci. Rep.* **2013**, *3*.

(83) Zhang, Q.; Kuang, G.; Pang, R.; Shi, X.; Lin, N. *ACS Nano* **2015**, *9* (12), 12521–12528.

(84) Zhao, A. *Science* **2005**, *309* (5740), 1542–1544.

(85) Ohta, N.; Arafune, R.; Tsukahara, N.; Kawai, M.; Takagi, N. *J. Phys. Chem. C* **2013**, *117* (42), 21832–21837.

(86) Mermin, N. D.; Wagner, H. *Phys. Rev. Lett.* **1966**, *17* (22), 1133–1136.

(87) *CRC handbook of chemistry and physics: a ready-reference book of chemical and physical data*, 86. ed.; Chemical Rubber Company, Lide, D. R., Eds.; CRC Press: Boca Raton, 2005.

(88) Godziela, G. M.; Goff, H. M. *J. Am. Chem. Soc.* **1986**, *108* (9), 2237–2243.

Acknowledgements

This thesis is the effect of four years of my life spent at PSI, but I could not have done it by myself. It is a result of collaboration with my co-workers at PSI and SLS as well as many international groups, who helped me greatly with their expertise. Everything I've learned during those 4 years I know thanks to you.

First of all I would like to thank my supervisor Thomas Jung for his trust, showed by hiring me as a PhD student. I thank him for his support, both scientific and non-scientific discussions and good team spirit. I am especially grateful that I was never forced into one or the other direction, but rather gently guided throughout my PhD studies; I am happy that I was free to explore what was interesting to me. I am also grateful to Nirmalya Ballav who was helping me to decide which project to focus on, even from India. I thank him for the many evenings we've spent together at different beamlines of the SLS discussing exciting results or dosing carbon monoxide.

I would like to express my gratitude to the Swiss Nanoscience Institute for not only funding my PhD studied, but also organizing interesting events and excursions, like the annual meetings in Lenzerheide. It was always a great opportunity to meet people from other branches of science, see their achievements during the day and have fun in the evening.

I am extremely grateful to all of my colleagues at PSI who were always there to talk to during difficult times, and were also there to share the excitement of successful experiments. Therefore I would like to thank Miloš Baljozović, Dipanwita Dutta, Jan Girovsky, Tatjana Hählen, Darek Jarząbek, Fotini Ravani, Harald Rossmann, Dorota Siewert and Christian Wäckerlin. I would like to especially thank Christian for his patience when introducing me to the laboratory, Miloš and Jan for the teamwork in the lab and during the synchrotron experiments well as to

Harald and Tatjana for their patience when preparing samples for the tired night-shift even when I was to sleepy to extract meaningful information from.

Due to the fact that beamtimes are very work-intensive, we often needed help from the NANOLAB group at University of Basel. I would like to thank Shadi Fatayer, Fatameh Mousavi, Thomas Nijs, Olha Popova and Aneliia Wäckerlin for their support and willingness to participate in beamtimes. It was great to enjoy some fondue with you before going to the beamline. I am also very grateful to Sylwia Nowakowska, who thought me how to use their STM and patiently helped me to measure. Most of the STM images in this thesis exist thanks to her.

There would be no beamlines without beamline scientists. I am grateful to Jan Dreiser, Armin Kleibert, Matthias Muntwiler and Cinthia Piamonteze because their hard work and dedication allowed me to use the synchrotron radiation to obtain results shown in this thesis.

A significant part of this work would not have been possible without the help of chemists from the University of Berne. I am very grateful to Silvio Decurtins and Shi-Xia Liu for synthesizing the molecules we imagined and for giving their fresh and professional view of the projects. The meetings with you were always exciting.

I am also grateful to our collaborators from the University of Hannover. I would like to thank Philipp Kröger and Herbert Pfnür as without their expertise, investigating single atoms on Bi would not be possible. I thank for the stimulating discussions and interesting results we obtained together.

In my opinion by far the best way to learn is by teaching others. During my PhD life I supervised and co-supervised many blockcourse, IAESTE and master students. I would like to thank all of them for filling the blanks in my knowledge with their clever questions. Three students I am most grateful to are Elise Aeby, Mariah O'Doherty and Gitika Srivastava who were always ready to help me do my job. Special thanks go to Mariah, as she also volunteered herself to proof-read my thesis to improve my non-native English.

I would not even have a laboratory to work in if not the dedication of technicians in building and maintaining it. I am grateful to Marco Martina and Rolf Schelldorfer for their support and patience, even when I broke something or had ‘crazy’ ideas at the last moment.

I am also grateful to everyone at the Laboratory of Micro and Nanotechnology, as they were always ready to help. The monthly LMN meetings were very interesting and expanded my interests and knowledge.

The biggest appreciation, however, has to go to my family. My wonderful parents, Izabela and Andrzej, supported me all along, even though it was not always easy. Thanks to their love and caring growing up with my sister Julia was full of both happiness and important life lessons. Thanks to these lessons I met and married my wife, Sylwia. Her support, both professional and personal, was incredibly important was during this thesis. Without her I would’ve given up a long time ago. Dziękuję Wam, Kochani.